Summer 8-15-2016

New Tools for Viscoelastic Spectral Analysis, with Application to the Mechanics of Cells and Collagen across Hierarchies

Behzad Babaei
Washington University in St. Louis

WASHINGTON UNIVERSITY IN ST. LOUIS

Department of Mechanical Engineering and Material Science

Dissertation Examination Committee:
Guy M. Genin, Chair
Victor Birman
Elliot L. Elson
David A. Peters
Srikanth Singamaneni
Simon Y. Tang
Stavros Thomopoulos

New Tools For Viscoelastic Spectral Analysis, With Application to The Mechanics of Cells and Collagen Across Hierarchies

by

Behzad Babaei

A dissertation presented to the
Graduate School of Arts and Sciences
of Washington University in
partial fulfillment of the
requirements for the degree
of Doctor of Philosophy

August 2016
Saint Louis, Missouri

Contents

List of Figures

List of Tables

Acknowledgments

First and foremost, I have to thank my research supervisors, Prof. Guy Genin, Prof. Elliot Elson and Prof. Stavros Thomopoulos. I am grateful to have had the opportunity to have known them and to have worked under their direction. Without their assistance and support these chains of projects would have never been accomplished. Specially, I acknowledge Prof. Guy Genin's fabulous friendship and support during these fours years.

I would like to thank Dr. Tony Pryse, Prof. Steven Abramowitch and William McConnaughey for their support and guidance, and, Ali Davarian and AJ Velasquez Mao for their friendship and help. Also, all friends who made Saint Louis a great place for me.

Finally, I thank my father and mother for their love, encouragement and support during these years. Although they were far from me, I always have felt them in my heart.

Behzad Babaei

Washington University in Saint Louis

August 2016

ABSTRACT OF THE DISSERTATION

New Tools For Viscoelastic Spectral Analysis, With Application to The Mechanics of Cells and Collagen Across Hierarchies

by

Behzad Babaei

Doctor of Philosophy in Biomechanics

Washington University in St. Louis

Professor Guy M. Genin, Chair

Viscoelastic relaxation spectra are essential for predicting and interpreting the mechanical responses of materials and structures. For biological tissues, these spectra must usually be estimated from viscoelastic relaxation tests. Interpreting viscoelastic relaxation tests is challenging because the inverse problem is expensive computationally. We present here (1) an efficient algorithm and (2) a quasi-linear model that enable rapid identification of the viscoelastic relaxation spectra of both linear and nonlinear materials. We then apply these methods to develop fundamental insight into the mechanics of collagenous and fibrotic tissues.

The first algorithm, which we term the discrete spectral approach, is fast enough to yield a discrete spectrum of time constants that is sufficient to fit a measured relaxation spectrum with an accuracy insensitive to further refinement. The algorithm fits a discrete spectral generalized Maxwell (Maxwell-Wiechert) model, which is a linear viscoelastic model, to results from a stress-relaxation test. The discrete spectral approach was tested against trial data to characterize its robustness and identify its limitations and strengths. The algorithm

was then applied to identify the viscoelastic response of reconstituted collagen and engineered fibrosis tissues, revealing that cells actively adapted the ECM, and that cells relax at multiple timescales, including one that is fast compared to those of the ECM.

The second algorithm, which we term the discrete quasi-linear viscoelastic (DQLV) approach, is a spectral extension of the Fung quasi-linear viscoelastic (QLV) model, a standard tool for characterizing biological materials. The Fung QLV model provides excellent fits to most stress-relaxation data by imposing a simple form upon a material's temporal relaxation spectrum. However, model identification is challenging because the Fung QLV model's "box" shaped relaxation spectrum, predominant in biomechanics applications, because it can provide an excellent fit even when it is not a reasonable representation of a material's relaxation spectrum. The DQLV model is robust, simple, and unbiased. It is able to identify ranges of time constants over which the Fung QLV model's typical box spectrum provides an accurate representation of a particular material's temporal relaxation spectrum, and is effective at providing a fit to this model. The DQLV spectrum also reveals when other forms or discrete time constants are more suitable than a box spectrum. After validating the approach against idealized and noisy data, we applied the methods to analyze medial collateral ligament stress-relaxation and sinusoidal excitation data and identify the strengths and weaknesses of an optimal Fung QLV fit.

Taken together, the tools in this dissertation form a comprehensive approach to characterizing the mechanics of viscoelastic biological tissues, and to dissecting the micromechanical mechanisms that underlie a tissue's viscoelastic responses.

Chapter 1

Introduction

The mechanical responses of nearly all materials and structures are viscoelastic, differing to some degree based upon the rate and duration of loading [134, 54, 18, 74, 164]. Characterizing viscoelasticity is important because viscoelasticity affects the transmission, storage, and dissipation of force and energy, and because variations in viscoelastic response as a function of loading duration or frequency can provide clues about micromechanical deformation, resilience mechanisms and molecular structure. Because cells and collagen-rich extracellular matrix (ECM) show strong viscoelastic behavior at physiological loading rates [68, 141, 194, 7], viscoelasticity is a factor in almost all biological tissues and organs. Indeed, viscoelastic responses have been studied as metrics of tissue function and health of arteries [32], brain parenchyma [155], liver tissues [26], the prostate [150], skin [29], breasts [23], articular cartilage [44], ligaments [3], and tendon [49] and its attachments to bone [173].

For engineering polymers, the characterization test of choice is often rotational rheometry, which can provide information about the frequencies and timescales of loading over which a material absorbs energy most effectively. However, rotational rheometry is often unsuitable for the characterization of biological tissues because of issues of gripping, orienting, and aligning specimens [8]. Instead, other viscoelastic protocols such as relaxation tests or dynamic excitation are typically used. In biomechanics, there are two well-known models

to analyze viscoelastic response of biological materials: 1) The Maxwell spring and dashpot model. 2) The Fung' quasi-linear viscoelastic model.

The Maxwell spring and dashpot model is common in biomechanics to analyze stress-relaxation response of biological materials. The Maxwell model is composed of a linear dashpot connected in series with a linear spring. A feature of this model is that it has a single relaxation time constant, $\tau = \eta/E$. However, this does not wholly simulate the viscoelastic behavior of most materials. For this reason, the generalized Maxwell (or Maxwell-Wiechert) model with multiple springs and dashpots is commonly applied. We found that the Maxwell model could fit most experimental stress-relaxation data with 2 or 3 time constants. This can be advantageous because a fit to subsequent analogous loadings could be obtained with little effort or complexity. However, this could be disadvantageous because such fitting may provide little information relevant to the characterization of intrinsic deformation mechanisms. In the following sections we present a simple, fast, and robust algorithm for overcoming this limitation. The discrete spectral approach is an algorithm that is fast enough to yield a discrete spectrum of time constants sufficient to fit a measured relaxation spectrum with an accuracy insensitive to further refinement. The algorithm fits a discrete spectral generalized Maxwell (Maxwell-Wiechert) model to results from a stress-relaxation test. It is analogous to the inverse fast Fourier transformation (FFT), except that the algorithm dissects the time domain relaxation data into a spectrum of viscoelastic time constants, each defined as a viscous coefficient η divided by an elastic modulus E. We broadly describe this model in Chapter 2. Then, we analyze several idealized, noisy, and incomplete data sets to establish the strengths and limitations of the approach. Thereafter, the approach will be applied to study the viscoelastic relaxation of reconstituted collagen.

In Chapter 3, we study how dermal fibroblasts alters the rate-dependent mechanical properties of collagen in engineered tissue constructs viscoelastically by using discrete spectral

approach. Fibroblasts remodel their extracellular neighborhood considerably when activated, stiffening and compressing their extracellular matrix (ECM) environment [27, 138, 84, 98, 110, 114, 113, 20, 16]. During remodeling, fibroblasts secrete ECM proteins, including collagens, proteoglycans, glycoproteins, and proteases, and cross-linking proteins and enzymes [27, 138, 84, 98, 106]. Fibroblasts exert traction on the ECM and each other [16, 100, 127, 203], and secrete soluble factors that affect neighboring cells and tissues in a paracrine manner [192]. This remodeling changes the tissue as a whole by establishing a network to link and organize individual cells [185, 1, 148, 165, 189, 35]. The ways that fibroblasts remodel their environment is central to wound healing, development of musculoskeletal tissues, and progression of pathologies such as fibrosis. However, the changes that fibroblasts make to the material around them and the mechanical consequences of these changes have proven difficult to quantify, especially in a realistic, viscoelastic three dimensional culture environments, leaving a critical need for quantitative data. Here, we observed the mechanisms and quantified the mechanical effects of fibroblast remodeling in engineered tissue constructs (ETCs) comprised of reconstituted rat tail (type I) collagen and human fibroblast cells. To study the effects of remodeling on tissue mechanics, stress-relaxation tests were performed on ETCs cultured for 24, 48, and 72 hours.

The Fung quasi-linear viscoelastic (QLV) model is a standard tool for representing the nonlinear history- and time- dependent soft tissue viscoelasticity of biological tissues [55, 33, 188, 2]. Based on the quasi-linear theory [56], the time-dependent response and elastic response of a viscoelastic material are separable, where nonlinearity is due to only the elastic nature of materials. Unfortunately, this model is not able to present unique time-dependent spectra for hysteresis at different strain-levels. Also, the QLV approach estimates a constant loss modulus over a wide range of frequencies,that is, the hysteresis of a quasi-linear viscoelastic materials is *not* frequency-dependent [56]. This contradicts many experiments [72, 107, 6, 79].

We present a simple model to overcome QLV model's challenges and termed it discrete quasi-linear viscoelastic (DQLV). The core of the technique is a finite series that, under special conditions, reduces to Fung's box spectrum relaxation function. We show that application of our DQLV model is a simple and effective way to identify material relaxation spectra in an unbiased manner from stress-relaxation data. The approach identifies ranges of time constants over which Fung's continuous box relaxation spectrum is appropriate, and is effective at fitting this box relaxation spectrum. It also identifies when discrete time constants are more appropriate than the box relaxation spectrum for representing damping responses. After presenting the DQLV model, we apply it to correctly identify spectra at particular strain levels from simple relaxation tests, and then demonstrate its utility on determining the quasi-viscoelastic response of the rabbit medial collateral ligament (MCL).

The time- and frequency-dependent properties of connective tissue define their physiological function, but are notoriously difficult to characterize. Well-established tools such as linear viscoelasticity and the Fung quasi-linear viscoelastic (QLV) model impose certain forms on responses that can mask true tissue behavior. In chapter 5, we present a more general discrete quasi-linear viscoelastic (DQLV) model to identify the static and dynamic time- and frequency-dependent behavior of rabbit medial collateral ligaments. Results of this study may suggest a mechanistic basis for the "stretching" regimens most favored by athletic trainers. Stretching is commonly performed by athletes for the purpose of optimizing body performance, but the mechanisms, optimal conditions, and efficacy of stretching are a source of debate. Stretching has been shown to enhance range of motion [120], but to either decrease or not affect peak athletic performance [118, 19]. The time period and character (ramped, ballistic, sustained) of the stretch appears to be a key determinant of efficacy, with ballistic stretching apparently less effecive than lower frequency dynamic stretching [77, 136, 179, 19]. The mechanisms underlying these effects are hypothesized to be some combination of connective tissue inelasticity, paracrine effects, and neural effects, the latter mediated by the

Golgi tendon organ and the muscle spindle stretch receptor, and somewhat less long-lasting in effect [34, 19].

The dissertation concludes in Chapter 6 with some reflections on the limitations and strengths of the work, and thoughts for future directions.

Chapter 2

Efficient and optimized identification of generalized Maxwell viscoelastic relaxation spectra

2.1 Introduction and background

The Maxwell model (Fig. 5.1(a)) is composed of a linear dashpot connected in series with a linear spring. A feature of this model is that it has a single relaxation time constant, $\tau = \eta/E$. However, this does not wholly simulate the viscoelastic behavior of most materials. For this reason, the generalized Maxwell (or Maxwell-Wiechert) model with multiple springs and dashpots is commonly applied (Fig. 5.1(b)). This model is composed of a spring of elastic modulus E_0 in parallel with M Maxwell elements, with the i^{th} Maxwell element having time constant τ_i and a spring of elastic modulus E_i. Since the components of the generalized Maxwell model are connected in parallel, all branches have the same strain $\epsilon(t)$ at all times t, and the overall stress of the system is the sum of the stresses in each branch. The response of a fully relaxed generalized Maxwell material to a strain history ϵ(t) is typically studied following convolution integral:

$$\sigma(t) = s_0 + \sum_{i=1}^{M} s_i(t) = \int_0^t \left(E_0 + \sum_{i=1}^{M} E_i e^{-(t-u)/\tau_i} \right) \dot{\epsilon} du \tag{2.1.1}$$

where $\sigma(t)$ is the generalized Maxwell prediction of the overall stress in a material sample, M is the number of Maxwell branches, s_0 is stress in the single spring and $s_i(t)$ is the stress within the ith Maxwell element.

When calibrating the generalized Maxwell model to a particular material, the objective is to find the strain-independent material properties E_i and τ_i and number of branches M.

Although Eq. (2.1.1) is particularly simple when the $\epsilon(t)$ represents a stepwise change in strain, approximating such a strain course experimentally is fraught with difficulty because inertial effects can cause overshoot in the loading frame and wave motion in the specimen that can in turn cause substantial error in parameter fitting [124]. Instead, strain is typically increased at some constant rate $\dot{\epsilon}$ over a time interval $0 \leq t \leq t_p$, and then held over the time interval $t_p \leq t \leq t_f$ (Fig. 5.1(c)). At discrete times t_j, the predicted stress response is (Fig. 5.1(d)):

$$\sigma(t_j) = \begin{cases} E_0 \dot{\epsilon} t_j + \sum_{i=1}^{M} E_i \tau_i \dot{\epsilon} \left(1 - \mathrm{e}^{-t_j/\tau_i}\right) & j = 1, 2, \ldots, p \\ E_0 \dot{\epsilon} t_p + \sum_{i=1}^{M} E_i \tau_i \dot{\epsilon} \left(1 - \mathrm{e}^{-t_p/\tau_i}\right) \left(\mathrm{e}^{-(t_j - t_p)/\tau_i}\right) & j = p, p+1, \ldots, f \end{cases} \tag{2.1.2}$$

where p and f are the number of data points in ramp and relaxation intervals, respectively. Note that the response to a very fast ramp ($t_p \to 0, \dot{\epsilon} \to \infty$) to a defined strain level ϵ_p has the simple form:

$$\sigma(t_j) = \left(E_0 + \sum_{i=1}^{M} E_i \mathrm{e}^{-t_j/\tau_i} \right) \epsilon_p \qquad j = 1, 2, \ldots, f \tag{2.1.3}$$

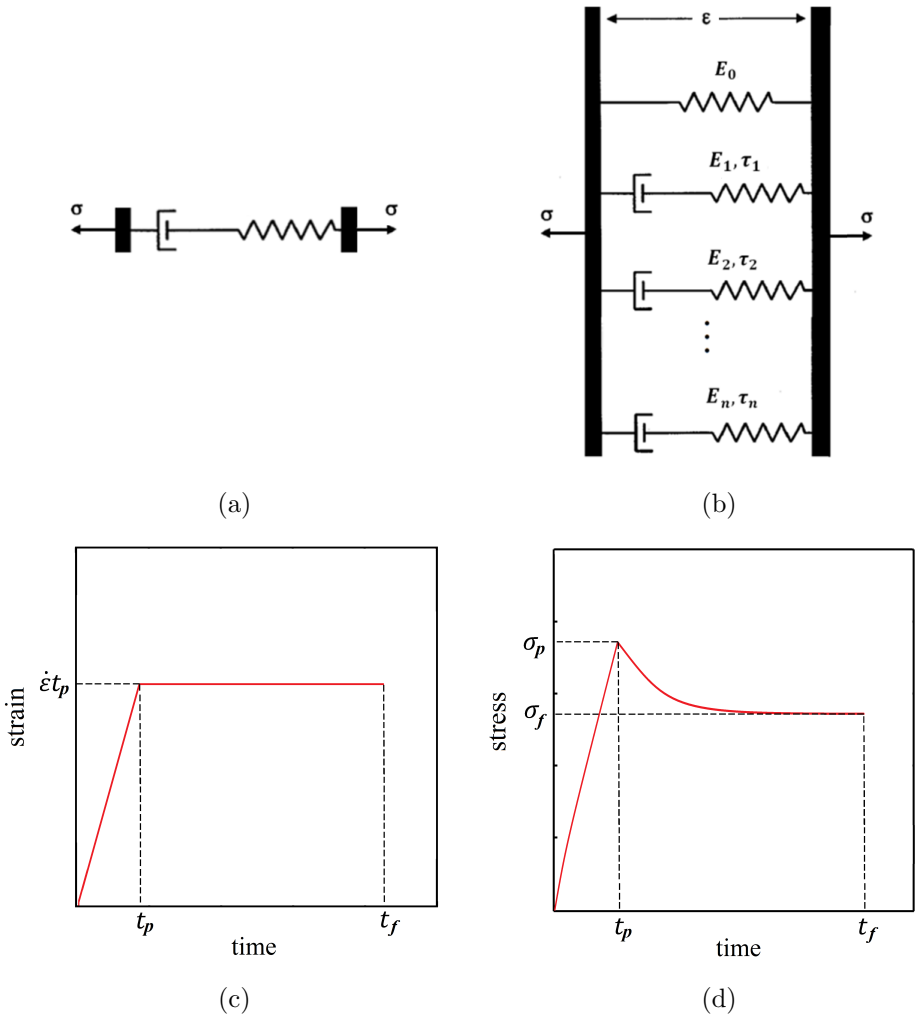

Figure 2.1: Schematics of the Maxwell model (a) and generalized Maxwell model (b). The strain profile of a stress-relaxation test showing a linear ramp to an isometric value of strain (c), and the associated stress response, showing a peak at the end of the ramp and a relaxation to a strain-dependent steady state.

where the substitution $t = \epsilon/\dot{\epsilon}$ was made into Eq. (5.2.3), and $\lim_{\dot{\epsilon}\to\infty} \dot{\epsilon}\left(1 - e^{-\epsilon/\dot{\epsilon}\tau_i}\right) = \epsilon/\tau_i$ was used.

2.2 Methods

2.2.1 Fitting of generalized Maxwell data

Two classes of approaches were used to fit a generalized Maxwell model to stress data $\bar{\sigma}(t_j)$ recorded at discrete times t_j as a material responds to a straining history $\epsilon(t_j)$: an *ad hoc* approach and a discrete spectral approach. We present here both approaches.

***ad hoc* approach**

The first approach was a simple and widely used *ad hoc* approach, requiring an *ad hoc* function to compute E_i and τ_i. Thus, the number M of Maxwell elements was guessed in advance, and the time constants τ_i and associated values of E_i were unknown. The values of τ_i and E_i could be estimated by minimizing the least squares error to fit a set of f observations with a relation for $2M$ unknown parameters ($f > 2M$). The approach started with a vector of initial guesses for E_i and τ_i and refined the estimates iteratively by minimizing the mean squared error:

$$MSE = \frac{1}{f}\sum_{j=1}^{f}\left(s_0 + \sum_{i=1}^{M} s_i(t) - \bar{\sigma}(t_j)\right)^2 \tag{2.2.1}$$

where s_0 and $s_i(t)$ were defined in Eq. (2.1.1) and $\bar{\sigma}(t)$ is the recorded stress history. We found that the *ad hoc* approach could fit most experimental stress-relaxation data with M=2 or 3. This can be advantageous because a fit to subsequent analogous loadings could be obtained with little effort or complexity. However, this could be disadvantageous because such fitting may provide little information relevant to the characterization of intrinsic deformation mechanisms. Further, if one analyzes a single set of experimental data with three different arbitrary exponential terms, e.g. M=1, 2 or 3, the results of these analyses are not comparable easily: the derived parameters such as τ_i and E_i are usually affected by the arbitrarily

chosen M. In the following sections we present a simple, fast, and robust algorithm for overcoming this limitation.

Discrete spectral approach

In the second approach, the time constants τ_i of Maxwell elements were chosen in advance, with τ_i spaced sufficiently closely to be approximately continuous on a logarithmic scale. For analysis of collagen, on the order of M= 1000-10000 time constants were distributed equidistantly in logarithmic space over an interval of 10^{-3} to 10^{5} s, an interval broader than any previously reported time constants of biological materials. The corresponding values of E_i were determined by fitting a generalized Maxwell model to relaxation data $\bar{\sigma}(t_j)$.

The problem of determining a low-rank solution is ill-posed. A range of methods exist for this problem, but they are relatively slow and are thus difficult to optimize [139, 163, 76]. Our contribution is a relatively fast algorithm that enables a well converged (although not necessarily optimal) approximation to experimental data. We converted (5.2.3) to a system of linear equations in matrix form that could be solved rapidly as:

$$\begin{bmatrix} \sigma_1 \\ \vdots \\ \sigma_p \\ \sigma_p \\ \vdots \\ \sigma_f \end{bmatrix} = \begin{cases} \begin{bmatrix} \dot{\epsilon}t_1 & a_{11} \dots & a_{M1} \\ \vdots & \vdots & \vdots \\ \dot{\epsilon}t_p & a_{1p} \dots & a_{Mp} \end{bmatrix} \begin{bmatrix} E_0 \\ E_1 \\ \vdots \\ E_M \end{bmatrix} \\ \begin{bmatrix} \dot{\epsilon}t_p & b_{1p} \dots & b_{Mp} \\ \vdots & \vdots & \vdots \\ \dot{\epsilon}t_p & b_{1f} \dots & b_{Mf} \end{bmatrix} \begin{bmatrix} E_0 \\ E_1 \\ \vdots \\ E_M \end{bmatrix} \end{cases} \tag{2.2.2}$$

where $a_{ij} = \tau_i \dot{\epsilon} \left(1 - \mathrm{e}^{-t_j/\tau_i}\right)$ for $i = 1, 2, \ldots, M$ and for $j = 1, 2, \ldots, p$; and $b_{ij} = \tau_i \dot{\epsilon} \left(1 - \mathrm{e}^{-t_p/\tau_i}\right) \mathrm{e}^{-(t_j - t_p)/\tau_i}$ for $i = 1, 2, \ldots, M$ and for $j = p, p+1, \ldots, f$.

The matrix form of (5.2.4) was written:

$$\begin{bmatrix} \sigma_1 \\ \vdots \\ \sigma_f \end{bmatrix} = \left\{ \begin{bmatrix} \epsilon_p & c_{11} \ldots & c_{M1} \\ \vdots & \vdots & \vdots \\ \epsilon_p & c_{1f} \ldots & c_{Mf} \end{bmatrix} \right. \begin{bmatrix} E_0 \\ E_1 \\ \vdots \\ E_M \end{bmatrix} \tag{2.2.3}$$

where $c_{ij} = \epsilon_p e^{-t_i/\tau_j}$ for $i = 1, 2, \ldots, M$ & $j = 1, 2, \ldots, p$.

A non-negative least squares regression [95, 21] was used to determine the values E_i from the stress-relaxation data. For a large dataset, corresponding to a large-scale matrix, solving the above equations was computationally expensive. Our approach was to use a singular value decomposition method [38, 87] to decrease the rank of the matrices and speed up the solution procedure. The procedure was repeated with increasingly large numbers M of Maxwell elements to ensure that approximations converged to those that would arise from infinitely large matrices. For all cases studied, spectra estimated using $M = 1000$ did not differ from those estimated using $M = 10000$. We therefore used $M = 1000$, and the algorithm calculated dominant time constants and moduli of relaxation data sets precisely, without needing to guess the requisite number of time constants in advance.

Convergence was achieved in 6.4 s when the algorithm was implemented in uncompiled Matlab (The Mathworks, Natick, MA) on a laptop running with an Intel Core i7-4710 CPU at 2.50 GHz and 8 GB of RAM for f=25,000 data points and M=1000 time constants.

2.2.2 Calibration

Fitting to idealized and incomplete data

Simulated stress-relaxation data were generated using the generalized Maxwell model and a strain history involving a ramp to 10% strain at a constant rate of 100%/s, followed by 500 s with the strain level held constant at the fixed level of 10%. The generalized Maxwell model had $M = 3$ Maxwell elements in parallel with a linear spring. The elastic modulus of the parallel spring was $E_0 = 100$ MPa; the time constants of Maxwell branches were $\{\tau_1, \tau_2, \tau_3\}$ = {1 s, 10 s, 100 s}; the elastic moduli of the springs within the Maxwell branches were $\{E_1, E_2, E_3\}$ = {18 MPa, 25 MPa, 9 MPa}. Data were generated at 50 data points per second.

Several permutations were studied, including fitting the generated data with a generalized Maxwell model having M=1, 2, 3 and 4 time constants, and fitting of truncated datasets. The latter studies aimed to assess the robustness of the procedure when data are acquired over time intervals that are not long compared to the longest time constant.

Sensitivity to noise

To study the stability of both *ad hoc* and discrete spectral fittings with respect to noise, random noise was added to the simulated stress-relaxation data. We superimposed upon the data noise chosen from the Gaussian distribution with amplitudes of 0%, 1%, 2%, 3% and 4% of the steady state stress. These noise amplitudes were in the range of experimental levels of noise. In this way, 50 noisy data sets were generated (10 sets for each noise percentage). For these new data sets, the time constants of the system were estimated. The sensitivity

to noise level was then quantified by relative error of the predicted parameters compared to the underlying input ones.

2.2.3 Estimation of the viscoelastic relaxation spectrum of reconstituted collagen

Viscoelastic relaxation spectra of reconstituted collagen gels were estimated from the data of Pryse et al.[141] using both the *ad hoc* and discrete spectral approaches. Briefly, type I rat tail collagen (Upstate Biotechnologies), was diluted to 2.5 mg/ml in Dulbecco's Modified Eagle Medium (DMEM) brought to pH 7 with sodium hydroxide. One milliliter of the collagen solution was pipetted into Teflon casting molds composed of an outer cylinder and an inner mandrel, and centrifuged gently and incubated at 37 °C to form ring-shaped specimens of 9.5 mm inner diameter, 2 mm thickness, and 10 mm height. Specimens were kept in molds at 37 °C for 15-18 hours before force measurements were performed. Ring gel specimens were then removed from the casting mold and mounted on a loading frame. Specimens were stretched to a strain of 6.7% in 20 ms and held isometrically while the force was monitored for 30 min at 5 Hz.

2.3 Results and Discussion

Because the generalized Maxwell model only approximates dominant elastic moduli and time constants of a real material, validation of the fitting method began with application to a fictional material whose mechanical response followed the generalized Maxwell model exactly. In this way, we checked the reproducibility of the approximations to further understand how

the approximations deviate from the optimum. Then, viscoelastic response of collagen gel [141] was reinterpreted by using the discrete spectral approach.

2.3.1 Characterization of relaxation spectra from idealized generalized Maxwell data

Ad hoc analysis

We began by evaluating what happens when data generated via the generalized Maxwell model with M=3 were interpreted using the *ad hoc* approach with M=1, 2, 3, or 4. When data from a model with M=3 Maxwell elements were fitted using a generalized Maxwell model with M=1 elements (i.e., a system including a spring and dashpot in series, in parallel with a single spring), the longest relaxation was estimated while two fast relaxation time constants were missed (Fig. 5.2(b)). The data were fitted based on their weights (with MSE regression); thus, the model estimated the time constants which had the highest weight in the data, which is τ=100 s. Correspondingly, the fitting (Fig. 5.2(a)) was good for longer times, but noticeably poor at shorter times. Different weighting functions could be applied to change this, but optimization based upon approach always captured the longest time constants.

For M=2, the two longer time constants were well estimated (Fig. 5.2(c)-(d)), and the fit to the data was much improved. For M=3 all three time constants were identified correctly (Fig. 5.2(e)-(f)).

When the process was repeated for M=4, in which the number of the viscoelastic terms was overestimated, a counterfeit peak appeared with a relatively small amplitude in the vicinity of the fastest time constant of the material's viscoelastic relaxation (Figs. 5.2(g)-(h)). This

small counterfeit peak disrupted estimation of the fastest time constant. With a sufficiently tight convergence criterion and no experimental noise, this peak would presumably disappear with a well-tailored algorithm and sufficient iteration. However, the peak was sustained to convergence criteria far tighter than are practical with experimental data. In each case, the value of R^2 for the fitting was very close to 1, even for the case of a fitting with M=1 (Table 2.1). We noted that the MSE of the fittings was a far more sensitive metric of goodness of fit and applied it in all subsequent analyses (Table 2.1).

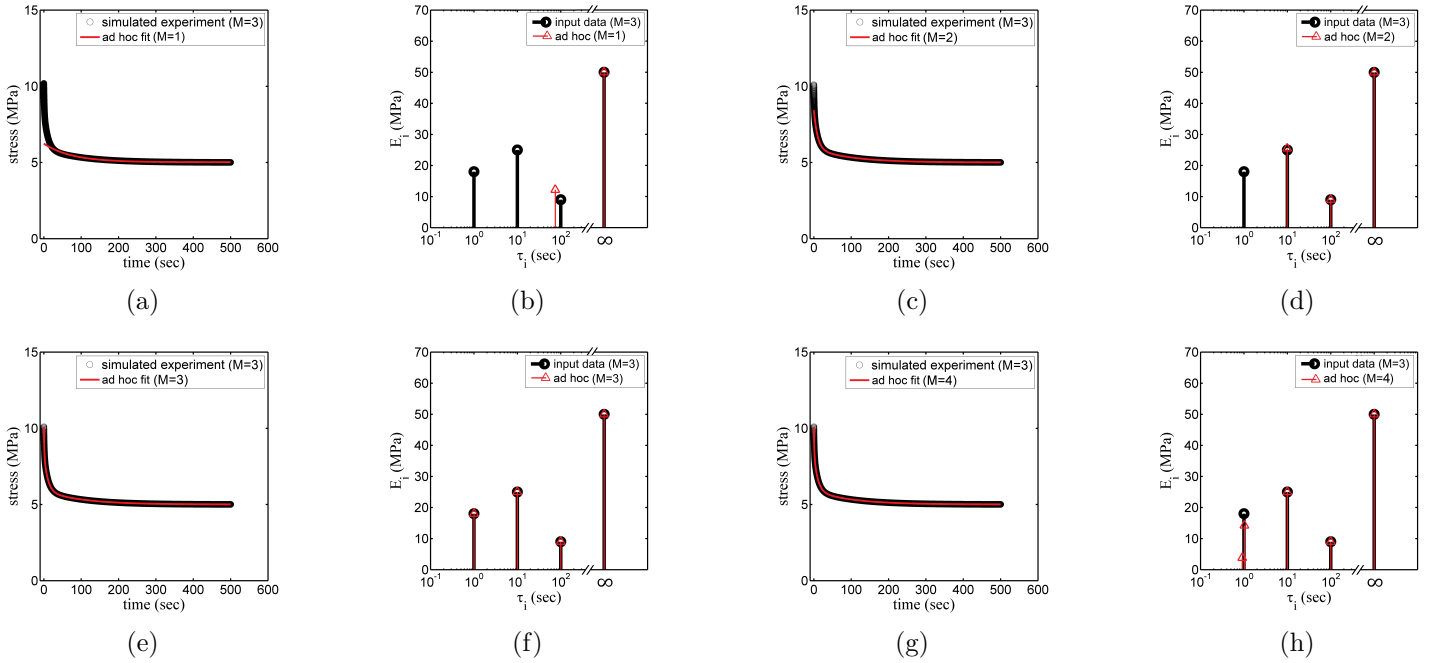

Figure 2.2: Stress relaxation data for an idealized generalized Maxwell material with M=3 time constants, fit with M=1 ((a) and (e)), M=2 ((b) and (f)), M=3 ((c) and (g)), and M=4 ((d) and (h)) time constants.

Table 2.1: Both the *ad hoc* and discrete spectral approaches were used to fit simulated, noise-free stress-relaxation data generated using M=3 Maxwell branches. R^2 and mean squared error (MSE) for each fitting were calculated. The results for M=1, 2, 3, and 4 correspond to Fig. 5.2 (*ad hoc* approach) while the results for M=1000 correspond to Fig. 5.3 (discrete spectral approach). The approaches required comparable CPU time (f=25000 data points, 1000 iterations).

M	1	2	3	4	1000
R^2	0.9957	0.9999	0.9999	0.9999	0.9999
MSE	0.6×10^{-2}	3.7×10^{-3}	1.6×10^{-9}	2.1×10^{-9}	1.8×10^{-9}
CPU time (s)	7.0	6.1	3.7	5.6	6.4

Discrete spectral analysis

With a sufficiently large number M of fixed time constants in the discrete spectrum, the number, elastic moduli, and time constants of Maxwell branches were well predicted using discrete spectral analysis (Fig. 5.3). Counterfeit peaks did not arise in the discrete spectrum as they did in the *ad hoc* spectrum.

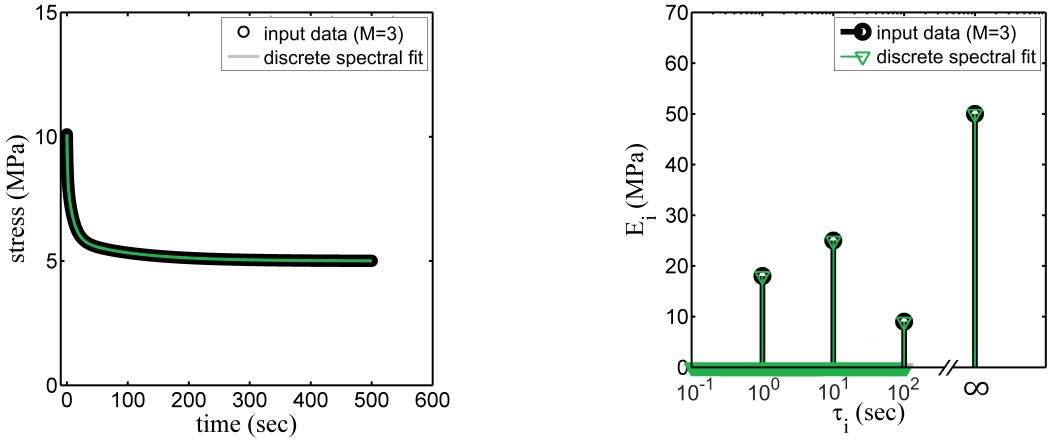

(a) (b)

Figure 2.3: Stress relaxation data for an idealized generalized Maxwell material with M=3 time constants, fit using the discrete spectral approach with 1000 time constants distributed equidistantly in log space over the interval $10^{-1}s \leq \tau \leq 10^{3}s$.

Effects of noise

Random noise added to the stress-relaxation data affected estimation time constants that were not long compared to the frequency of the noise. The effect increased with the amplitude of noise added (Fig. 5.4). Although estimates of the time constants were affected, the noise did not introduce new, artifactual time constants into the viscoelastic relaxation spectrum.

To study the effect of noise estimates derived using the *ad hoc* approach, a best case scenario was assumed in which the correct number of Maxwell branches ($M = 3$) was known in advance. In this best-case scenario, the fastest time constant of the system,τ_1, for 4% noise, was estimated with less than 8% error, while the other time constants were estimated with less than 1.5% error. For comparison, the time constants were estimated correctly to within floating point precision for the ideal case of no noise. The errors associated with interpreting these data using the discrete spectral approach were smaller still (Fig. 5.4). For 4% noise, the fastest time constant was estimated with less than 4% error while the other time constants were estimated with less than 2% error. These results suggest that for the interpretation of noisy data from a generalized Maxwell material, the discrete spectral approach is at least as accurate as the *ad hoc* approach, and has the additional advantages of being fast computationally and of avoiding the need to guess the number M of time constants *a priori*.

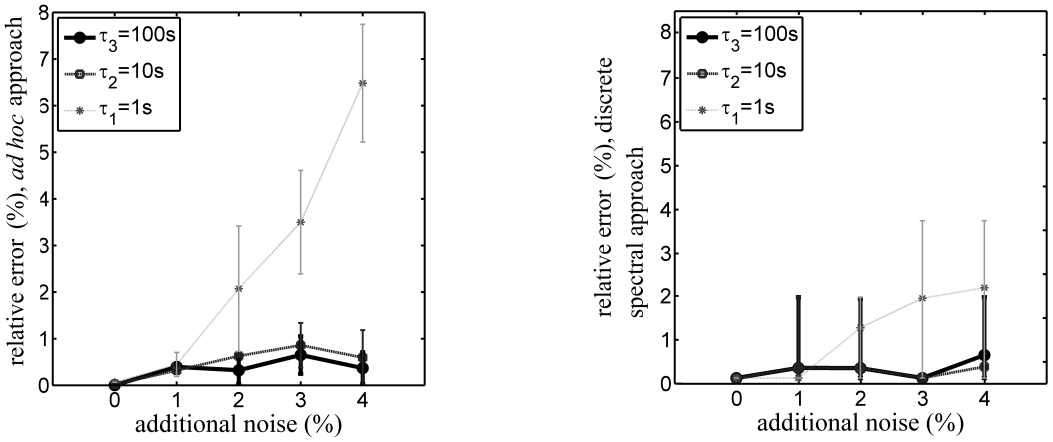

(a) (b)

Figure 2.4: 50 sets of Gaussian noise were generated (10 sets for each of 5 noise amplitudes) and added to ideal simulated stress-relaxation data. The simulated noisy stress relaxation data were then analyzed using the (a) *ad hoc* and (b) discrete spectral approaches.

2.3.2 Interpretation of incomplete relaxation data

With the efficacy of the discrete spectral approach established, we evaluated its performance against incomplete data. This is useful because biological systems often preclude the possibility of holding a specimen sufficiently long for complete relaxation to occur. For example, in biological tissue constructs consisting of living cells in a reconstituted collagen matrix, relaxation has been shown to persist to times sufficient for cellular remodeling to occur [97]; in such a case, the tissue construct as a whole becomes a different material before relaxation is complete, and only partial data can be used.

For the stress relaxation data studied in Fig. 5.2, the first test involved analyzing the first 50 s of stress relaxation data (Fig. 5.5(a)), a time interval that is only 50% of the slowest finite viscoelastic time constant in the input data. The interpretation of the spectrum succeeded in identifying the three time constants and the infinite time constant (Fig. 5.5(b)). The first, second and infinite time constants had accurate positions, but the third time constant

estimation deviated about 7% from input time constant. When 100 s of the stress relaxation data were studied (Fig. 5.5(c)), a time interval equal to the longest time constant of the input data, the interpretation succeeded in capturing the first two fast time constants (Fig. 5.5(d)), but the interpretation again captured the third peak with about 7% error. With 200 s of stress-relaxation data, the interpretation succeeded in capturing the peaks at the all three time constants and also the correct amplitude of the infinite time constant (Fig. 5.5(e)-(f)). Here, we considered an estimate of the time constant with less than 2% error as successful.

The guidelines demonstrated in this simple test are that a predicted time constant can be trusted as being represented in the actual spectrum of a tested material if it is infinite or if it is less than half the duration of the viscoelastic relaxation data. Error was on the order of 10% or less for a time constant that is twice the duration of the viscoelastic relaxation data.

2.3.3 The viscoelastic relaxation response of reconstituted collagen

We reinterpreted the experimental data studied by Pryse et al.[141] using the *ad hoc* and discrete spectral approaches (Figs. 5.6, columns 1 and 2, receptively). For the fitting of these data collagen gel data, the highest absolute error was associated with the *ad hoc* approach, but the mean errors were comparable (Fig. 5.6(e)-(f)).

Consistent with the analyses of Pryse et al. [141], *ad hoc* analysis estimated that collagen gel has three relaxation mechanisms that manifest themselves as viscoelastic relaxation time constants of 4.6 s, 30.6 s and 1250 s (Fig. 5.6(c)). However, the discrete spectral approach revealed a region with relatively fast time constants (Fig. 5.6(d)). The studies described in the previous sections suggest that these time constants are not artifacts arising from noise or from the duration of the test. The spectrum suggested six main relaxation time constants of about 0.3 s, 0.7 s, 2.6 s, 16.1 s, 72.7 s, and 1520 s (Fig. 5.6(d)). Because the time constants found were either infinite or less than twice the 1800 s duration of the isometric stretch, they can be expected to have an error of less than 10%. In addition to being consistent with the analysis of Pryse et al.[141], they are further consistent with some of the slower time constants identified by Gupta et al.[70] and Xu et al.[194]. The faster time constants might have been absent in the work of Gupta et al.[70] because their study was of tendons rather than of reconstituted collagen. Alternatively, it is possible that, either because their approach was analogous to the *ad hoc* approach or because that study used a data acquisition rate whose inverse was slow compared to the fastest time constants observed here, they were able to obtain an excellent fit in the absence of the contributions of faster time constants. The slowest time constant of 1500 s was not present in the work of Gupta et al.[70], possibly reflecting once more a difference between collagen within reconstituted tissues and collagen within the fibers and fibrils of a tendon.

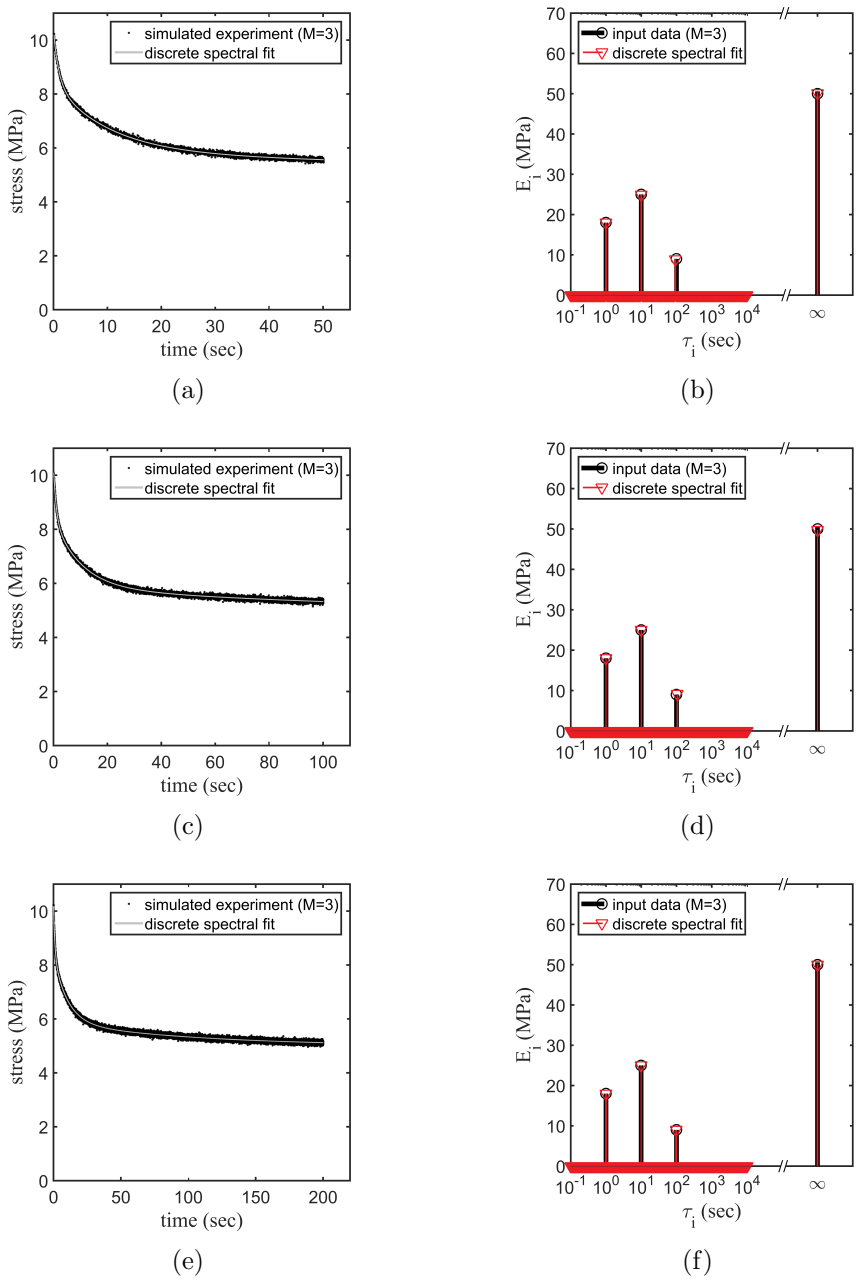

Figure 2.5: Discrete spectral analyses of noisy data following 50 s ((a) and (b)), 100 s ((c) and (d)), or 200 s ((e) and (f)) of relaxation.

2.3.4 Prospects for application to collagenous tissues

A central theme of this study is the potential of a viscoelastic spectrum as a tool for assessing the health and function of a biological tissue. We envision that this potential will be strong for assessing pathologies such as hypertrophic cardiomyopathy, in which relaxation is central to the progression of pathology [12]. However, several important factors need to be considered when extending our application of the method to living tissues, especially collagenous tissues such as tendon. First, viscoelastic time constants of collagenous tissues are well known to depend upon the degree of hydration of the tissue. This is known from studies at the molecular [59], fibril [158], and tissue [180] levels, for both unmineralized and mineralized tissues [104]. Therefore, the viscoelastic spectra estimated by our approaches will likely be sensitive to the nature of the medium in which tendons are tested.

Second, such tissues are highly nonlinear and anisotropic. Although these two material factors are well understood from the perspective of linear elasticity, the nature of the viscoelastic nonlinearity and anisotropy is not yet certain [144, 167, 130]. While we expect that the tools presented in this article will be of value in defining these effects, we note that characterization and comparison of viscoelastic spectra may be sensitive to the details of strain state and direction of loading.

Third, we expect viscoelastic spectra to be sensitive to the details of the composition of tissues. A key motivation for our group is understanding viscoelastic responses at interfaces between tendon and bone, where composition is known to vary in a graded fashion. Understanding such spatial variations will be complicated by the nature and media-sensitivity of glycosaminoglycans and by the spatial disposition of mineral. Although outstanding models exist for the viscoelastic responses of proteoglycan rich tissues, the extension of these to spectral representations will be a challenge.

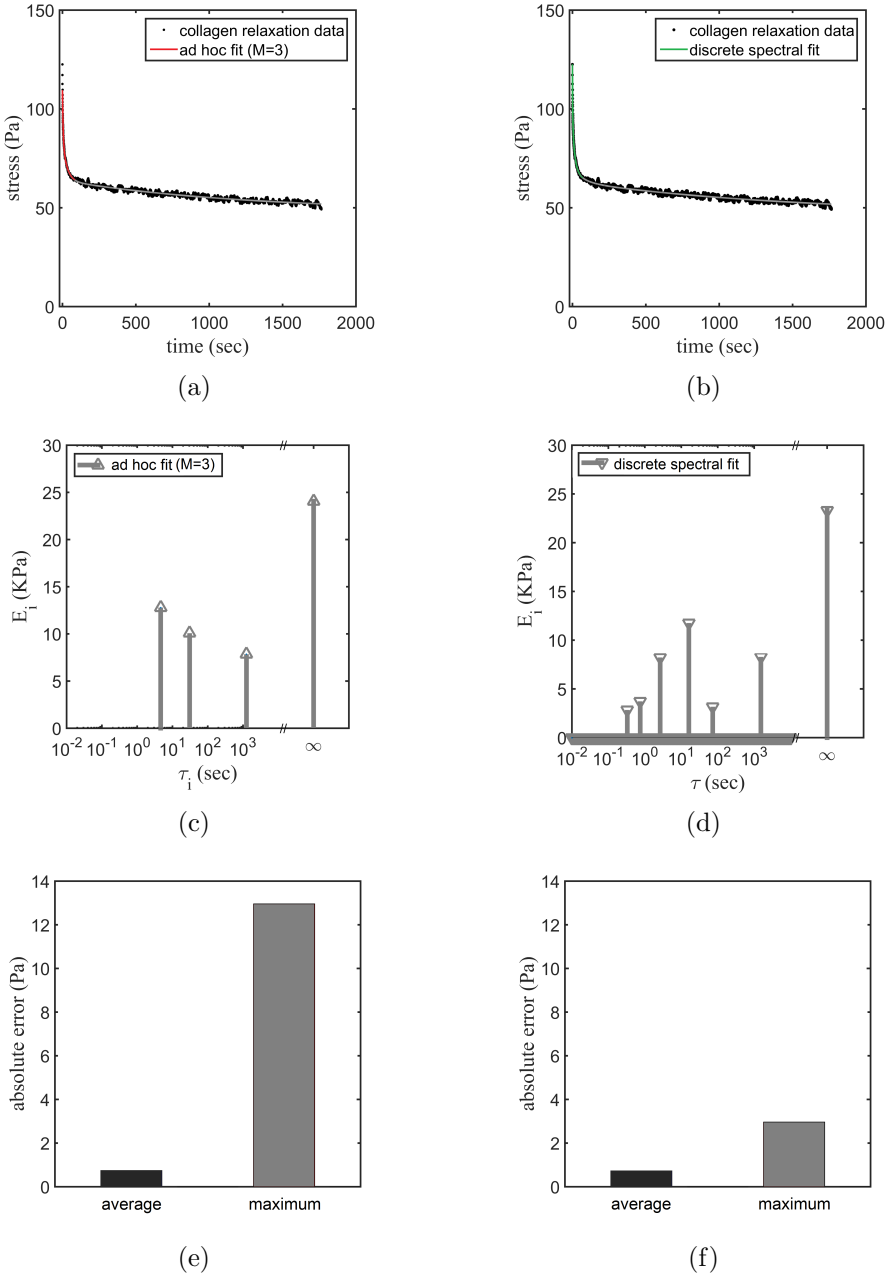

Figure 2.6: Fittings for stress-relaxation data acquired from a collagen gel stretched 20% strain under a fast strain rate (100 %/s) fitted by (a,c,e) the *ad hoc* and (b,d,f) discrete spectral approaches. (c) Three time constants were estimated at 4.63 s, 30.6 s and 1250 s using the *ad hoc* approach. Using the discrete spectral approach the spectrum shows that relaxation of the collagen has six main time constants at about 0.3 s, 0.7 s, 2.6 s, 16.1 s, 72.7 s and 1520 s.

2.4 Conclusions

We presented a fast and general discrete spectral approach to estimating viscoelastic relaxation spectra from force or stress relaxation data, and compared it to an *ad hoc* approach. When using an *ad hoc* approach with a fixed number M of variable viscoelastic time constants, the fitting process was sensitive to M: by underestimating M, faster relaxation mechanisms were missed; by overestimating M, artifactual fast time constants were introduced. These problems were not clearly evident when comparing goodness of fit using R^2, because R^2 was near 1 for all of the fittings. The precision of fittings was more distinguishable by considering MSEs.

The discrete spectral approach predicted the number of time constants and corresponding elastic moduli with very low MSE, only slightly higher than when the correct number of viscoelastic time constants was known *a priori*. The discrete spectral approach was less sensitive to noise, but for ideal data, without any noise, the *ad hoc* method was more efficient.

Application of the discrete spectral approach to reconstituted collagen gels revealed six time constants, with the slower time constants analogous to those captured by *ad hoc* analyses in the literature. As with the work of others, the discrete spectra that arise are of value in relating viscoelastic responses to micro-mechanical phenomena that occur across length scales [196, 9, 67]. Results suggest that the discrete spectral approach is a computationally efficient and informative approach to analyzing viscoelastic relaxation data.

Chapter 3

Remodeling by dermal fibroblasts alters the rate-dependent mechanical properties of collagen in engineered tissue constructs

3.1 Introduction

Although several studies have estimated the effects of this remodeling on ECM elasticity [110, 17], much less is known about the viscoelastic effects of ECM remodeling. Fibroblasts are known to affect viscoelastic tissue relaxation in pathologies such as congestive heart failure. However, these effects have not been quantified, and there is a pressing need for data on viscoelastic remodeling of tissues.

Additionally, the cells themselves change during remodeling. Cytoskeletal disposition is known to change in response to perturbations in mechanical loading [89, 80, 90]. During wound healing, cytoskeletal structure is regulated to develop force against the ECM to close

the wound [183]. Cell transformation and tumorigenicity are associated with a decrease in cell viscosity and elasticity [42]. Although well established techniques exist for estimating cell elasticity within engineered tissues [46, 110], protocols are still needed to acquire information about cell viscoelasticity.

Engineered tissue constructs (ETCs) comprised of reconstituted rat tail (type I) collagen and human dermal fibroblast cells serve as *in vitro* models of this remodeling, and provide simplified systems in which to assess how remodeling affects the mechanics of cells and ECM [92, 186]. These systems have been applied to study both linear and nonlinear elasticity of cells and ECM, but variations of time-dependent tissue mechanics by ECM remodeling has not been well characterized quantitatively.

The goal of this study was to establish the ways that fibroblast cells modulate their ECM viscoelastically and contribute to ETC-level viscoelasticity over the course of ETC remodeling. We studied these effects by performing viscoelastic relaxation tests on ETCs at three different timepoints. Following techniques that are standard for evaluation of ECM elasticity, ECM viscoelasticity was evaluated by treating ETCs with deoxycholate, a mild detergent which dissolves cell membranes and disperses cytoplasmic structures such as the cytoskeleton. Tests were interpreted using a discrete spectral generalized Maxwell approach [12], which yields both elastic moduli and viscoelastic relaxation finite time constants. Results showed that cells actively adapted the ECM, and that cells relax at multiple timescales, including one that is fast compared to those of the ECM.

3.2 Materials and methods

3.2.1 Engineered tissue construct (ETC) preparation

ETCs were synthesized using procedures described in detail elsewhere [183]. Briefly, human dermal fibroblasts (Lonza, Allendale, NJ, USA) were cultured in Dulbecco's modified Eagle's medium (DMEM, Gibco) at 37°C and 5% CO_2. The media were changed every 3-4 days and the cells were split when cell confluency reached >80% of the dish surface. The cells were used for culturing ETCs at the 7th-10th passage. 0.5 million cells were mixed with 1 ml of a solution consisting of DMEM and 0.5 mg/ml type I rat tail collagen (harvested in our laboratory). The pH of this mixture was brought to neutrality using 0.2 M NaOH. 0.5 ml of this mixture was poured into hollow, cylindrical Teflon molds; the molds contained a central rod to create an annular well with outer and inner diameters of 14.9 mm and 9.5 mm, respectively. The final mixture was incubated at 37°C with 5% CO_2 for 30 minutes to allow the collagen to polymerize. Then, the molds were filled with DMEM supplemented with 5% fetal bovine serum (FBS) and were kept in an incubator for 24, 48 or 72 hours to allow the cells to remodel the collagen. Three specimens were tested at each of the three remodeling times, a total of nine specimens.

3.2.2 Stress-relaxation testing apparatus and protocol

Stress-relaxation tests were performed on the ring-shaped ETCs. ETCs were mounted within glass organ baths filled with HEPES-buffered DMEM (pH 7.4) and 5% FBS, and kept at 37°C, conditions standard for culturing engineered tissues [64]. One end was attached to an actuator connected to a stepper motor, and the other to a force transducer, as described elsewhere [183]. Tissues were allowed one hour to accommodate to the new media before the

stress-relaxation test. The protocol started with 10 minutes of force monitoring to establish a baseline. This was followed by tissue preconditioning consisting of 5 sequential cycles of a 20% axial stretch, followed by a 30 minute recovery interval. A preconditioning protocol is standard in testing of collagenous tissues [55]. Using a strain rate analogous to that of the subsequent characterization experiments and a strain magnitude twice that used in the characterization experiments yields repeatable results in the testing of ETCs [46, 182].

In the characterization experiments, ETC rings were stretched 10% at 20%/s then held isometrically for 3600 s while force was recorded at 50 Hz. Nominal stress data were inferred from force data by dividing the force by the cross-sectional area measured for each specimen at the conclusion of the test, as described below. Note that, despite the preconditioning, the specimens likely experienced some permanent deformation over the course of the loading; by considering a transversely isotropic specimen with a Poisson ratio of 0.5 locked into its deformed configuration, the difference between the actual first Piola Kirchoff stress and that we report can be estimated to be less than 10%. The strain amplitude of 10% strain was chosen because it represents the upper end of the linear range for a tendon [73]. Achieving this over 0.5 seconds is representative of strains in response to a brisk walking cadence and to stretching by the cardiovascular system. The stretch rate and prolonged monitoring were furthermore suitable for characterizing the temporal range of physiological responses [12, 10].

3.2.3 Deoxycholate treatment

The specimens were returned to their baseline configurations and allowed to recover for 30 minutes to prepare for testing the contribution of the remodeled ECM to viscoelastic behavior of the ring constructs. For this purpose, DMEM+HEPES was replaced with 0.05% w/v deoxycholate in PBS (pH 7.4), and allowed to incubate for 60 minutes. The stretch-and-hold protocol was then repeated. Deoxycholate was chosen over inhibitors such as cytochalasin D

and latrunculin because it enables lysis of cells without altering the mechanics of the protein structure in the remaining porous ECM [184, 46].

3.2.4 Measurement of ETC dimensions

After the end of each experiment, specimens were mounted on spacers and stretched to their reference length, then fixed in 4% formaldehyde for 20 minutes at room temperature. Afterwards, specimens were cut into two equal pieces and placed within four-well plates filled with PBS. The width and thickness of each tissue were measured using Confocal microscopy (LSM 510, Zeiss). The thickness was measured near the upper and lower borders as well as in the middle of the tissue. The cross sectional area of the tissue was calculated as the mean of the three measurements. All measurements were conducted by the same person.

3.2.5 DNA quantification

We synthesized an additional 9 specimens (three each at 24, 48, and 72 hours of incubation) to estimate the final cell concentration in ETCs using a total DNA quantification assay. Right after the measurement of tissue dimensions, the constructs were centrifuged with 2 ml PBS in capped tubes. PBS was removed and, after 1 ml of lysis buffer was added, the tubes were sonicated. 30 μl of this sample was mixed with 3 ml of Hoechst solution (30 nM of Hoechst 33258 per ml of PBS) (Sigma, St. Louis, MO). The fluorescence of this mixture was read at excitation-emission of 346 nm-460 nm max, respectively. A known number of human dermal fibroblast cells was used as a calibration to estimate the number of cells in the mixtures.

3.2.6 Analysis of stress-relaxation data

The generalized Maxwell model was used to interpret the relaxation behavior of the specimens tested. We used a discrete spectral implementation described elsewhere [12], based on a large number ($n = 1000$) of exponential terms. In the discrete spectral approach, the relaxation times, τ_i, were logarithmically distributed equidistantly over a range broader than probable range of time constants of a material. The best fit elastic moduli E_i for each pre-selected τ_i were estimated by minimizing the mean squared error between the experimental data and the fitting arising from the estimated viscoelastic spectrum. We note that MSE is superior to R^2 for identifying viscoelastic relaxation spectra from relaxation spectra because even a mediocre fit can yield $R^2 \approx 1$ [12]. The spectrum arising by plotting E_i versus the pre-selected τ_i yielded an unbiased relaxation spectrum that enabled simple, graphical material identification.

3.2.7 Staining and imaging

The actin cytoskeletons of the fixed tissues were stained with rhodamine phalloidin (Sigma, St. Louis, MO) and imaged using confocal microscopy. Images were obtained with a Zeiss 510 confocal microscope using a 40x, 1.2 NA, water objective. In backscattering reflectance mode confocal microscopy, collagen fibers of ETCs can be observed directly without staining and with good axial and lateral resolution.

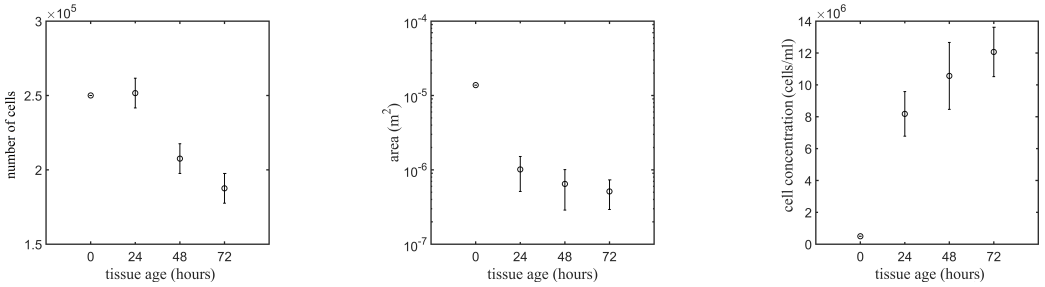

(a) (b) (c)

Figure 3.1: Development of engineered tissue constructs (ETCs) over 72 hours, including variations of their cross-sectional area, of the number of cells within them, and of the number of cells per unit volume (cell concentration). (a) The cross-sectional areas of the ETCs reduced to a minimum of $\sim 5 \times 10^{-7}$ m^2 over approximately 36 hours as the cells remodeled the collagen. (b) The cell population varied during this compaction, with the number of cells within each (initially 0.5 ml) ETC rising from 250×10^3 over the first 24 hours of observation, then decreasing to approximately 190×10^3 over 72 hours. (c) Throughout incubation, the cell concentration rose steadily. All error bars represent standard deviation.

3.3 Results

3.3.1 Remodeling of ETCs

Over three days of remodeling, cells proliferated and compressed the ETCs (Fig. 5.1a), with the initial cross-section area (thickness $\times$ width) decreasing from 13.8×10^{-6} m^2 (initial solution poured into the mold) to 1.01×10^{-6} m^2 during the first 24 hours, and to 0.51×10^{-6} m^2 after 72 hours. The starting population of 250×10^3 cells (in 0.5 ml of solution) was sustained for 24 hours, and decreased to about 190×10^3 after 72 hours (Fig. 5.1b). The initial cell concentration for all ETCs was 0.5 million cells/ml. Over 24, 48 and 72 hours of incubation, cell concentration rose to approximately $8, 10$ and 12 million cells/ml, respectively (Fig. 5.1c).

3.3.2 Mechanical responses

In response to the ramped stretch, the stress needed to maintain an ETC at its length increased to a peak value. As the ETC was held isometrically, this stress dropped over time as a result of viscoelastic relaxation (Fig. 5.2). The relaxation responses of both the control (Figs. 5.2a, 5.2c and 5.2e) and deoxycholate-treated (Figs. 5.2b, 5.2d and 5.2f) ETCs reached nearly complete equilibrium at 3600 s, and we therefore termed this the steady state.

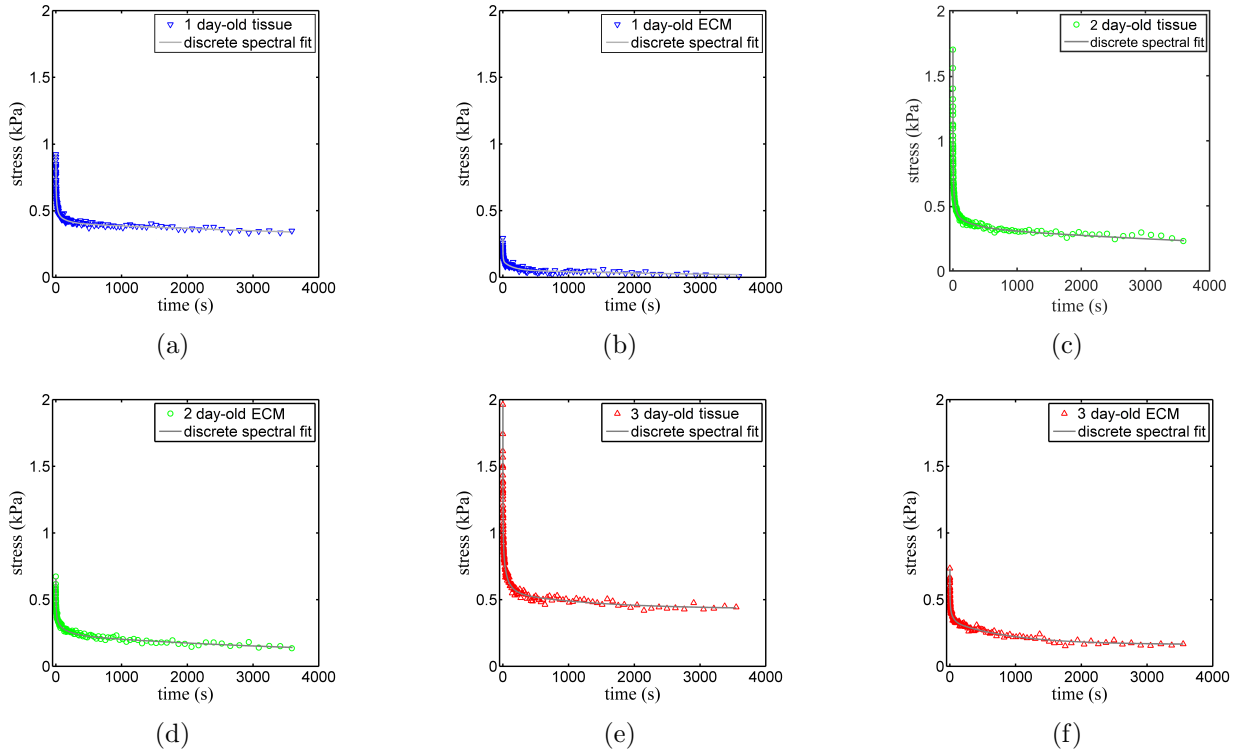

Figure 3.2: Stress relaxation curves showing the variation of stress over time in engineered tissue constructs (ETCs) that were held isometrically at 10% stretch immediately following a linear ramp to 10% stretch over 0.5 s. The isometric force required to sustain ETCs at 10% stretch relaxed viscoelastically. Left column (a, c, e): ETCs tested in nutritional medium; right column (b, d, f): ETCs tested in nutritional medium plus deoxycholate to lyse cells. Three time points were considered: 24 hours (a, b), 48 hours (c, d), and 72 hours (e, f). The data presented are representative; replicate data are presented in the supplementary document, Figures S1 (24 hours), S3 (48 hours), and S5 (72 hours).

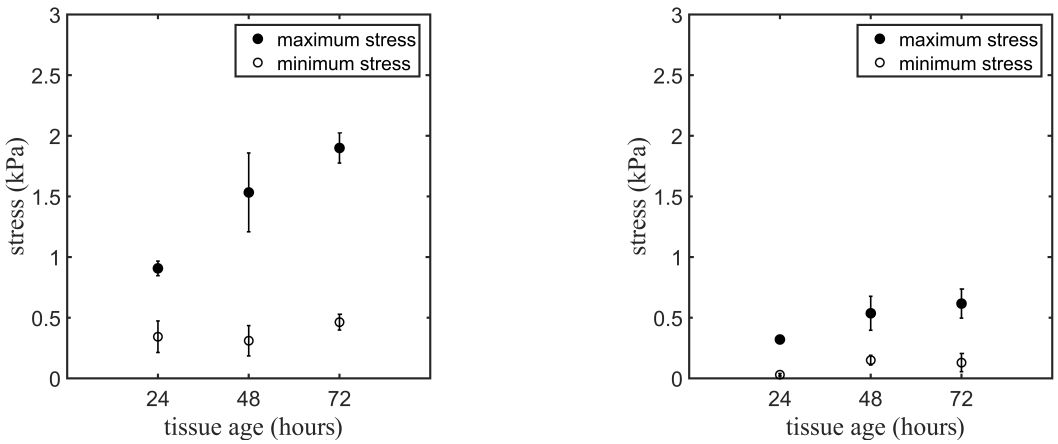

Figure 3.3: Variations of the peak stress (immediately following ramp loading, solid circles) and minimum stress (reached after 3600 s of relaxation, hollow circles) attained during stress relaxation tests on engineered tissue constructs (ETCs) that remodeled for 24, 48, or 72 hours prior to testing. (a) In ETCs tested in nutritional medium only, a statistically significant increase was observed in peak stress between 48 and 72 hours. (b) In ETCs tested following treatment with deoxycholate, a significant increase was observed in the minimum stress between 24 and 48 hours. Error bars: standard deviation. Criterion for significance: $p < 0.05$ in Student's T-test.

These stress-relaxation curves changed as the course of remodeling progressed, and were analyzed to quantify the effects of remodeling. The peak stresses attained immediately following cessation of the ramp tended to increase as the cells continued remodeling the ETCs over time for both the control and deoxycholate-treated ETCs. From the 24 to the 72 hour time points, peak stress doubled for the control ETCs (Fig. 5.3a) and more than doubled for the deoxycholate-treated ETCs (Fig. 5.3b); these trends were significant statistically ($p < 0.001$). Additionally, the peak force in the ETCs rose significantly between 24 and 48 hours, indicating that the stiffening extended beyond that associated with syneresis (Fig. S7). Treatment with dexoxycholate more than halved the peak stress in each case. The minimum stress in the deoxycholate-treated ETCs rose from the 24- to the 48-hour time point ($p < 0.05$, Fig. 5.3b).

The transition from the peak to the steady state stress was analyzed using a spectral approach that, through integration with tests involving deoxycholate, quantified the rheological responses of the cells and ECM over a range of loading time constants. The analyses demonstrated that the relaxation mechanisms of ETCs cannot be described by one simple exponential term (Fig. 5.4).

The analysis showed subtle but significant transitions in some of the viscoelastic relaxation time constants over the course of ECM remodeling, with a slower finite time constant ($\sim$ 7000 s) emerging between 24 and 48 hours of remodeling, and with some faster time constants (0.5-2 s) merging into a single time constant between 48 and 72 hours of remodeling. As discussed below, these changes were retained following deoxycholate treatment, indicating that the changes occurred in the ECM rather than in the cells. In the deoxycholate treated ETCs, with cells eliminated, the 0.2 s time constant disappeared at all time points. At 24 hours, the $\sim$ 8 s time constant disappeared with deoxycholate treatment, and at 48 and 72 hours, the 30 s time constant disappeared (Figs. 5.4b, 5.4d and 5.4f). The elastic moduli decreased for the deoxycholate treated ETCs with respect to control samples (Figs. 5.4a, 5.4c and 5.4e) at finite time constants faster than 100 s. Variance amongst the relaxation spectra was greatest for the 48-hour time point.

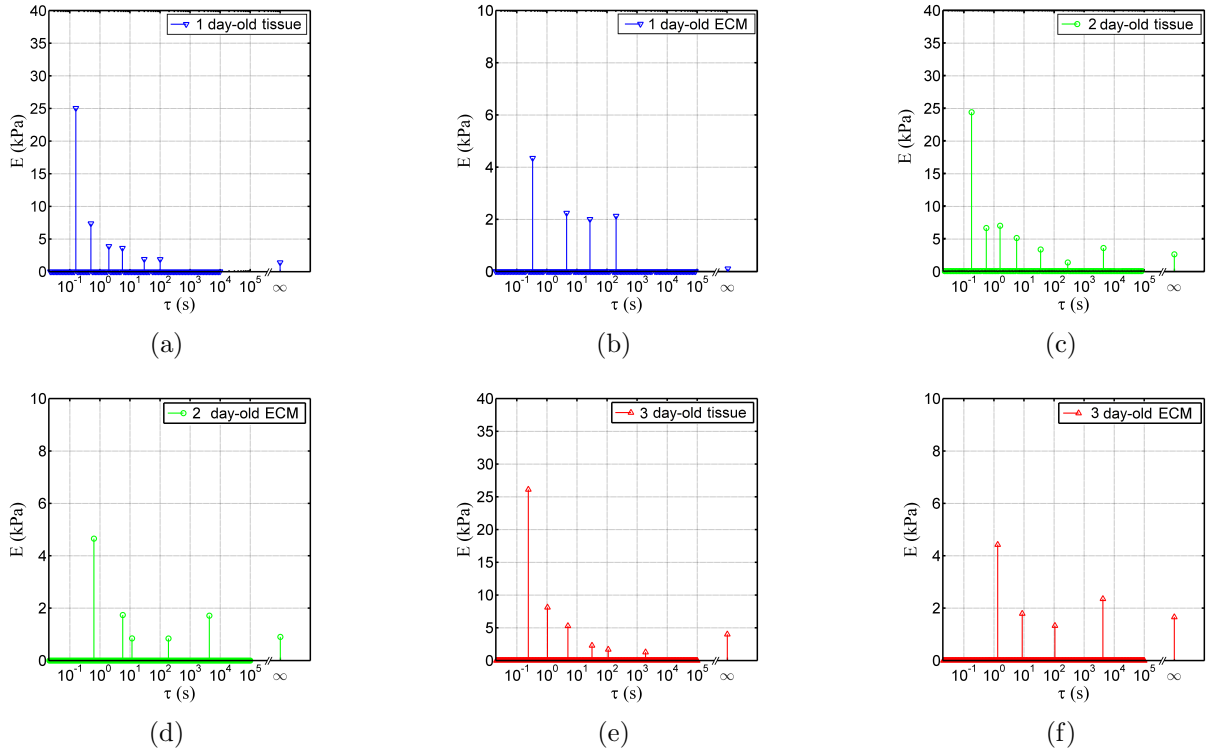

Figure 3.4: Viscoelastic relaxation spectra of ETCs tested in nutritional medium (left column, panels a, c, and e) or nutritional medium plus deoxycholate to lyse cells (right column, panels b, d, and f). Cells and ECM displayed distinguishable contributions to the ETC viscoelasticity, with the latter changing over the course of ECM remodeling. Three time points were considered: 24 hours (a, b), 48 hours (c, d), and 72 hours (e, f). The time constants of the ETCs were similar at the three different tissue ages. The exception was that during 48-72 hours of the remodeling the two time constants between 1 and 10 s merged into a single time constant at about 2 s. In the deoxycholate treated ETCs the 0.2 s and 30 s peaks were absent. Each panel corresponds to a single, representative specimen. Replicate spectra are presented in the supplementary document, Figures S2 (24 hours), S4 (48 hours), and S6 (72 hours).

Imaging of ETCs

Imaging of 24-hour-old-old ETCs showed a disordered collagen fibers (representative image, Fig. 5.5a). For 48-hour-old ETCs, a transitional state could be observed in which collagen fibers were more organized and began to exhibit a preferred orientation (representative image, Fig. 5.5b). Finally, a very compact pattern of collagen fibers appeared in 72-hour-old ETCs (representative image, Fig. 5.5c).

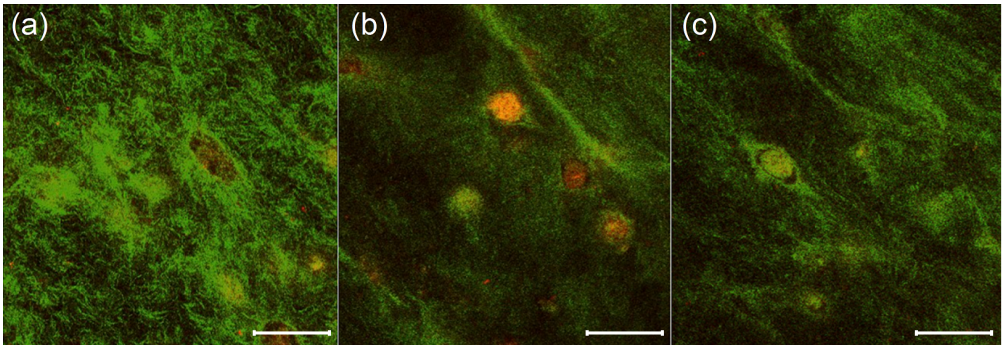

Figure 3.5: Confocal reflectance microscopy images of collagen fibers (green) superimposed upon images of cells (red) in engineered tissue constructs. Although little effect was evident in the viscoelastic time constants, remodeling corresponded to a substantial change in ECM morphology. (a) A random collagen distribution was evident at 24 hours. (b) The collagen fibers were more organized and began to exhibit a preferred orientation at 48 hours. (c) A very compact pattern of collagen fibers was observed at 72 hours. Red: cell membranes; green: signal from confocal reflectance. Scale bar, 50 μm.

This compact pattern could be found at a multitude of locations throughout the ETCs, not only close to the edges. Cells in ETCs could establish a network that linked and organized cells not only in the direction of circumferential restraint but also perpendicular to it (Fig. 5.6). The ECM contained several clusters of adjacent cells forming ring-like structures (e.g., Fig. 5.6).

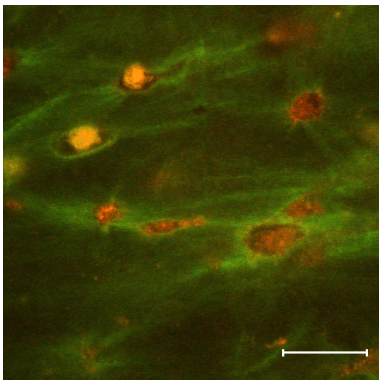

Figure 3.6: A confocal reflectance microscopy image of collagen fibers (green) superimposed upon images of cells (red) in engineered tissue constructs. During the remodeling, the cells established a connective network, with some clusters of adjacent cells forming ring-like structures. The network appeared to link and organize individual cells in the ECM. Mechanical signals sent to amongst cells over a timescale faster than the fastest time constant in these collagen bundles are not attenuated by the bundles. Scale bar, 50 μm.

3.4 Discussion

3.4.1 Cells remodeled the ECM locally

Many consequences of the interactions between cells and ECM were evident by observing the ETCs. Reflectance mode confocal microscopy, in which collagen fibers of ETCs can be observed directly without staining and with good axial and lateral resolution, showed that collagen fibers remodeled over time into a network showing elements of structural organization (Fig. 5.5). The latter typically aligned with the direction of circumferential constraint in the ring-shaped ETCs, and also connected cells or groups of cells (Fig. 5.6). Cells reduced ETC cross-sectional area as they collectively remodeled the ECM (Fig. 5.1).

Our images (Fig. 5.5 and Fig. 5.6) and data (Fig. S7, supplementary document) were consistent with previous experimental results [112, 185, 1] showing that remodeling involves more than simple syneresis. Remodeling mechanisms are believed to include increasing cross-linking of the collagen network, which helps collagen retain a compressed state and increases

collagen fibril stiffness [39, 36]. Additionally, contractility [185, 1], enzymatic activity [30], and matrix synthesis [148] play roles.

The structural aspects of remodeling are central to the mechanics of ETCs [203, 64], and are particularly important for promising new therapies to improve cardiac function after myocardial infarction through guiding scar development [75]. They are also key to understanding how myofibroblasts invade an infarct region [147, 63]. Additionally, these factors are central to healing of tendons, ligaments, and their bony attachments [65, 104, 103, 171, 172, 149, 24, 10]. In all of these, percolation phenomena involving formation of a continuous structural network are important, and variance is typically highest in conditions close to percolation [65]. Indeed, in our study, the variance in relaxation spectra was highest in samples at the 48-hour time point, when images showed the beginnings of interconnection amongst remodeled regions of ECM. Although visualizing and quantifying the underlying mesoscale effects are open challenges [128, 22], an understanding of how viscoelasticity is mediated by such changes will be an important future component of such studies.

3.4.2 ETC remodeling occurred over specific ranges of relaxation time constants

A remarkable feature of the remodeling process was that the majority of the ETC relaxation time constants were *not* altered significantly (Fig. 5.4). Many others have quantified tremendous stiffening of ECM by cells [81, 101, 109] and substantial effects on the cells themselves [45], which appear to become more compliant with ECM stiffening in 3D [112] and more compliant in 2D [161]. Stiffening is typically small in tissue constructs that begin with cell concentrations below those in our study [48, 110]. However, measurable contributions of cells to ETC mechanics are evident even at cell concentrations far below those used in the current study[88]. A number of recent studies have shown that, when cell density is sufficiently high,

cells can adapt the fibrous structure of the ECM to form connections and structures like those shown in Figs 5.5 and 5.6 [71, 1, 13, 123, 159, 185].

In the work reported here, remodeling of ETCs by fibroblasts showed a major effect on peak stresses in stress-relaxation tests (Fig. 5.2 and Fig. 5.3). In this light, the relative lack of viscoelastic effects comes as a surprise. The only exceptions were was that between 24 and 48 hours, a relatively long finite time constant emerged in both the ETCs and the ECM, and that between 48 and 72 hours of remodeling, two time constants 0.5 and 2 s merged into a single, intermediate time constant with a stronger amplitude. Because relaxation spectra are correlated to discrete structure of collagenous tissues [175, 70, 157], the merging of the two peaks indicates a decrease in the structural heterogeneity of the tissue during the remodeling process. These time constants are near those that others have been attributed to intra-fibril relaxation ($\sim 4 - 7$ s) [157, 70, 195]. One possible source of this merging of time constants is syneresis of inter-molecular water [62, 60]. Time constants in the 1s range are of particular interest for the cardiovascular system because this is associated with frequency of the heart. In fibrotic cardiomyopathy, a disease characterized by remodeling of heart tissue by activated cardiac myofibroblasts, a central pathology involves retarded diastolic filling [57, 207], possibly due in part to viscoelastic remodeling. Although the fibroblasts within the heart are believed to differ in subtle ways from those in the skin, viscoelastic remodeling in this frequency range warrants further study.

3.4.3 Specific time constants can be attributed to cells, ECM, and components of the ECM

Responses of the tissue constructs to mechanical stretching were quantified using a spectral approach that, through integration with tests involving specific inhibitors, quantified the rheological responses of the cells and extracellular matrix (ECM) over a range of loading

time constants. Through these tests, some responses of cells and remodeled ECM could be dissected. We note that the analysis techniques are robust against data that have not reached a complete steady state [12]. A time constant estimated by the discrete spectral approach can be trusted if it is infinite or if it is less than twice the duration of the viscoelastic relaxation data: error was found to be on the order of 7% for a time constant that is twice the duration of the viscoelastic relaxation data [12]. In Fig. 5.4, the slowest finite time constant was about 7000 s, which is within this trusted range.

The decrease in the minimum stress of the deoxycholate-treated with respect to non-treated (control) ETCs shows that at least a part of the time-independent (elastic) behavior of tissues, which corresponds to the single spring in the generalized Maxwell model, is due to elastic contributions of the cells. Other studies confirm that the cells have elastic (time-independent) properties [146, 82].

Because deoxycholate treatment removed cells from ETCs, comparison of control and deoxycholate-treated ETCs enabled attribution of specific time constants to cell responses and to effects of ECM remodeling (Fig. 5.4). Six peaks in the relaxation spectra of 24 and 72-hour-old ETCs demonstrate six relaxation mechanisms, while for the 48-hour-old ETCs this number increased to seven. Two of the spectral peaks disappeared following treatment with deoxycholate (those at 0.2 s and 30 s for 48 hour and older specimens; 0.2 s and 8 s for 24-hour-old specimens) indicating that these are attributable to cells or cell-ECM interactions. Although cells might be expected to exhibit different relaxation behaviors under different environmental conditions, our results for the time constants of cells are within the range reported in other studies [146, 82, 133]. Wong et al. [191] reported that the major viscoelastic components of the cell cytoskeleton are responsible for vital mechanical functions, and found a slowest time constant for a cell of 0.28 s, a number within the range of our findings. Nekouzadeh et al. [127] and Trepat et al. [176] found that very fast relaxation was associated with cytoskeletal fluidization; although they did not quantify the relaxation spectrum, we note that this is

one possible explanation for the fastest time constant we observed. We note as well that the elastic moduli decreased for deoxycholate-treated ETCs for finite time constants below 100 s (Fig. 5.4), possibly due to loss of fibroblast contractility and contributions of voids in the ECM left by the lysis of cells.

The remaining four time constants (five after 48 hours) were all associated at least in part with the ECM. These time constants include several within the range of those found by others. Pryse et al. [143] found three plus an infinite time constant (approximately 5, 40, and 600s); Xu et al. [195], who estimated a regularized, continuous spectrum, found dominant time constants between 0.3-1 s, 3-90 s and > 200 s for collagen matrices. We note that ETCs exhibited some faster relaxation time constants than did collagen matrices, likely due to the action of cells.

Much work in the literature has focused on identifying the hierarchical structural origins of the elastic (time-independent) and viscous (time-dependent) behaviors in collagenous tissues [102, 69], including work on effects of microstructural changes on the microscopic viscoelastic properties of collagen at different hierarchical levels [145, 62]. The idea is that by analyzing the stress-relaxation data, and by assuming that different time constants correspond to specific hierarchical structures, one can gain insight into hierarchical contributions and distinguish different materials [131, 137, 41]; the elastic modulus at each time constant of the relaxation spectrum reflects the contribution of that time constant to ETC relaxation. Potential sources of viscous relaxation exist across collagen's hierarchical organization [62, 160]: triple-helix collagen molecules; cross-linked fibrils a few hundred nm in diameter assembled from these molecules in a roughly triclinic lattice, and infiltrated by water and non-collagenous proteins; and cross-linked fibers assembled from these fibrils.

The work of Gupta et al. [70] and Shen et al. [158] identify the 7-10 and 100-110 s time constants as being associated with intra-fibril relaxation, and 2 and 33 s time constants as being

associated with inter-fiber relaxation. Gupta et al. [70] notes that no intra-fiber relaxation was evident in their experiments. Relaxation time constants for intra-fiber interactions have not yet been characterized in any study of which we are aware. The 7000 s time constant we observed might be associated with this, or might be a feature of the larger structures within the tissue construct. The relaxation time constants of the tropocollagen molecules are on the order of microseconds [62] and appear to be masked at the level of tissue constructs.

An additional factor is water flow. At the molecular level, tropocollagen molecules bond covalently [62] and are surrounded by a hydration layer [25]. At the next hierarchical level, water plays a structural role, possibly maintaining spacing between collagen fibrils, while dehydration causes the tighter packing of fibrils and enhances mechanical rigidity by increasing intra-molecular hydrogen bonds [181, 117, 115]. Gautieri et al. [61] found that the dominant fibril-level deformation mechanism shifted from molecular sliding to molecular stretching with dehydration, with the latter exhibit higher stiffness.

Debate exists in the literature about how cross-linking affects stress-relaxation. Xu et al. [195] concluded that the viscoelastic response of a collagen gel depends upon cross-linking, while Feng et al. [50], comparing viscosity of artificial and native tissues, concluded that it does not. From the observations of remodeling dependent viscoelastic responses in this study, which includes effects of cross-linking, one can speculate that both groups are correct. The 100-110 s intra-fibril time constant persists throughout remodeling, while the 7-10 s time constant associated with intra-fibril relaxation seems coupled with cell responses in ETCs tested at 24 hours.

3.4.4 Caveats

A limitation of the current work is that the data acquired are strictly uniaxial. The off-axis contributions of cells to tissue viscoelasticity cannot be quantified. However, previous data do show that under the conditions of these experiments, the additive decomposition of the contributions of cells and ECM is a reasonable approximation [113, 114]. Moreover, for elongated cells appearing in these tissue constructs, the contributors of the transverse behavior of cells to the mechanics of the tissue construct is on the order of only a few percent [111].

A question that is raised in the study and elastic analysis of ETC mechanics is whether the mechanics of the porous ECM arising from deoxycholate treatment is representative of the true ECM mechanics. Although this is issue is largely resolved in the elastic analysis of tissue constructs [46], the question bears scrutiny in our viscoelastic analyses. Two questions arise. First, does deformation of pores in which cells resided an important (and irrelevant) deformation mechanism? If this were the case, then a new time constant or set of time constants associated with such deformation would be expected to appear in the relaxation spectrum. However, no such time constants appeared, and time constants associated with cells or cell/ECM interactions disappeared. Second, although deoxycholate does not change the short-term or long-term elastic response of the ECM [110], does it change the viscoelastic response? Again, no substantial shifting of time constants or appearance of new time constants was observed in the ECM relaxation spectra. Although the possibility exists that some of the time constants attributed to cells disappeared because of the action of deoxycholate, the absence of elastic effects combined with the overall insensitivity of the remaining time constants makes this possibility appear remote. However, now that tools for doing so are becoming available, quantifying the viscoelastic effects of deoxycholate in addition to the

other agonists, inhibitors, and detergents that are applied commonly in the study of ETCs represents an important direction of future inquiry.

3.5 Conclusions

Although the hierarchical origins of the time constants observed are still an issue of debate, the spectral analyses we presented indicate that cells remodel the viscoelastic nature of their environment, and have the potential to communicate through a viscoelastic ECM at higher frequencies. Our spectral analyses revealed that human dermal fibroblasts remodeled their environments in such a way as to strengthen some temporal responses relative to others. These changes resulted in an increase in the energy absorption in the 1 Hz range, indicating increased damping in the range associated with heart contraction in humans. The cells themselves exhibited damping at time constants sufficiently fast that the ECM would effectively appear elastic, indicating that cells are capable of absorbing and transmitting mechanical signals from one another at these ranges. Results highlight the multifaceted nature of the signals that cells receive, and indicate that the well-known ECM stiffening effects of fibroblasts are enacted over a specific range of viscoelastic time constants. The possible effects of this on cell-cell communication and pathologies of fibrosis warrant continued study.

Chapter 4

A Discrete Spectral Analysis for Determining Quasi-linear Viscoelastic Properties of Biological Materials

4.1 Introduction and background

The Fung quasi-linear viscoelastic (QLV) model is a standard tool for representing the nonlinear history- and time- dependent soft tissue viscoelasticity of biological tissues [55, 33, 188, 2]. The QLV model provides a simple fit to stress-relaxation tests, which are preferred over standard rotational rheometry for biological tissues due to issues of gripping and anisotropy. These tests involve stretching a specimen a prescribed amount and then analyzing the relaxation over time of the force needed to sustain this level of stretch. However, confidence interval for estimation of the parameters of the box shaped temporal relaxation function that Fung suggested in his book [55] are typically large [2], which complicates comparison of materials. Further, the usual box form of the temporal relaxation function is sufficiently restrictive that many have found the need to apply different relaxation functions [169, 125, 177] or apply different QLV representations altogether [142]. Finally, identifying when the box

spectrum is too restrictive to describe a specific biological materials time-dependent mechanical responses is a challenge [173, 153, 154, 132, 135, 93, 151, 91, 5] because, with this box spectrum, the Fung QLV model can fit relaxation data even for materials whose responses to dynamic loading it would fail to predict [79, 6].

We present here a simple technique to overcome these challenges. The core of the technique is a finite series that, under special conditions, reduces to Fung's box spectrum relaxation function. In this proposal, we show that application of our discrete QLV (DQLV) form of the Fung QLV model is a simple and effective way to identify material relaxation spectra in an unbiased manner from stress-relaxation data. The approach identifies ranges of time constants over which Fung's continuous box relaxation spectrum is appropriate, and is effective at fitting this box relaxation spectrum. It also identifies when discrete time constants are more appropriate than the box relaxation spectrum for representing damping responses. After presenting the DQLV model, we apply it to correctly identify spectra at particular strain levels from simple relaxation tests, and then demonstrate its utility on determining the quasi-viscoelastic response of the rabbit medial collateral ligament (MCL).

We begin with overview of the integral form of linear and quasi-linear viscoelastic models with the goal of setting the stage for the specific discrete relaxation function we present in section 3.2.2.

4.1.1 Integral form of linear viscoelasticity

The behavior of a linear viscoelastic material in one dimensional can be represented by the following convolution integral [166, 105].

$$\sigma(t) = \int_{-\infty}^{t} \psi(t,u)\frac{\partial \epsilon}{\partial u}du \tag{4.1.1}$$

where $\psi(t,u)$ is a material modulus function, t is time, σ is engineering stress, and ϵ is linearized strain. For hereditary or non-aging materials, this reduces to:

$$\sigma(t) = \int_{-\infty}^{t} \phi(t-u)\frac{\partial \epsilon}{\partial u} du \tag{4.1.2}$$

where the relaxation function $\phi(t)$ describes the mechanical character of a material, ranging from an elastic solid (ϕ=constant) to a Newtonian fluid ($\phi(t) = \eta\delta(t)$, where η is a coefficient of viscosity and $\delta(t)$ is Diracs delta function. For a material with both elastic and viscous properties, $\phi(t)$ must be a generalized function that defines the whole spectrum of material behavior. $\phi(t)$ is determined in general by fitting to data from an experiment such as a stress-relaxation test, in which a sample is subjected to a linear ramp at strain rate $\dot{\epsilon}$ over time $0 \leq t \leq t_p$, followed by an isometric relaxation phase over $t_p \leq t \leq t_f$ (Figure 4.1(a) and (b)).

4.1.2 Fung's quasi-linear viscoelastic (QLV) model

In a biological material, $\phi(t)$ is typically inadequate because the relaxation function depends upon the degree to which the material is strained. Fung's QLV model, reviewed extensively and in more detail by others [126, 177, 132, 93, 151, 79, 6, 166, 105, 40, 200, 154, 43, 153, 66, 202], provides a simple strain-dependent extension of 4.1.2 in which the temporal decay of stress is independent of strain:

$$K(\epsilon, t) = G(t)\ \sigma^{(e)}(\epsilon) \tag{4.1.3}$$

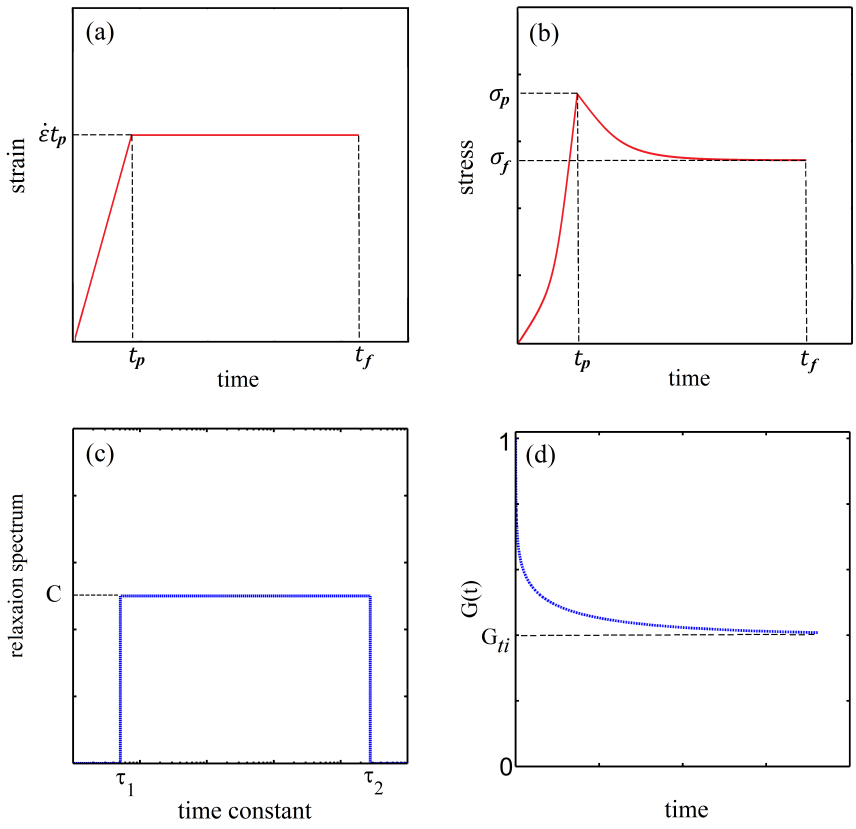

Figure 4.1: Characterization of a viscoelastic material through a standard ramp-and-hold test. (a) In a ramp-and-hold relaxation test, uniaxial strain is increased at a constant rate $\dot{\epsilon}$ over a time t_p then held at an isometric level $\dot{\epsilon}t_p$ until time t_f. (b) In response, the stress varies with time, rising to a peak value σ_p and then relaxing to a value σ_f. (c) For biological tissues, such data are often interpreted using Fungs QLV theory, involving a box-shaped relaxation spectrum of height C. (d) The parameters describing this box spectrum can be rearranged to predict the "reduced relaxation function" that appears in the Fung QLV constitutive law

where $G(t)$ is a normalized function of time so that $\lim_{t\to\infty} G(t) = G_{ti}$ (time-independent component of G) and $\lim_{t\to 0} G(t) = 1$ (Figure 4.1 (d)); $K(\epsilon, t)$ represents stress; and $\sigma^{(e)}(\epsilon)$ presents the elastic response. Based upon the concave-up force-displacement curves common to collagenous tissues, Fung proposed using an exponential relationship that he attributes to Kenedi et al. [55, 56], for the elastic stress component:

$$\sigma^{(e)}(\epsilon) = A(e^{B\epsilon} - 1) \tag{4.1.4}$$

The stress responses to a small strain increment, applied at time u, $G(t-u)\frac{\partial\sigma^{(e)}(\epsilon)}{\partial\epsilon}\delta\epsilon(u)$, can be summed using the Boltzmann superposition principle, so that the stress for t0 can be written:

$$\sigma(\epsilon, t) = \int_0^t G(t, u)\frac{\partial\sigma^{(e)}(\epsilon)}{\partial\epsilon}\frac{\partial\epsilon}{\partial u}du \tag{4.1.5}$$

$G(t)$ is a monotonically decreasing function [105]; as in the fading memory model, the recent strain history determines material response. Fung termed $G(t)$ the "reduced relaxation function" and suggested the form:

$$G(t) = \frac{1 + \int_0^\infty S(\tau)e^{-t/\tau}d\tau}{1 + \int_0^\infty S(\tau)\ d\tau} \tag{4.1.6}$$

where $S(\tau)$ is the following function, first proposed independently by others including Neubert [129]:

$$S(\tau) = \begin{cases} \frac{C}{\tau} & \tau_1 < \tau < \tau_n \\ 0 & \text{otherwise} \end{cases} \tag{4.1.7}$$

in which C, τ_1 and τ_2 are material constants to be determined experimentally (Figure 4.1). Substituting, one arrives at the form that is ubiquitous in the biomechanics literature:

$$G(t) = \frac{1 + \int_{\tau_1}^{\tau_2} (C/\tau) e^{-t/\tau} d\tau}{1 + \int_{\tau_1}^{\tau_2} (C/\tau)\ d\tau} = \frac{1 + C(E_1(t/\tau_2) - E_1(t/\tau_1))}{1 + C\ ln(\tau_2/\tau_1)} \tag{4.1.8}$$

where $E_1 = \int_0^\infty e^{-\tau} \tau d\tau$ is the exponential integral function. This version of the Fung QLV model is predicated upon the requirements of equations 4.1.3, 4.1.4, and 4.1.7. Although the typical implementation focuses on small strain applications, straightforward extensions of the Fung QLV model to finite strain exist [28, 37, 190]. However, the suitability of the assumption of equation 4.1.3 must be checked carefully for any material to which these extensions are applied.

In section 3, we present a simple tool to identify whether the relaxation response $S(\tau)$ follows the box spectrum of Equation 4.1.7, and whether this response is independent of strain (cf. Equation 4.1.3). We further propose a simple technique for modeling a material if these requirements prove unsuitable.

4.1.3 Schematic representations of the Fung QLV model

Two graphical representations of the Fung QLV model bear mention. These provide a foundation for interpreting the fitting and model identification tools presented in section 3.

4.1.4 Standard linear solid models in series

The Fung QLV model can be represented as an infinite number of standard linear solid elements in series, modified so that linear springs are replaced by nonlinear springs (Figure 4.2(a)). $S(\tau)$ for each of those elements varies between two constants: $S(\tau_2) < C/\tau < S(\tau_1)$.

Noting that the stress in each element is equal, a relationship can be written between the first and the last elements:

$$\frac{1+(C/\tau_1)e^{-t/\tau_1}d\tau}{1+(C/\tau_1)\ d\tau}A(e^{B\epsilon_1}-1)=\frac{1+(C/\tau_2)e^{-t/\tau_2}d\tau}{1+(C/\tau_2)\ d\tau}A(e^{B\epsilon_2}-1) \tag{4.1.9}$$

where A, B, C, τ_1 and τ_2 are the five QLV parameters to be fit. The first element ($S = C/\tau_1$) has the highest strain, ϵ_1, while the last ($S = C/\tau_2$) has the smallest, ϵ_2. Equation 4.1.9 shows a major difference between the QLV and generalized Maxwell models [190]. Because the viscoelastic elements in the QLV model are in series, changing τ_1 or τ_2 changes the stress in all of the individual models (Figure 4.2(a)). Thus, in contrast with the generalized Maxwell model, τ_1 and τ_2 are not the fastest and slowest viscoelastic time constants, respectively. Rather, they are time-domain parameters whose values affect the entire stress-relaxation curve.

4.1.5 Temporal QLV decomposition

A second useful schematic depiction of the Fung QLV model involves decomposition into time-independent and time-dependent parts. This decomposition is instructive and useful because it introduces a constraint upon the five QLV parameters. Following a ramp to a sustained level of isometric stretch (cf. Figure 4.1(a)), the relaxation function, $G(t), (t > t_p)$ is:

$$G(t)=G_{ti}+G_{td}(t)=\frac{1}{1+C\ ln(\tau_2/\tau_1)}+\frac{C(E_1(t/\tau_2)-E_1(t/\tau_1))}{1+C\ ln(\tau_2/\tau_1)} \tag{4.1.10}$$

where G_{ti} represents the time-independent and G_{td} the time-dependent parts of the reduced relaxation function. The stress can likewise be separated into time-independent and time-dependent parts (Figure 4.2(b)). For example, for a specimen that is fully relaxed at time t=0 that is stretched at a constant strain rate $\dot{\epsilon}$ from $t = 0$ to $t = t_p$ then held isometrically until $t = t_f$ (Figure 4.1(a)),

$$\sigma(t) = \begin{cases} \frac{A(e^{B\epsilon}-1)}{1+C(\tau_2/\tau_1)} + \int_0^t \frac{C(E_1((t-u)/\tau_2))-E_1((t-u)/\tau_1)))}{1+C\ ln(\tau_2/\tau_1)} e^{B\dot{\epsilon}u} & 0 \le t \le t_p \\ \\ \frac{A(e^{B\epsilon_p}-1)}{1+C(\tau_2/\tau_1)} + \int_0^{t_p} \frac{C(E_1((t-u)/\tau_2))-E_1((t-u)/\tau_1)))}{1+C\ ln(\tau_2/\tau_1)} e^{B\dot{\epsilon}u} & 0 \le t \le t_p \end{cases} \tag{4.1.11}$$

or

$$\sigma(t) = \begin{cases} \sigma_{ti}(\epsilon) + \sigma_{td}(t) & 0 \le t \le t_p \\ \sigma_{ti}(\epsilon_p) + \sigma_{td}(t) & t_p \le t \le t_f \end{cases} \tag{4.1.12}$$

Schematically, the first term on the right side of these equations represents the stress in a nonlinear time-independent (strain-dependent) spring, and the second term represents a nonlinear spring, with linear viscous damping, which is time-dependent (Figure 4.2(b)). After sufficient relaxation, the second term on the right hand side of equation 4.1.11 or 4.1.12 approaches 0, and $\sigma(t)$ approaches a steady-state:

$$\sigma(\infty) = \sigma_{ti}(\epsilon_p) = \frac{A(e^{B\epsilon} - 1)}{1 + C\ ln(\tau_2/\tau_1)} \tag{4.1.13}$$

where $\epsilon_0 = \epsilon t_p$. Thus, a way to ensure that the five QLV parameters are estimated correctly from a data set is to compare the stress asymptote in the data to $\frac{A(e^{B\epsilon_p}-1)}{1+C(\tau_2/\tau_1)}$ from equation 4.1.13 (Figure 4.1(b)), assuming the isometric portion of the experiment was sufficiently long to provide an accurate estimate of $\sigma(\infty)$.

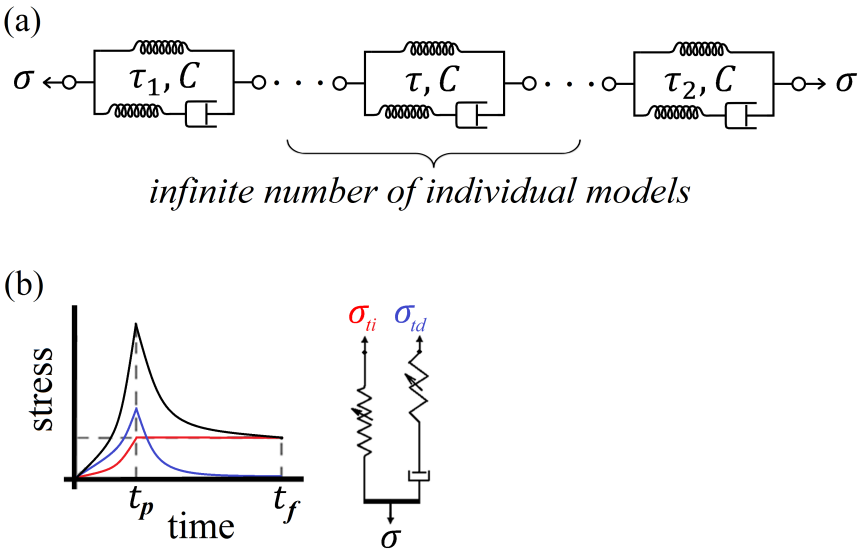

Figure 4.2: Schematic representations of the Fung box spectrum model. (a) The box spectrum model can be represented schematically by a continuous series of nonlinear viscoelastic elements, each associated with a time constant between the limits τ_1 and τ_2 of the box relaxation spectrum, and with the height C of the box relaxation spectrum (cf. Figure 4.1(c)). (b) In another representation, with a different type of nonlinear spring, the time-independent and time-dependent stress responses can be separated as in equation 4.1.12.

4.2 Methods

4.2.1 Continuous quasi-linear viscoelastic spectrum

To analyze a materials relaxation spectrum without any specific pre-assumption for $S(\tau)$, suppose $S(\tau)$ is

$$S(\tau) = \begin{cases} \frac{h(\tau)}{\tau} & \tau_1 < \tau < \tau_n \\ 0 & \text{otherwise} \end{cases} \tag{4.2.1}$$

where for $h(\tau) = C$, equation 4.2.1 reduces to the Fung QLV model (cf. equation 4.1.7). Plugging equation 4.2.1 into equation 4.1.6, the relaxation function can be written:

$$G(t) = \frac{1 + \int_0^\infty S(\tau) e^{-t/\tau} d\tau}{1 + \int_0^\infty S(\tau)\ d\tau} = \frac{1 + \int_{\tau_{min}}^{\tau_{max}} \frac{h(\tau) e^{-t/tau}}{\tau} d\tau}{1 + \int_{\tau_{min}}^{\tau_{max}} \frac{h(\tau)}{\tau} d\tau} \tag{4.2.2}$$

Then, for a fully relaxed specimen stretched at a constant strain rate $dot\epsilon$ over the time interval 0 to t_p and held isometrically until time t_f, the stress history can be written:

$$\sigma(t) = \begin{cases} \frac{A(e^{B\epsilon}-1)}{1+\int_{\tau_{min}}^{\tau_{max}} \frac{h(\tau)}{\tau} d\tau} + \int_0^t \frac{\int_{\tau_{min}}^{\tau_{max}} \frac{h(\tau) e^{-(t-u)/\tau}}{\tau} d\tau}{1+\int_{\tau_{min}}^{\tau_{max}} \frac{h(\tau)}{\tau} d\tau} e^{B\dot{\epsilon}u} du & 0 \le t \le t_p \\ \\ \frac{A(e^{B\epsilon_p}-1)}{1+\int_{\tau_{min}}^{\tau_{max}} \frac{h(\tau)}{\tau} d\tau} + \int_0^{t_p} \frac{\int_{\tau_{min}}^{\tau_{max}} \frac{h(\tau) e^{-(t-u)/\tau}}{\tau} d\tau}{1+\int_{\tau_{min}}^{\tau_{max}} \frac{h(\tau)}{\tau} d\tau} e^{B\dot{\epsilon}u} du & t_p \le t \le t_f \end{cases} \tag{4.2.3}$$

In the above equations, $A, B, h(\tau), \tau_{min}$ and τ_{max} are unknowns that should be estimated by fitting $\sigma(t)$ to experimental stress-relaxation data. This, unfortunately, is an ill-posed problem. However, a broad range of techniques exists to find a solution [105, 52, 178, 47] that is suitable and repeatable, if not unique.

4.2.2 Discrete quasi-linear viscoelastic spectrum

A discretization technique simplifies this ill-posed problem. Although several approaches exist for discretizing viscoelastic responses, including the Prony series approach, our specific objective is to arrive at an approach that yields a graphical representation to easily identify the suitability of the the Fung box spectrum over a particular range of loading conditions. The approach we take begins with a discrete form of the integral $\int_{\lambda_1}^{\lambda_{n+1}} \frac{h(\tau)}{\tau} d\tau$, with the interval $(\lambda_1, \lambda_{n+1})$ divided into equidistant logarithmic subintervals:

$$\int_{\lambda_1}^{\lambda_{n+1}} \frac{h(\tau)}{\tau} d\tau = \int_{\lambda_1}^{\lambda_{n+1}} h(\tau) d(ln(\tau)) = \sum_{i=1}^{n} \int_{\lambda_1}^{\lambda_{i+1}} h(\tau) d(ln(\tau)) = \sum_{i=1}^{n} ln(\frac{\lambda_{i+1}}{\lambda_1}) H_i \quad (4.2.4)$$

For the case of λ_i distributed equidistantly over the range $\lambda_1 \leq \lambda_i \leq \lambda_n$, one can further simplify to write:

$$\int_{\lambda_1}^{\lambda_{n+1}} \frac{h(\tau)}{\tau} d\tau = T \sum_{i=1}^{n} H_i \quad (4.2.5)$$

where the constant $T = ln(\frac{\lambda_{i+1}}{\lambda_1}) = ln(\frac{\lambda_2}{\lambda_1})$, and H_i is the height of the ith rectangle and τ_i is the corresponding time constant (Figure 4.3). The spectrum $H_i(\tau_i)$ represents a tool for model identification, which we term a "discrete quasi-linear viscoelastic" (DQLV) spectrum, which simplifies to the continuous Fung box spectrum when appropriate. Throughout, we use the superscript DQLV to distinguish parameters arising from a DQLV fitting from those arising from a box spectrum fitting. The discrete form of equation 4.2.2 is:

$$G^{(DQLV)}(t_j) = \frac{1 + T \sum_{i=1}^{n} H_i e^{-t_j/\tau_i}}{1 + T \sum_{i=1}^{n} H_i} \quad (4.2.6)$$

and that of equation (3.1) is:

$$S^{(DQLV)}(\tau_i) = \begin{cases} \frac{H_i}{\tau_i} & \tau_1 < \tau < \tau_n \\ 0 & \text{otherwise} \end{cases} \quad (4.2.7)$$

where H_i are parameters to be fit and τ_1 and τ_n, as described below, are chosen to encompass a range broader than that needed to describe a material. In contrast to the Neubert [31]

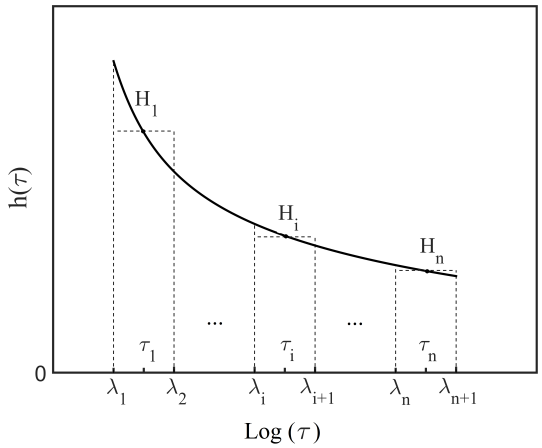

Figure 4.3: Schematic of the discretization of the continuous function $h(\tau)$. A partition of an interval $[\gamma_1, \gamma_(n+1)]$ is a finite sequence of n subintervals on a logarithmic x-axis. $[\gamma_i, \gamma_(i+1)]$ is the width and H_i is the height of the ith rectangle and τ_i time constant corresponding to H_i.

and Fung box spectrum models [1], the values of H_i need not be identical. Schematically, the DQLV model is analogous to the box spectrum model, except with a finite number of elements, H_i, that represent the relaxation spectrum (Figure 4.4). For materials that are not well fit by the box spectrum model, the insertion of equation (4.2.9) into equation (4.2.8) provides for a simple extension of the QLV model. We note that, although the DQLV spectrum reduces to a box spectrum, it is different in that the values of Hi need not be constant. Further, although this physical meaning of τ_1 and τ_n is analogous to these constants within a Prony series, we note that the DQLV spectrum reduces to a box spectrum when a box spectrum is indeed the correct representation of a materials relaxation response. The model does not reduce to the spectral representation that would be obtained using the generalized Maxwell model [39].

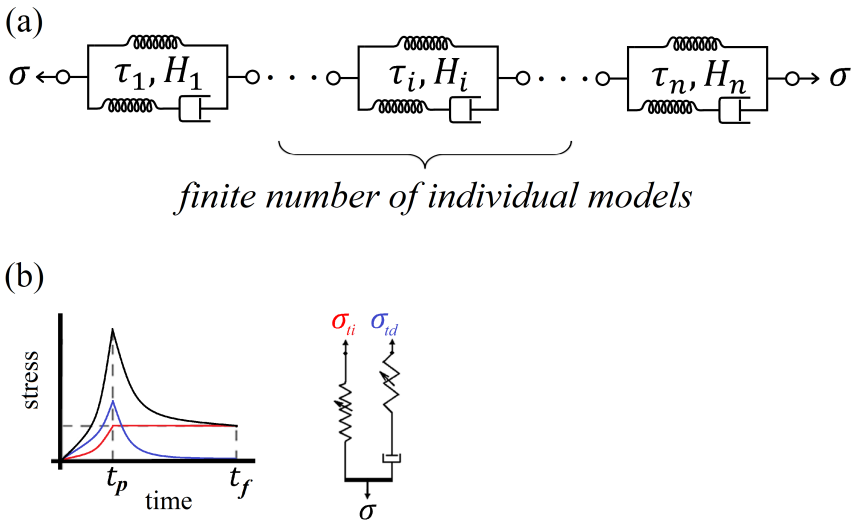

Figure 4.4: The DQLV model differs from the Fung box spectrum model in that it has a finite number n of elements analogous to those in Figure 4.2(a), each with a discrete time constant τ_i and with a potentially different height H_i. (b) The time-independent and time-dependent stress responses can be separated as in 4.2(b).

4.2.3 Numerical fitting algorithms

As in equation 4.1.12, we can split $G^{(DQLV)}(t)$ into time-independent and time-dependent parts:

$$G^{(DQLV)}(t) = G_{ti}^{(DQLV)} + G_{td}^{(DQLV)}(t) = \frac{1}{1 + T\sum_{i=1}^{n} H_i} + \frac{T\sum_{i=1}^{n} H_i e^{-t/\tau_i}}{1 + T\sum_{i=1}^{n} H_i} \tag{4.2.8}$$

Because of the nature of ill-posed problems, we expect predictions to show some deviation from a Fung box spectrum even for artificial data generated from the Fung model [163, 162, 85, 15]. Thus, we used a simple regularizing criterion, which acted as a penalty against unwanted states and ensured that the fitting algorithm did not become trapped in local minima. In this approach, H_i were smoothed by a regularization function and were identified by minimizing:

$$\frac{1}{f}\sum_{j=1}^{f}(\sigma_j^{(exp)}-\sigma_j^{(DQLV)})+\alpha\sum_{i=2}^{n-1}(H_{i-1}+2H_i-H_{i+1})^2 \tag{4.2.9}$$

where f is the number of data points, $\sigma_j^{(exp)}$ are known stress data or a calculable relationship, and α is a regulating factor. Parameters were determined using a non-negative least-squares regression [21]. For any α on the order of 1, the parameter estimates were insensitive to the specific choice of α. $\alpha = 1$ was used in the model validation studies below. $\sigma_j^{(DQLV)}$ are DQLV estimates of $\sigma_j^{(exp)}$:

$$G(t)=\frac{1+\int_0^\infty S(\tau)e^{-t/\tau}d\tau}{1+\int_0^\infty S(\tau)\ d\tau}=\frac{1+\int_{\tau_{min}}^{\tau_{max}}\frac{h(\tau)e^{-t/tau}}{\tau}d\tau}{1+\int_{\tau_{min}}^{\tau_{max}}\frac{h(\tau)}{\tau}d\tau} \tag{4.2.10}$$

Then, for a fully relaxed specimen stretched at a constant strain rate $\dot{\epsilon}$ over the time interval 0 to t_p and held isometrically until time t_f, the stress history can be written:

$$\sigma_j^{(DQLV)}=\begin{cases}\frac{A(e^{B\dot{\epsilon}t_j}-1)}{1+T\sum_{i=1}^n H_i}+\int_0^{t_j}\frac{T\sum_{i=1}^n H_i e^{-(t_j-u)/\tau_i}}{1+T\sum_{i=1}^n H_i}e^{B\dot{\epsilon}u}du & (j=1,2,...,p)\\ \\ \frac{A(e^{B\dot{\epsilon}t_p}-1)}{1+T\sum_{i=1}^n H_i}+\int_0^{t_p}\frac{T\sum_{i=1}^n H_i e^{-(t_j-u)/\tau_i}}{1+T\sum_{i=1}^n H_i}e^{B\dot{\epsilon}u}du & (j=p+1,p+2,...,f)\end{cases} \tag{4.2.11}$$

where p and f are the number of data points in ramp and relaxation intervals, respectively.

4.2.4 Validation of software to estimate DQLV spectra

A code to obtain the DQLV spectrum of a material from stress versus time data in a relaxation test was generated in the Matlab environment. The code is available from the authors. Because the DQLV model represents an approximation of the real spectrum of a material

[163], it was important to validate the model and check the reproducibility of the approximation. Validations were performed by using the DQLV model to fit stress-relaxation data generated using either the Fung QLV model with a box spectrum or using the generalized Maxwell model, the latter having three time constants (including the infinite time constant) (see, e.g., [206, 52]). The stability of the model with respect to noise was then studied. Random noise was added to the simulated Fung QLV stress-relaxation data to evaluate how noise affects DQLV analysis results. We superimposed upon the data noise chosen from a uniform distribution with amplitudes of $5\%, 10\%, 15\%, 20\%$ or 25% of the steady state stress. 50 noisy data sets were generated (10 sets for each noise percentage). Relaxation spectra, $H(\tau)$, for these new data sets were estimated using the DQLV approach. The sensitivity to noise level was then quantified by the mean square error (MSE) of the predicted stress-relaxation compared to the underlying input stress-relaxation data.

4.2.5 Characterization of MCL relaxation

As an example of DQLV characterization of an orthopedic tissue, we studied the either the left or right medial collateral ligament (MCL) from N=6 skeletally mature female New Zealand white rabbits. The study was done in compliance with the National Institutes of Health guidelines for animal care and the Institutional Animal Care and Use Committee (IACUC) at the University of Pittsburgh. Prior to dissection, knees were wrapped in saline soaked gauze and then sealed in plastic bags and fresh frozen at $-20°C$ [193]. On the day of testing, knees were thawed to room temperature and MCLs were dissected and cut free at the insertion sites [122, 187]. The geometry was standardized by cutting the ligaments into dog bone shapes with a length-to-width ratio of 6.8 ± 0.8 (width $1.6\pm0.2\ mm$). The tissue samples were fixed in custom-made soft tissue clamps, and the cross-sectional area was determined with a laser micrometer system ($1.0 \pm 0.3\ mm^2$ [193, 99]. Measurements were taken in three

locations along the length of the tissue sample and averaged for stress calculations. The tissue sample-clamp construct was then mounted to a tensile testing machine (Enduratec Elf 3200, Bose Corporation, Framingham, MA). Reflective markers were placed on the tissue sample to track strain using an optical system (VP110, Motion Analysis, Santa Rosa, CA). A saline drip was utilized to hydrate the tissue sample and maintain temperature at a constant $37°C$. The tissue sample was aligned along the loading axis using an x-y table and then was left unloaded for 30 minutes to acclimate. Specimens were elongated to strain levels of $1.25\%, 2.5\%$ and 5% and held isometrically at each level for 35 minutes to reach equilibrium [119]. Force data were acquired at 3 Hz throughout the ramp and 35 minute relaxation intervals. The ramp time for all three samples was $9.2sec$; thus, the specimens strain rates were $0.135\%/sec$, $0.271\%/sec$ and $0.543\%/sec$, respectively. The experimental data were fit using both the DQLV and Fung box spectrum models [2].

4.3 Results and discussion

4.3.1 Fitting of simulated data

In the first validation study, stress-relaxation data were calculatedfor a Fung QLV material whose relaxation response followed abox spectrum, and the DQLV model was applied to estimate the parameters used to generate these data. The parameters chosen were those reported by Abramowitch et al. [2] for a goat medial collateral ligament (MCL) that was strained to 2.76% over 18.4 s then held isometrically for $3600s$ (Figure 4.5(a) and band table 4.1). The DQLV model was applied using equation (3.10), which constrains the DQLV model to fit stress-relaxation data. A spectrum that approximated a box spectrum was predicted, indicating that the material would be well-modeled by a box spectrum representation. Several sets of time constants and different regularization parameters were evaluated to ensure

that the DQLV spectrum was repeatable. The predicted spectra were insensitive to the choice of α for α on the order of 1, and α=1 was adopted for all subsequent analyses. The spectrum shown in Figure 4.5(c) had n=100 time constants. Increasing n provided a better quantitative fit to the stress-relaxation data, but did not change the qualitative nature of the predicted DQLV spectrum. An interesting feature of the DQLV analysis is that the predicted DQLV spectrum, despite its deviation from a box shape, yielded error of less than 0.01% of the peak stress when predicting stress-relaxation data generated using a flat box spectrum.Indeed, the Fung box spectrum and DQLV fits were both indistinguishable from the input relaxation data (Figure 4.5(c)). The logical course of action for a DQLV spectrum such as this would thus be to adopt the simpler box spectrum fitting for subsequent analysis ofthis material. We next studied whether the DQLV model could identify when stress-relaxation data should not be represented by a Fung box spectrum. The input data in this case were generated using a generalized Maxwell model [52] including two Maxwell elements in addition to a linear spring, all acting in parallel. The data chosen were those reported by Shen et al. [158] for fitting the response of a sea cucumber (Cucumariafrondosa) collagen fibril following a $20s$ ramp to a strain of 20% and a subsequent $520s$ isometric hold (Figure 4.6 and band table 4.2). The DQLV fitting recovered a Maxwell-type spectrum with two distinct peaks at the two non-infinite time constants used to generate the input data (4.6(c).

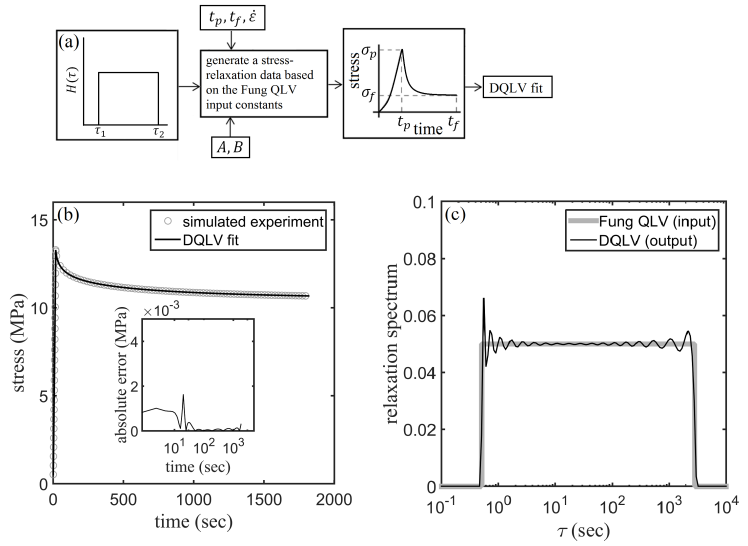

Figure 4.5: Validation of the DQLV fitting method against simulated stress-relaxation data from an ideal Fung QLV material with a box spectrum. (a) Simulated stress-relaxation data were generated for an idealized Fung QLV material with a box spectrum, then fit with the DQLV model. (c) The DQLV spectrum approximated a box-shape. (d) DQLV fitting provided and excellent fit to the input data.

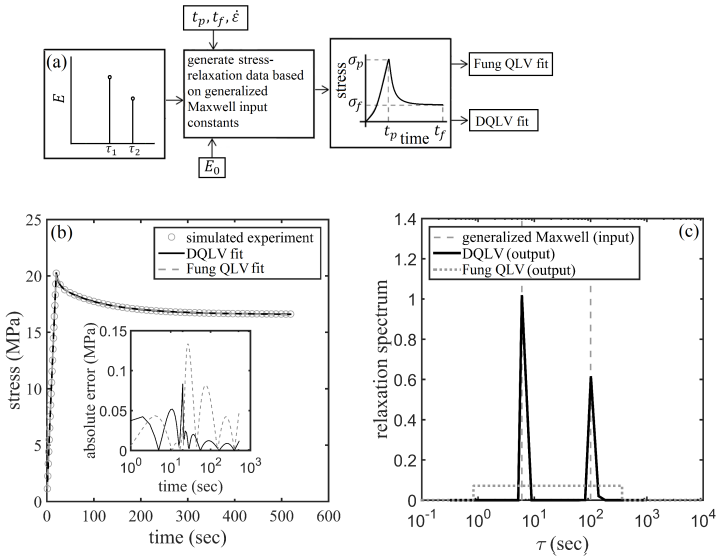

Figure 4.6: Validation of the DQLV fitting method to simulated stress-relaxation data from an ideal generalized Maxwell material. (a) Simulated stress-relaxation data were generated for an ideal generalized Maxwell model with two time constants, then fit with the DQLV model. (b) Despite the inappropriateness of a Fung box spectral fitting, both fittings provided excellent fits to the input data. (c) The DQLV spectrum identified the two discrete time constants accurately.

Table 4.1: Constants describing the parameters of reduced relaxation function, the instantaneous elastic response and the strain profile for goat MCL [2].

A(MPa)	B	C	τ_1	τ_2	t_p	t_f	$\dot{\epsilon}(s^{-1})$
32.86	13.5	0.05	0.51	2786	18.4	3618.4	0.0015

However, the box spectrum fitting (Figure 4.6(c)), also yielded an excellent fit to the stress-relaxation data. The fitting error, as observed in the plot of the residuals (inset of Figure 4.6(b)), was only slightly higher than that of the DQLV fitting. This very small difference in residual error highlights the peril of fitting a Fung QLV box spectrum in the absence of a spectral evaluation such as that which the DQLV model provides: although the box spectrum model capturedthe relaxation data very well, this prediction captures the frequency-dependence of the material response very poorly at the extremes of the range of time constants [79, 6]. As we emphasize in the sequel to this article, the errors become substantial when attempting to predict material response under dynamic loading. Finally, the

fittings were remarkably robust against Gaussian random noise for both the DQLV (Figure 4.7(a)) and box spectrum (Figure 4.7(b)) models. MSEs increased with noise, but were less than $2MPa$ for 25% noise in both models, compared to a peak stress of about $13MPa$.

Table 4.2: Constants describing the elastic moduli, the relaxation time constants and the strain profile for isolated collagen fibrils of Cucumaria frondosa [158].

E_0(MPa)	E_1(MPa)	E_2(MPa)	τ_1	τ_2	t_p	t_f	$\dot{\epsilon}(s^{-1})$
83	19	14	6	100	20	520	0.0100

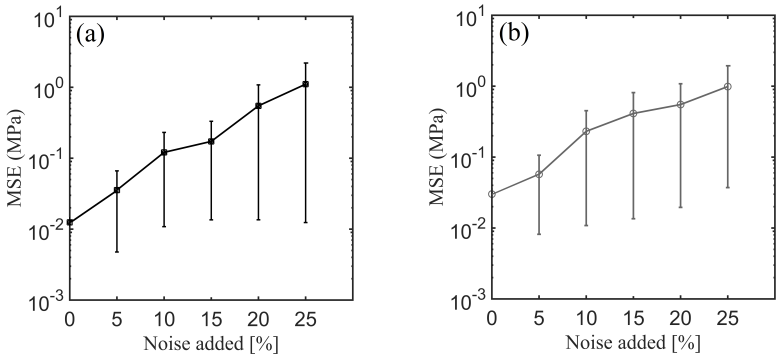

Figure 4.7: Assessment of the susceptibility of the DQLV and Fung QLV fitting methods to experimental noise. (a) DQLV and (b) Fung QLV fittings of simulated data reproduced the stress-relaxation curves in a way that was robust against noise. The DQLV model showed lower MSE than the Fung QLV model. Shown is the mean squared error (MSE) of the fit to the stress-relaxation data for fitting of 10 different noisy sets of relaxation data at each of 5 different levels of noise. For comparison, the peak stress was about 13 MPa. Noise was introduced by adding a Gaussian random fraction of the quantity $\beta(\sigma_f)$ to each data point, where $\beta \in [0\%, 5\%, 10\%, 15\%, 20\%, 25\%]$.

4.3.2 DQLV fitting of stress-relaxation data of rabbit MCL

The stress-relaxation data for rabbit MCLs at strain levels of $1.25\%, 2.5\%$ and 5% all showed a characteristic rise during stretching, then gradually decreased to plateau at about $2000s$ (Figure 4.8(a), (c) and (e)). Both the DQLV and box spectrum models fit the experimental data with acceptable error, but the DQLV had higher precision (Figure 4.8(a), (d) and (f)).By comparing the DQLV spectra (Figure 4.9(a)) to the Fung box spectra (Figure 4.9(b)) of the three stress-relaxation tests, it is clear that the box spectra weakly estimated the lower

boundary of dominant time constants of the system.The DQLV model estimation, on the other hand, was more consistent. Moreover, the DQLV model illuminated a structurally fast time constant at about $10s$ and a slow time constant at about $1000s$ that were not detectable by the Fung boxspectra. These observations are consistent with dynamic testing reported for other tissues [79, 6, 166].

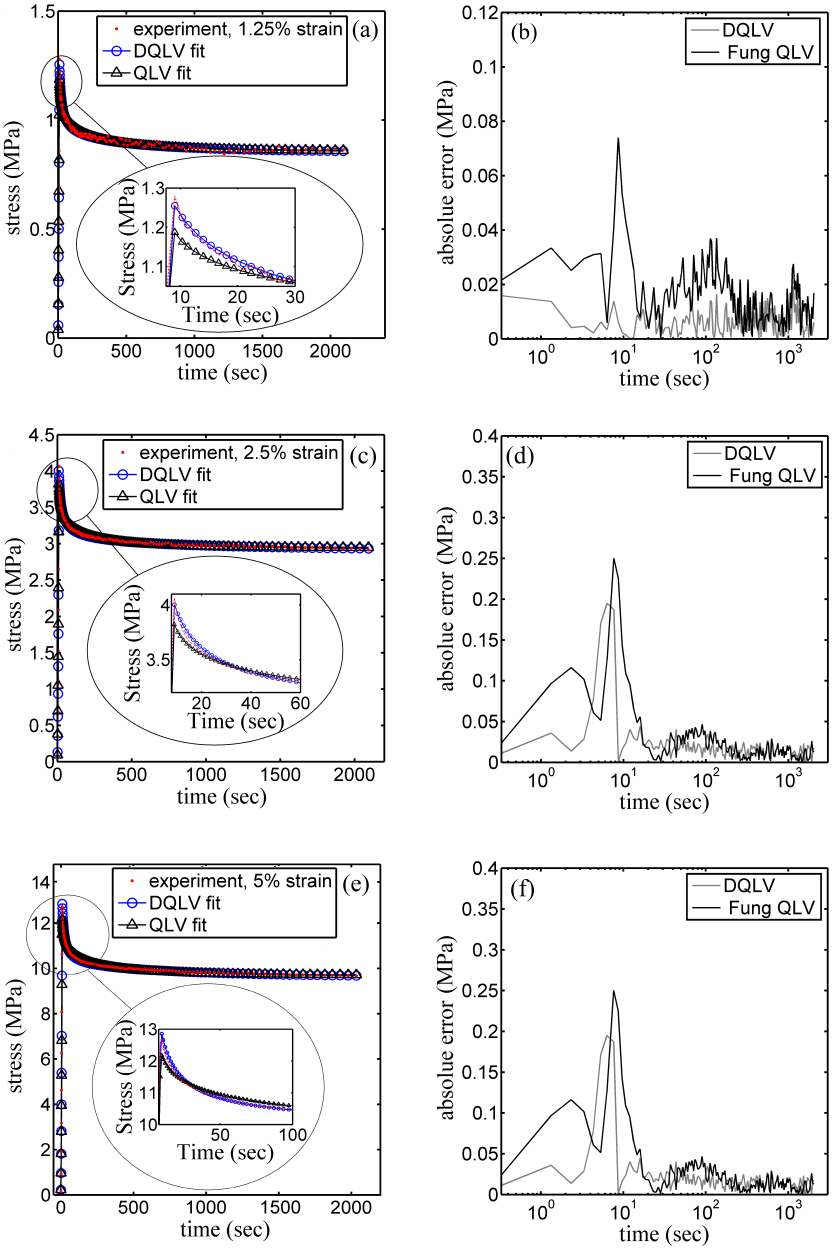

Figure 4.8: Demonstration of the fitting methods on experimental stress-relaxation data from a ligament. DQLV and Fung QLV fittings of stress-relaxation data acquired from a rabbit MCL stretched to (a) 1.25%, (c) 2.5% and (e) 5% strain. The residuals were substantially lower for the DQLV fittings at all three strain levels: (b) 1.25%, (d) 2.5%, and (f) 5% strain.

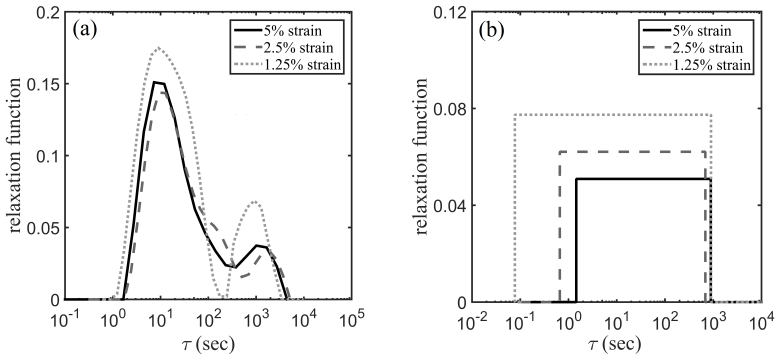

Figure 4.9: DQLV and Fung QLV spectra of the rabbit MCL. (a) The DQLV spectra were very similar at all three strain levels, which is a fundamental requirement for using the Fung QLV model. However, the spectra showed two dominant peaks (about $10s$ and about $1000s$) rather than a box spectrum, which precludes use of the Fung QLV model. (b) The Fung QLV model produced a poor fit to this spectrum, with the lower range of τ mispredicted and the minor variations of the spectrum with respect to strain exaggerated.

The DQLV spectrum showed reasonable repeatability for the three strain levels, suggesting that the Fung QLV model's criterion of a strain-independent reduced relaxation function-would be metreasonably well for the rabbit MCL specimens tested. However, the other condition, that of a flat, box-like spectrum was not met: the continuous spectrum of equation (3.1) must have constant dimensionless heighth $(\tau) = C$ over some range of τ_1 to τ_2, but the values of τ_1, τ_2 and C varied substantially for the best fits to the three tests. Errors associated with applying the box spectrum model become evident at the lower boundary of the time constants (Figure 4.9(b)).

4.3.3 Choosing amongst models

For a tissue such as the rabbit MCL studied above, a more detailed description of the spectrum would be required, especially under dynamic loading. Two logical choices are a normalized, generalized form of the Maxwell model and the DQLV model. Both are related in that they involve a Prony series, and both have strengths and limitations. The generalized

Maxwell model is an excellent tool for fitting most experimental stress-relaxation data, and can usually do so with only two or three exponential terms [12].This is a strength because of its simplicity, but is also a limitation because the limited number of time constants may be inadequate to reveal either the range of relaxation mechanisms or the subtle differences between materials. The DQLV model can represent the reduced relaxation spectrum of a material such as the rabbit MCL, and is convenient for several reasons. First, estimating a DQLV spectrum is a logical first step in choosing a material model for a biological material: by using a regularizing function, the approach identifies ranges of time constants over which Fung's continuous box relaxation spectrum provides a suitable approximation, and is effective at fitting this box relaxation spectrum. Second, a DQLV spectrum identifies when discrete time constants are more effective than a box relaxation spectrum for representing damping responses, and provides a reasonable material model with no further fitting. Third, the DQLV spectra from multiple strain states reveal the assumption of strain-independent relaxation (cf. Equation (2.3)) is supported; for example, the MCL data (Figure 4.9(a)) showed DQLV spectra that are very similar for three different strain levels, indicating that the DQLV model would be an reasonable simplification. Finally, the parameters H_i are insensitive to the number of time constants chosen. Increasing the number of time constants will improve precision of the discretization of a continuous relaxation spectrum, but our experience is that the nature of this spectrum eventually converges, becoming insensitive to further increases in the number of time constants.Application of this approach is a simple and effective way to identify material relaxation spectra in an unbiased manner from stress-relaxation data.

4.4 Conclusion

Application of the DQLV model is a simple and effective way to identify material relaxation spectra in an unbiased manner from stress-relaxation data. The approach identifies ranges

of time constants over which Fung's continuous box relaxation spectrum provides a suitable representation of material behavior, and is effective at fitting this box relaxation spectrum. It also identifies when discrete time constants are more appropriate than a box relaxation spectrum for representing damping responses. Although the Fung QLV model with abox spectrum can fit most stress-relaxation data, including data generated using a relaxation spectrum that differs substantially from a box spectrum, errors associated with applying the box spectrum become evident at the lower boundary of the time constants. The improvement in fit to relaxation data using the DQLV model can be substantial, especially when considering behavior over narrow ranges of material time constants. The DQLV model was able to identify correctly spectra at particular strain levels from simple stressrelaxation tests.

Chapter 5

Identifying time- and frequency-dependent properties of the medial collateral ligament

5.1 Introduction

"Stretching" is commonly performed by athletes for the purpose of optimizing body performance, but the mechanisms, optimal conditions, and efficacy of stretching are a source of debate. Stretching has been shown to enhance range of motion [120], but to either decrease or not affect peak athletic performance [118, 19]. The time period and character (ramped, ballistic, sustained) of the stretch appears to be a key determinant of efficacy, with ballistic stretching apparently less effecive than lower frequency dynamic stretching [77, 136, 179, 19]. The mechanisms underlying these effects are hypothesized to be some combination of connective tissue inelasticity, paracrine effects, and neural effects, the latter mediated by the Golgi tendon organ and the muscle spindle stretch receptor, and somewhat less long-lasting in effect [34, 19].

We focus here are the first factor and, more broadly, characterization of the dynamic, viscoelastic responses of connective tissue. The dynamic responses of connective tissue demonstrate viscoelastic damping that is dominated by syneresis and rearrangement of the fibrous structures of the connective tissue, both of which elongate the stress-free state of the tissue [121, 53, 59, 104, 170]. Because both of these factors dissipate energy in ways that are rate-dependent [125, 70], we hypothesized that stretching cycles applied to ligament would show rate-dependent energy dissipation, and that this would be greatest at the timescale of tens of seconds cited as the optimal ramp time for a stretching routine [19].

While linear viscoelastic models exist for predicting the viscoelastic nature of soft tissues under cyclic loadings such as those associated with stretching [51], these models are not sufficient to describe the complex, non-linear behavior of soft tissues. Specifically, linear viscoelastic constitutive equations describing the relationships between stress, strain, and strain rate are not sufficient to model all aspects of tissue viscoelastic behavior under different loading patterns and stimuli. The most common extension of these linear viscoelastic constitutive relations is Fung's quasi-linear viscoelastic (QLV) model [56], but we show here that this model imposes a certain character to viscoelastic responses that can mask the frequency dependence of tissue hysteresis. We therefore applied the discrete quasi-linear viscoelastic (DQLV) model [10] to interpret our experiments.

The experiments focused on quantifying the time- and frequency-dependent viscoelastic properties of rabbit medial collateral ligaments (MCLs). The model stretching regimen was a combined static-dynamic (ramp-hold-sinusoidal) testing procedure applied over a range of frequencies (from 0.01 to 50 Hz), with three levels of baseline strain levels (1.25%, 2.5% and 5%). This pre-strain was required to ensure that, as in the body, the ligament was never slack during a sinusoidal stretching cycle and to assess the nonlinearity of the response.

A theoretical framework was derived for characterizing material behavior of nonlinear biological materials under sinusoidal loadings using the DQLV approach, then applied to rabbit MCL data and compared to linear and QLV fits of the same data. Results supported our hypothesis, and further suggested a mechanical basis for the stretching regimens most favored by athletic trainers.

5.2 Background

5.2.1 Quasi-linear viscoelasticity

The rabbit MCLs tested showed rate-dependence and non-linearity. The usual model of choice for quantifying the behavior of such a tissue is Fung's QLV model, in which the stress $\sigma(\epsilon, t)$ at time strain ϵ and time t is obtained by solving the following convolution integral [56]:

$$\sigma(\epsilon, t) = \int_{-\infty}^{t} G(t-u)\frac{\partial \sigma^{(e)}}{\partial \epsilon}\frac{\partial \epsilon}{\partial u}du, \tag{5.2.1}$$

where $\sigma^{(e)}(\epsilon)$ represents the (possibly nonlinear) elastic stress response of the tissue, and $G(t)$ is the relaxation function, normalized so that $\lim_{t\to 0} G = 1$, and $\lim_{t\to\infty} G = c$, where c is a constant for a specific material (Figure 5.1a). For $\sigma^{(e)}(\epsilon)$, Fung proposed the exponential relationship he attributed to Kenedi et al. [86, 56]:

$$\sigma^{(e)} = A(e^{B\epsilon} - 1), \tag{5.2.2}$$

where A and B are material constants. For $G(t)$, Fung proposed the following form:

$$G(t) = \frac{1 + \int_{\tau_1}^{\tau_2}(C/\tau)e^{-t/\tau}d\tau}{1 + \int_{\tau_1}^{\tau_2}(C/\tau)\ d\tau} \tag{5.2.3}$$

where C, τ_1 and τ_2 are material constants to be determined experimentally.

Many viscoelastic biomaterials exhibit frequency-dependent dissipation that is not represented well by Equation (5.2.3) [142, 12, 11]. A more general choice for $G(t)$ is the discrete DQLV form of Equation (5.2.3) [10]:

$$G(t) = \frac{1 + T\sum_{j=1}^{n} H_i e^{-t/\tau_i}}{1 + T\sum_{i=1}^{n} H_i}, \tag{5.2.4}$$

where τ_i are the n time constants, typically chosen in advance and spaced equidistantly on a temporal logarithmic axis, T is the logarithmic distance between two adjacent time constants on this temporal logarithmic axis [10], H_i are dimensionless spectrum amplitudes, and n is a number sufficiently large to capture the material behavior of interest (typically, n=100-1000).

For the common viscoelastic test consisting of a linear ramp in strain followed by a sustained, isometric strain at the ramp's peak strain, a simple analytical solution for Equation (5.2.1) can often be found. However, for more complex strain profiles, such as the ramp-hold-sinusoidal loading protocol considered here, numerical approaches are preferred. Although when solving Equation (5.2.1) numerically the choices for $\sigma^{(e)}(\epsilon)$ and $G(t)$ need not be restricted to those that admit simple analytical solutions, simple forms like those described above are often desirable for interpreting fits to experimental data.

5.2.2 Memory effects in viscoelastic materials

The experimental protocol we applied in this work involved sinusoidal straining of a viscoelastic tissue. A challenge for such a loading is that applying a complete cycle of tension and compression is impractical for connective tissues due to their tendency to buckle. Therefore, application of a sinusoidal loading require that the sample first be placed in tension with

a pre-stress greater than the amplitude of the sinusoidal loading. Because the instantaneous response of a viscoelastic material depends upon the history of loadings it has experienced, the history must be factored into material characterization. To clarify this point, consider a sinusoidal straining of a material:

$$\epsilon(t) = \epsilon_0 \sin(\omega t), \tag{5.2.5}$$

where ϵ_0 is a defined amplitude and ω is angular frequency. The stress response to this straining of a linear viscoelastic material that was fully relaxed at $t = 0$ (Figure 5.1b) shows, as expected from (5.2.1)-(5.2.4), that $\epsilon(t = 0) = \sigma(t = 0) = 0$. However, as the sinusoidal response approaches a steady state, the peak stress changes and the stress profile falls behind the strain profile by a phase lag ϕ:

$$\sigma(t) = \sigma_0 \sin(\omega t + \phi), \tag{5.2.6}$$

where σ_0 is the stress amplitude. A central focus of the current work is therefore taking proper account of strain history when interpreting experimental data.

5.2.3 Complex modulus of a Fung QLV material

The viscoelastic response of a linear viscoelastic material is often represented by a complex modulus $G^*(\omega)$, defined by a one-sided Fourier transform [83]:

$$G^*(\omega) = j\omega \int_0^\infty G(u) \mathrm{e}^{-j\omega u} du = G'(\omega) + jG''(\omega), \tag{5.2.7}$$

where $j = \sqrt{-1}$ and $G'(\omega)$ and $G''(\omega)$ are the storage and loss moduli, respectively. The storage modulus represents the material response of the elastic portion (corresponding to

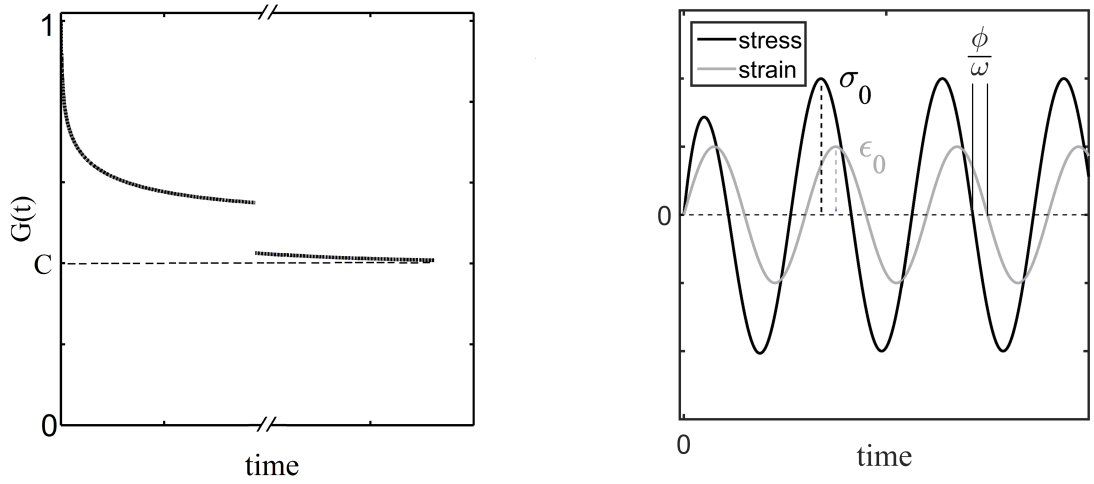

(a) (b)

Figure 5.1: Relaxation function, input strain and stress response of a viscoelastic material under sinusoidal excitation using a simulated experiment. (a) Relaxation function $G(t)$, which is normalized so that $G(0) = 1$. The rate of relaxation to a constant c depends on the viscoelastic response of a material. (b) In response to a sinusoidal straining, the stress response requires several cycles to reach a steady state amplitude and phase delay with respect to the strain.

the stored energy), and the loss modulus represents the viscous portion (corresponding the dissipated energy).

For the reduced relaxation function of Equation (5.2.3), the normalized storage and loss moduli are [56]:

$$G' = \frac{1 + \frac{C}{2}[\ln(1+\omega^2\tau_2^2) - \ln(1+\omega^2\tau_1^2)]}{1 + C\ln(\tau_2/\tau_1)} \quad \text{and} \quad G'' = \frac{C[\tan^{-1}(\omega\tau_2) - \tan^{-1}(\omega\tau_1)]}{1 + C\ln(\tau_2/\tau_1)}. \quad (5.2.8)$$

5.3 Materials and methods

5.3.1 Characterization of MCL relaxation and damping responses

MCLs were dissected and cut free at the insertion sites of N=6 rabbit knees. The geometry was standardized by cutting the ligaments into a dog-bone shape with a length-to-width ratio of 6.8 ± 0.8 (width 1.6 ± 0.2 mm). The tissue samples were affixed to custom-made soft tissue clamps, and the cross-sectional area was determined with a laser micrometer system (1.0 ± 0.3 mm^2). Measurements were taken at three locations along the length of the tissue sample and averaged for stress calculations. Then, the tissue sample-clamp construct was mounted on an Enduratec Elf 3200 testing machine (Bose, Framingham, MA). Reflective markers were placed on the tissue sample to track strain using a Motion Analysis Corporation strain tracking system (Santa Rosa, CA). A heated saline drip was utilized to hydrate the tissue sample and maintain temperature at a constant 37°C. The tissue sample was aligned along the loading axis using an $x - y$ table and then was left unloaded for 30 min to acclimate. A 0.5 MPa pre-stress was placed on the tissue sample and this position served as the starting point for all subsequent tests.

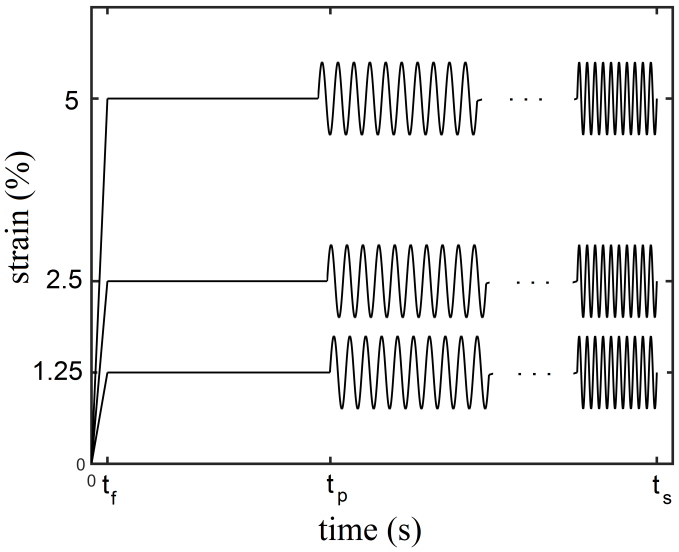

Figure 5.2: Specimens were elongated to one of three baseline strain levels {1.25%, 2.5%, 5%} over an interval of t_p=9.2 s and were then held isometrically for 2100 s as specimens relaxed to a steady state at time t_f. Thereafter, 60 sinusoidal strain perturbations were applied, with cycles 10 at each of six frequencies (0.01, 0.1, 1, 10, 25, and 50 Hz). The sequence of frequencies was randomized.

The subsequent testing protocol (Figures 5.3 and 5.2) began with a ramp to a baseline level of strain ($0 \leq t \leq t_p$, t_p = 9.2 s) followed by an isometric hold of 2100 s ($t_p \leq t \leq t_f$, t_f = 2100 s) at this baseline strain to enable the specimen to reach a steady state stress. Specimens were elongated to three different levels of baseline strain (1.25%, 2.5%, or 5%). Afterwards, the baseline strain level was maintained, and each specimen was subjected to sinusoidal perturbations in strain (amplitude 0.25% strain) at frequencies of $(\omega/2\pi)$ = {0.01 Hz, 0.1 Hz, 1 Hz, 10 Hz, 25 Hz, 50 Hz}. This protocol was repeated for each baseline strain level with 1 hour of recovery between tests at each baseline strain level (Figure 5.2). In addition, the order of testing was randomized for strain level. For each frequency, 10 cycles of stress and strain versus time data were collected following the first 10 cycles of loading and unloading.

5.3.2 Numerical fitting algorithm

The DQLV and QLV models were applied to fit the ramp-hold-sinusoidal loading data. A simple regularizing criterion was used to penalize unwanted states and to ensure that the fitting algorithm did not become trapped in local minima. For the DQLV model, H_i were regularized and identified by minimizing:

$$MSE = \sum_{k=1}^{m} \left(\sigma_k^{(model)} - \sigma_k^{(exp)} \right)^2 + \alpha \sum_{i=1}^{n-1} (H_i - H_{i+1})^2, \tag{5.3.1}$$

where m is the number of data points, $\sigma_k^{(exp)}$ are known stress data or a calculable relationship, α is a regulating factor and $\sigma_k^{(model)}$ is the model estimate of $\sigma_k^{(exp)}$. For the QLV approach, $\alpha = 0$ and $H_i = C$.

As shown in Figure 5.2, the strain profiles were treated as:

$$\epsilon(\omega_l, t_k) = \begin{cases} \gamma t_k & k = 0, 1, 2, ..., p \\ \gamma t_p & k = p+1, p+2, ..., f \\ \gamma t_p + \epsilon_0 \sin(\omega_l t_k) & k = f+1, f+2, ..., q \end{cases} \tag{5.3.2}$$

where p, f and q, respectively, represent the time when the ramp, hold and sinusoidal loading phases are ended, and $(\omega_l/2\pi) = \{0.01$ Hz, 0.1 Hz, 1 Hz, 10 Hz, 25 Hz, 50 Hz$\}$ represents the frequency of sinusoidal loading.

5.3.3 Complex modulus of a DQLV material

Results are presented in terms of complex moduli. After the terms H_i were fit, normalized storage and loss moduli for the DQLV fitting were obtained by substuting Equation (5.2.2)

into Equation (5.2.7):

$$G'(\omega) = \frac{1 + T\sum_{i=1}^{n} H_i \frac{\omega^2\tau_i^2}{1+\omega^2\tau_i^2}}{1 + T\sum_{i=1}^{n} H_i} \qquad \text{and} \qquad G''(\omega) = \frac{T\sum_{i=1}^{n} H_i \frac{\omega\tau_i}{1+\omega^2\tau_i^2}}{1 + T\sum_{i=1}^{n} H_i}. \tag{5.3.3}$$

5.3.4 Statistics

Paired T-tests were performed to assess whether damping was frequency dependent. Responses at six frequencies were compared to each other, and the BenjaminiHochberg procedure was applied to control the false discovery rate at 0.05 Hz [116].

5.4 Results

The stress-relaxation data for rabbit MCLs at the three baseline strain levels of 1.25%, 2.5%, and 5% exhibited a characteristic non-linear rise during stretching, then a gradual decrease to a plateau by ∼1500 s (Figure 5.3). The responses exhibited two hallmarks of non-linear viscoelastic behavior. First, whereas linear viscoelastic models such as the standard linear solid model [52] have linear dashpots that relax the linear proportionality of stress and strain to produce concave-down stress-strain curves, the stress-strain curves for the MCLs were concave up (Figure 5.3). Second, whereas linear viscoelasticity requires that stress levels be proportional to strain levels, the stress peaks were 1.5 MPa, 4.2 MPa and 12.7 MPa, for slow ramps up to 1.25%, 2.5% and 5% strain, respectively.

The DQLV approach was applied to fit ramp-hold-sinusoidal experimental data at the three baseline strain levels using equations (5.3.1) and (5.3.2). The DQLV spectra that approximated the time-dependent properties of the MCLs at 1.25% and 2.5% baseline strain showed four peaks at about $\tau = 0.002$ s, 0.2 s, 20 s and $1000 - 2000$ s (Figure 5.4a). These peaks

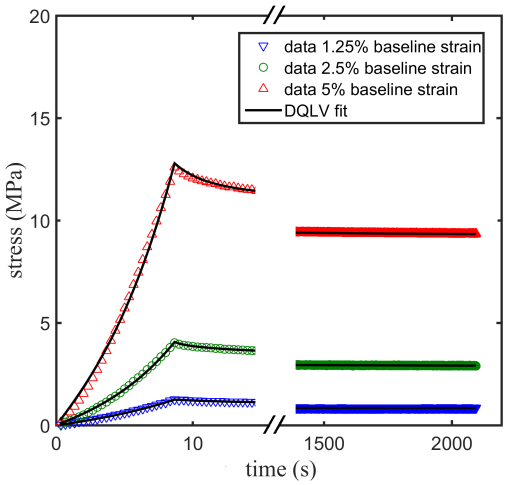

Figure 5.3: Representative data for force relaxation during application of baseline strain. The DQLV fits shown represent the parameter that best fit not only the data for ramp loading and relaxation, but also the subsequent sinusoidal oscillation of the specimens.

shifted slightly with straining, so that at 5% the baseline strain they appeared at about τ 0.001 s, 0.02 s, 20 s and 1000 s (Figure 5.4a).

The QLV approach was also used to fit these data, but the tissue was clearly not a perfect Fung QLV material (Figure 5.4b). The upper estimated time constants (τ_2) were fairly consistent at all three levels of baseline strain, but the damping coefficients, C (plateau level in Figure 5.4b), decreased with strain, and the lower estimated time constants (τ_1) varied non monotonically (Figure 5.4b).

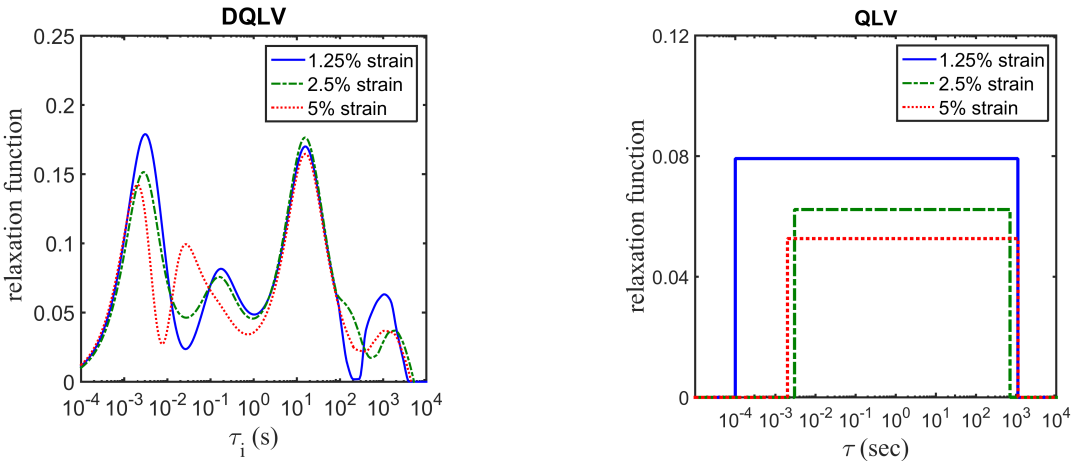

Figure 5.4: Representative DQLV and Fung QLV relaxation spectra of a rabbit MCL specimen (replicate data in the Supplementary document). (a) The DQLV spectra were similar at all three strain levels, a key requirement for application of quasi-linear theory. The spectra showed four dominant peaks (around $\tau = 0.002s, 0.2s, 20s$ and $1000 - 2000s$), which shifted only slightly as a function of strain. (b) The Fung box spectra overstated minor variations of the spectrum with respect to strain, and were not strain independent.

The elastic parameter A and non-linearity parameter B for each strain level, estimated using equation (5.2.2), were similar for QLV and DQLV estimates (Tables 5.1 and 5.2). However, the DQLV fits matched the cyclic strain data more closely than the Fung QLV fits, with the differences most pronounced at the 1 Hz loading (Figure 5.5).

Table 5.1: Estimated elastic parameters using the DQLV model

	1.25 % strain	2.5 % strain	5% strain
A(MPa)	1.505 ± 0.26	2.17 ± 0.31	10.43 ± 1.71
B	56.57 ± 5.4	43.57 ± 7.8	18.22 ± 3.3

Table 5.2: Estimated elastic parameters using the Fung QLV model

	1.25 % strain	2.5 % strain	5% strain
A(MPa)	1.395 ± 0.21	2.31 ± 0.29	11.03 ± 1.89
B	42.62 ± 8.18	37.59 ± 5.81	20.42 ± 8.43

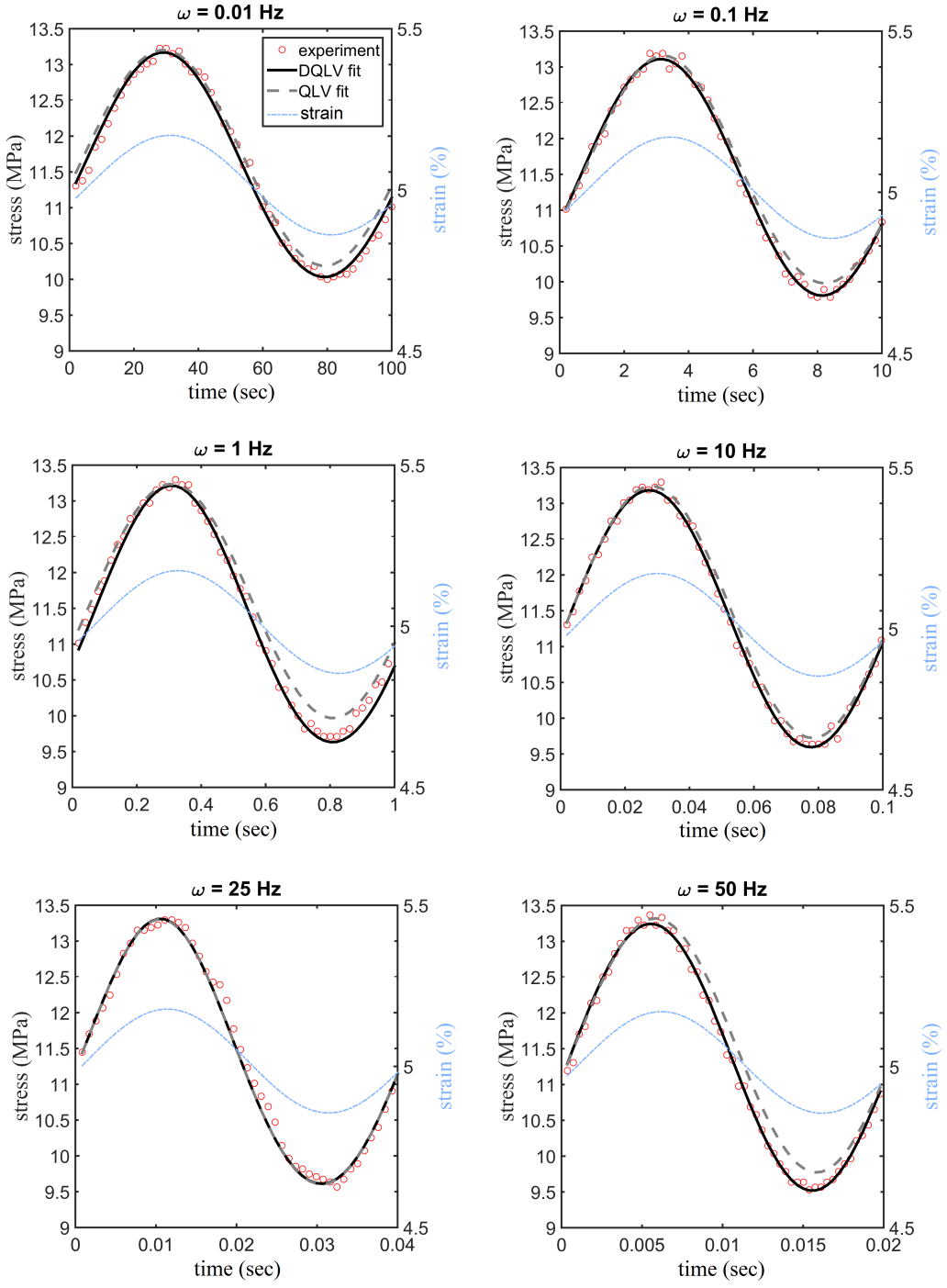

Figure 5.5: Data for the final sinusoidal oscillation of a specimen at each of the six frequencies, with DQLV and QLV fits. The DQLV fit captured the small differences between loading and unloading responses better than the QLV fit.

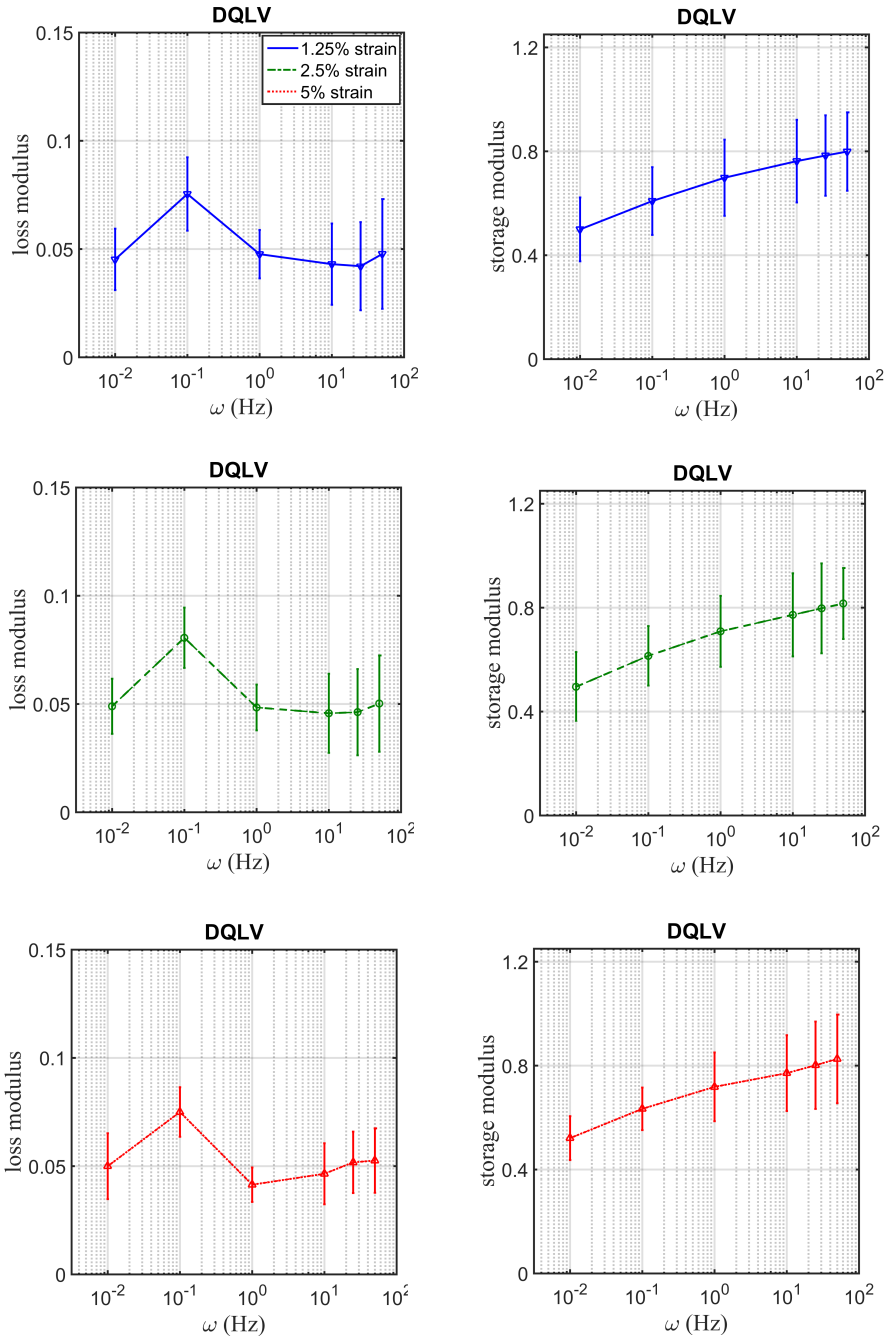

Figure 5.6: Storage and loss moduli obtained using the DQLV fittings of the data. Storage moduli estimated using the DQLV model increased with loading frequency, and did not change significantly as a function of strain. As load increased, more energy was stored in rabbit MCL. Loss moduli estimated using the DQLV model were highest at $\omega/2\pi$=0.1 Hz, indicating that inelastic energy absorption was highest for stretching on the order of tens of seconds.

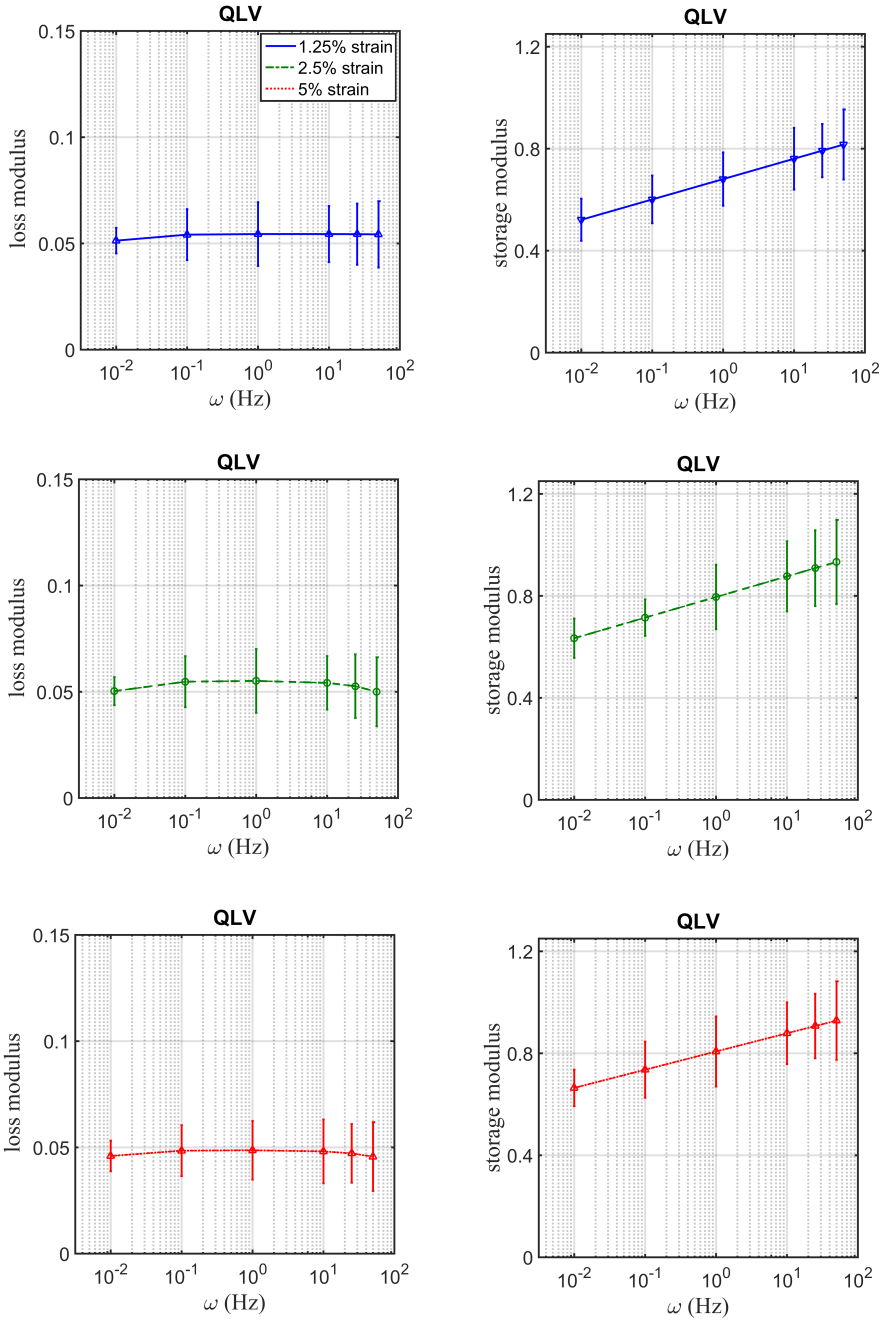

Figure 5.7: Storage and loss moduli obtained using the Fung QLV fittings of the data. Storage moduli estimated using the Fung QLV model were similar to those estimated using the DQLV model. Loss moduli estimated using the Fung QLV model were independent of strain and frequency.

As represented in equations (5.2.8) and (5.3.3), the normalized storage and loss moduli depend on ω and the relaxation spectra (including τ_i, T and H_i). For the DQLV model, the frequency-dependent storage and loss moduli for MCLs at all three baseline strains increased monotonically with respect to frequency from $\omega/2\pi$=0.01 Hz to $\omega/2\pi$= 50 Hz (Figure 5.6, the right column). The loss moduli, however, showed a substantial and statistically significant increase in damping at a frequency of $\omega/2\pi$=0.1 Hz (Figure 5.6, the left column): BenjaminiHochberg tests revealed that the damping response at 0.1 Hz differed substantially from the responses at all other frequencies (BenjaminiHochberg $p < 0.05$ for comparison to 0.01 Hz; BenjaminiHochberg $p < 0.01$ for comparison to all other loading frequencies). The QLV approach predicted a similar monotonic increase in storage modulus (Figure5.7), although for 1.25% baseline strain data, the modulus estimate was about 25% lower than for the 2.5 and 5% baseline strains. The QLV approach predicted a frequency-independent loss modulus at each strain level.

5.5 Discussion

Based on QLV theory, the time-dependent and elastic responses of a viscoelastic material are separable, with nonlinearity arising only from the nonlinear elastic nature of biomaterials. This serves as the workhorse for modeling of viscoelastic biological materials, and is effective in many ways, especially compared to linear viscoelasticity. For example, the definition of complex modulus based upon linear viscoelasticity permits no strain dependence for the frequency response spectrum of a material, and is therefore inappropriate for nearly all biological materials.

However, although it provides a strong foundation, the Fung QLV model is not adequate for identifying the frequency-dependent hysteretic behavior of the MCL at different strain-levels

(Figure 5.4b). The Fung QLV model predicts a constant loss modulus over a wide range of frequencies; that is, it predicts that the hysteresis of a quasi-linear viscoelastic materials is frequency-independent [56]. This is contradicted by many experiments [79, 72, 107, 6]. As shown in Figure 5.4d, the QLV approach predicts a frequency-independent hysteresis for MCLs as well.

The DQLV approach resolves this problem. It identified robust, nearly strain-independent temporal relaxation spectra (Figure 5.4a) and complex moduli (Figures 5.4a and b) from ramp-hold-sinusoidal data in an unbiased way. The more refined relaxation spectra led to substantially improved predictions of the stress versus time responses of the specimens at each strain level (Figure 5.5).

The ramp-hold-sinusoidal protocol analyzed here provided a fuller picture of the relaxation spectra of rabbit MCLs than is available through other means. In an analysis of stress-relaxation data alone for rabbit MCLs presented elsewhere [10], only a portion of the time-dependent material properties were accessible, (over the range of $10^0 < \tau < 10^4$). Here, we showed that by applying high frequency sinusoidal loading, the fast time constants of MCLs can be estimated as well. In other words, high frequency loading excited very fast time constants, which were not detectable in a simple stress-relaxation test.

From the perspective of material damping, the DQLV interpretation of the data revealed an interesting increase in damping at a loading rate of 0.1 Hz. This frequency-dependence of the MCL's mechanical response is not evident in the QLV interpretation, again because the QLV model by its nature enforces a prediction of frequency-independent hysteresis.

Although stretching protocols prior to exercise typically target muscles and tendons rather than ligaments [19], this result is interesting in that it shows increased energy absorption of a collagenous tissue at a critical loading rate of 10s of seconds, which is in the range of loading times recommended for stretching. For example, Bandy et al. [14] showed that the optimal

stretching period for increasing hamstring flexibility is a 30 s cycle. Although a great many hypotheses exist about what stretching accomplishes physiologically for those who subscribe to the hypothesis that permanent rearrangement of collagenous tissues is a beneficial aspect of stretching, the data presented here suggest that loading over 10s of seconds appears to be optimum for applying energy inelastically to such tissues.

5.6 Conclusions

The DQLV approach, when applied to ramp-hold-sinusoidal testing data, provides a robust spectral characterization of rabbit MCL tissues that enable more accurate prediction of mechanical response than the QLV approach. Data show for the first time that the rabbit MCL damped energy most effectively over 10 second loading cycles. These results have implications for stretching protocols prior to athletic events. More broadly, the protocol presented provides a straightforward mechanism for characterizing the high frequency responses of biological tissues, and for overcoming limitations of the Fung QLV model when studying the frequency-dependence of hysteresis.

Chapter 6

Future work

This dissertation proposed a new linear discrete approach to estimate the viscoelastic spectrum of a material from the time variation of isometric force responses in chapter 2, then applied this to perform spectral analysis of engineered tissue constructs in chapter 3. A discrete quasi-linear viscoelastic model was presented in chapters 4 and 5, and applied to analyze the isometric and dynamic time- and frequency-dependent behavior of rabbit medial collateral ligaments. Together, the methods comprise a comprehensive toolbox for the analysis of viscoelastic tissues. However, the work is far from complete, and we suggest several important directions for future studies.

6.1 Dissipation energy and rate dependence in connective materials

Soft tissues that serve a structural role are in continual states of varying static and dynamic tension, compression, and shear. As a result, these structures are constantly under varying degrees of deformation and recovery, and are at constant risk of injury. We developed two models to describe the behavior of connective tissues under ramp-isometric hold loading,

but less is known about two important concepts of a biological tissue system under dynamic loading: (1) instantaneous stress response and (2) energy dissipation. Also, the proportionate response of cells and ECM in a tissue is not well studied. As an example, Figure 6.1 shows decomposed behaviors of ECM and cells in a 3D engineered tissue construct. Although it is widely accepted that almost all biological materials behave nonlinearly, there is no universal method of characterizing or predicting a nonlinear stress response. An important area of future inquiry is the development of protocols for dynamic testing of tissues, such as sinusoidal or saw-tooth strain excitation, to describe linear behavior and non-linear behaviors of connective tissues. These efforts must necessarily incorporate numerical solutions.

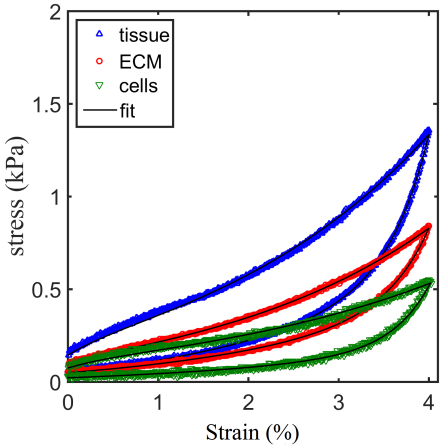

Figure 6.1: Stress response and energy dissipation of tissue, ECM and cells under sawtooth loading.

6.2 A universally adaptable numerical tool for viscoelastic model identification and fitting

Although almost all standard viscoelastic tests are well-developed in theory, they are impractical to some extent. For example in a stress-relaxation test, with a very fast ramp, loadings often overshoot their target deformation or undershoot their target strain rates near the end

of a ramped strain due to inertial effects. Thus, closed-form stress-relaxation models can not predict stress responses of specimens (Figure 6.2(a)). Moreover, predicting viscoelastic responses of connective tissues require a pre-strain, as they often can not undergo both tension and compression in a loading cycle. In practice we need to predict behavior of connective tissues under ramp-hold-sinusoidal loading, which is analytically almost impossible, but a numerical approach can capture material response very well (Figure 6.2(b)). Thus, future work should include a universal viscoelastic model to enable the mechanical characterization of materials under conditions that are not sufficiently described by standard viscoelastic tests.

6.3 Photoacoustic viscoelasticity imaging

Photoacoustic imaging is a mixed imaging method, imaging ultrasounic waves generated by pulsed laser heating. This high optical contrast and resolution method has made great improvements in medical applications such as tumor detection [94, 201], noninvasive monitoring of vasculature networks [205, 198] and brain functional imaging [197, 204, 58]. The common viscoelastic model in photoacoustic viscoelasticity imaging is the Kelvin-Voigt model, a two-element model including a spring and dashpot in parallel. Although the Kelvin-Voigt model is simple and facilitates material property estimation, application of this model could be disadvantageous because the simplifications it requires may mask information relevant to the characterization of intrinsic time- and frequency-dependent material properties. We suggest the generalized Maxwell model instead to identify local spectral viscoelastic properties at regions of interest within biological tissues.

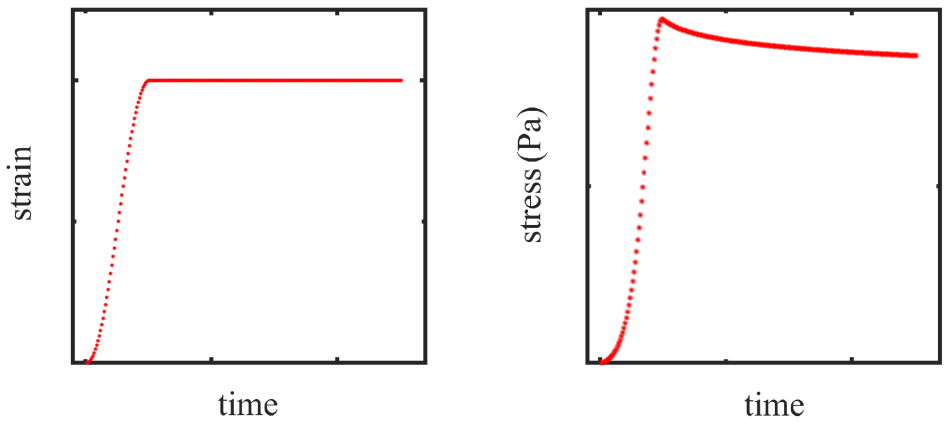

(a)

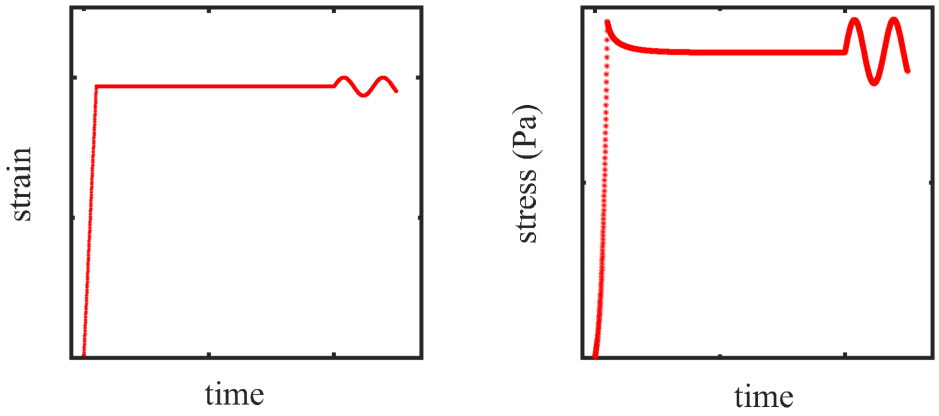

(b)

Figure 6.2: A universal viscoelastic model can predict uncommon perturbations. (a) Response of a material to under-shooting of strain in a stress-relaxation test. (b) Response of a material to sequential ramp-hold-sinusoidal excitation.

Bibliography

[1] AS Abhilash, Brendon M Baker, Britta Trappmann, Christopher S Chen, and Vivek B Shenoy. Remodeling of fibrous extracellular matrices by contractile cells: Predictions from discrete fiber network simulations. *Biophysical journal*, 107(8):1829–1840, 2014.

[2] Steven D Abramowitch and Savio L-Y Woo. An improved method to analyze the stress relaxation of ligaments following a finite ramp time based on the quasi-linear viscoelastic theory. *Journal of biomechanical engineering*, 126(1):92–97, 2004.

[3] Steven D Abramowitch, Savio LY Woo, Theodore D Clineff, and Richard E Debski. An evaluation of the quasi-linear viscoelastic properties of the healing medial collateral ligament in a goat model. *Ann. Biomed. Eng.*, 32(3):329–335, 2004.

[4] Steven D Abramowitch, Savio LY Woo, Theodore D Clineff, and Richard E Debski. An evaluation of the quasi-linear viscoelastic properties of the healing medial collateral ligament in a goat model. *Annals of biomedical engineering*, 32(3):329–335, 2004.

[5] Steven D Abramowitch, Xiaoyan Zhang, Molly Curran, and Robert Kilger. A comparison of the quasi-static mechanical and non-linear viscoelastic properties of the human semitendinosus and gracilis tendons. *Clinical Biomechanics*, 25(4):325–331, 2010.

[6] D Ron Anderson, Savio L-Y Woo, Michael K Kwan, and David H Gershuni. Viscoelastic shear properties of the equine medial meniscus. *Journal of orthopaedic research*, 9(4):550–558, 1991.

[7] Elizabeth E Antoine, Pavlos P Vlachos, and Marissa Nichole Rylander. Review of collagen i hydrogels for bioengineered tissue microenvironments: characterization of mechanics, structure, and transport. *Tissue Eng. Part B Rev.*, 20(6):683–696, 2014.

[8] Kristy B Arbogast and Susan S Margulies. Material characterization of the brainstem from oscillatory shear tests. *J. Biomech.*, 31(9):801–807, 1998.

[9] H Ashrafi and M Shariyat. A nano-indentation identification technique for viscoelastic constitutive characteristics of periodontal ligaments. *Journal of Biomedical Physics and Engineering*, 2015.

[10] Behzad Babaei, Steven D Abramowitch, Elliot L Elson, Stavros Thomopoulos, and Guy M Genin. A discrete spectral analysis for determining quasi-linear viscoelastic properties of biological materials. *Journal of The Royal Society Interface*, 12(113):20150707, 2015.

[11] Behzad Babaei, Ali Davarian, Sheng-Lin Lee, Kenneth M Pryse, William B McConnaughey, Elliot L Elson, and Guy M Genin. Remodeling by fibroblasts alters the rate-dependent mechanical properties of collagen. *Acta Biomaterialia*, 2016.

[12] Behzad Babaei, Ali Davarian, Kenneth M Pryse, Elliot L Elson, and Guy M Genin. Efficient and optimized identification of generalized maxwell viscoelastic relaxation spectra. *Journal of the mechanical behavior of biomedical materials*, 55:32–41, 2015.

[13] Brendon M Baker, Britta Trappmann, William Y Wang, Mahmut S Sakar, Iris L Kim, Vivek B Shenoy, Jason A Burdick, and Christopher S Chen. Cell-mediated fibre recruitment drives extracellular matrix mechanosensing in engineered fibrillar microenvironments. *Nature materials*, 2015.

[14] William D Bandy, Jean M Irion, and Michelle Briggler. The effect of time and frequency of static stretching on flexibility of the hamstring muscles. *Physical therapy*, 77(10):1090–1096, 1997.

[15] Romina B Barello and Martin Lévesque. Comparison between the relaxation spectra obtained from homogenization models and finite elements simulation for the same composite. *International Journal of Solids and structures*, 45(3):850–867, 2008.

[16] Victor H Barocas, Alice G Moon, and Robert T Tranquillo. The fibroblast-populated collagen microsphere assay of cell traction force. part 2: Measurement of the cell traction parameter. *Journal of biomechanical engineering*, 117(2):161–170, 1995.

[17] Victor H Barocas and Robert T Tranquillo. An anisotropic biphasic theory of tissue-equivalent mechanics: the interplay among cell traction, fibrillar network deformation, fibril alignment, and cell contact guidance. *Journal of biomechanical engineering*, 119(2):137–145, 1997.

[18] Jörg Baschnagel. *Viscoelasticity Atomistic Models Statistical Chemistry*, volume 152. Springer Berlin Heidelberg, 2000.

[19] David G Behm and Anis Chaouachi. A review of the acute effects of static and dynamic stretching on performance. *European journal of applied physiology*, 111(11):2633–2651, 2011.

[20] Eugene Bell, Bengt Ivarsson, and Charlotte Merrill. Production of a tissue-like structure by contraction of collagen lattices by human fibroblasts of different proliferative potential in vitro. *Proceedings of the National Academy of Sciences*, 76(3):1274–1278, 1979.

[21] Rasmus Bro and Sijmen De Jong. A fast non-negativity-constrained least squares algorithm. *J. Chemom.*, 11(5):393–401, 1997.

[22] Markus J Buehler and Guy M Genin. Integrated multiscale biomaterials experiment and modelling: a perspective. *Interface Focus*, 6(1):20150098, 2016.

[23] SA Carp, Juliette Selb, Qianqian Fang, Richard Moore, DB Kopans, Elizabeth Rafferty, and DA Boas. Dynamic functional and mechanical response of breast tissue to compression. *Opt. Express*, 16(20):16064–16078, 2008.

[24] Ryan M Castile, Nathan W Skelley, Behzad Babaei, Robert H Brophy, and Spencer P Lake. Microstructural properties and mechanics vary between bundles of the human anterior cruciate ligament during stress-relaxation. *Journal of biomechanics*, 2015.

[25] George E Chapman, Steven S Danyluk, and KA McLauchlan. A model for collagen hydration. *Proceedings of the Royal Society of London B: Biological Sciences*, 178(1053):465–476, 1971.

[26] Shigao Chen, William Sanchez, Matthew R Callstrom, Brian Gorman, Jason T Lewis, Schuyler O Sanderson, James F Greenleaf, Hua Xie, Yan Shi, Michael Pashley, et al. Assessment of liver viscoelasticity by using shear waves induced by ultrasound radiation force. *Radiology*, 266(3):964–970, 2013.

[27] Matthias Chiquet, Ana Sarasa Renedo, François Huber, and Martin Flück. How do fibroblasts translate mechanical signals into changes in extracellular matrix production? *Matrix biology*, 22(1):73–80, 2003.

[28] Jacopo Ciambella, Michel Destrade, and Ray W Ogden. On the abaqus fea model of finite viscoelasticity. *Rubber Chemistry and Technology*, 82(2):184–193, 2009.

[29] Neil T. Clancy, Gert E. Nilsson, Chris D. Anderson, and Martin J. Leahy. A new device for assessing changes in skin viscoelasticity using indentation and optical measurement. *Skin Res. Technol.*, 16(2):210–228, 2010.

[30] Ivan E Collier, Wesley Legant, Barry Marmer, Olga Lubman, Saveez Saffarian, Tetsuro Wakatsuki, Elliot Elson, and Gregory I Goldberg. Diffusion of mmps on the surface of collagen fibrils: the mobile cell surface-collagen substratum interface. *PLoS One*, 6(9):e24029–e24029, 2011.

[31] Bruno Corman, Micheline Duriez, Pierre Poitevin, Didier Heudes, Patrick Bruneval, Alain Tedgui, and Bernard I Levy. Aminoguanidine prevents age-related arterial stiffening and cardiac hypertrophy. *Proceedings of the National Academy of Sciences*, 95(3):1301–1306, 1998.

[32] Bruno Corman, Micheline Duriez, Pierre Poitevin, Didier Heudes, Patrick Bruneval, Alain Tedgui, and Bernard I Levy. Proc. natl. acad. sci. u.s.a. *Proc. Natl. Acad. Sci. U.S.A.*, 95(3):1301–1306, 1998.

[33] Damian Craiem, Francisco J Rojo, José Miguel Atienza, Ricardo L Armentano, and Gustavo V Guinea. Fractional-order viscoelasticity applied to describe uniaxial stress relaxation of human arteries. *Physics in medicine and biology*, 53(17):4543, 2008.

[34] Nathalie Cuissard, Jacques Duchateau, and Karl Hainaut. Muscle stretching and motoneuron excitability. *European Journal of Applied Physiology and Occupational Physiology*, 58(1-2):47–52, 1988.

[35] Rumi De, Assaf Zemel, and Samuel A Safran. Dynamics of cell orientation. *Nature Physics*, 3(9):655–659, 2007.

[36] Riccardo De Pascalis, I David Abrahams, and William J Parnell. On nonlinear viscoelastic deformations: a reappraisal of fung's quasi-linear viscoelastic model. *Proceedings of the Royal Society of London A: Mathematical, Physical and Engineering Sciences*, 470(2166):20140058, 2014.

[37] Riccardo De Pascalis, I David Abrahams, and William J Parnell. On nonlinear viscoelastic deformations: a reappraisal of fung's quasi-linear viscoelastic model. In *Proceedings of the Royal Society of London A: Mathematical, Physical and Engineering Sciences*, volume 470, page 20140058. The Royal Society, 2014.

[38] James W. Demmel. *Applied Numerical Linear Algebra*. Society for Industrial and Applied Mathematics, Philadelphia, PA, USA, 1997.

[39] Todd C Doehring, Evelyn O Carew, and Ivan Vesely. The effect of strain rate on the viscoelastic response of aortic valve tissue: a direct-fit approach. *Annals of Biomedical Engineering*, 32(2):223–232, 2004.

[40] Todd C Doehring, Evelyn O Carew, and Ivan Vesely. The effect of strain rate on the viscoelastic response of aortic valve tissue: a direct-fit approach. *Annals of Biomedical Engineering*, 32(2):223–232, 2004.

[41] NG Dong, XF Ye, ZQ Sun, JW Shi, YM Qiu, and JJ Chen. [experimental study on mechanical properties of decellularized porcine aortic valve and effects of precoating methods of biological scaffold on histocompatibility]. *Zhonghua wai ke za zhi [Chinese journal of surgery]*, 45(16):1128–1131, 2007.

[42] LJMG Dortmans, AAHJ Sauren, and EPM Rousseau. Parameter estimation using the quasi-linear viscoelastic model proposed by fung. *Journal of biomechanical engineering*, 106(3):198–203, 1984.

[43] LJMG Dortmans, AAHJ Sauren, and EPM Rousseau. Parameter estimation using the quasi-linear viscoelastic model proposed by fung. *Journal of biomechanical engineering*, 106(3):198–203, 1984.

[44] Lorna Edelsten, Janet E Jeffrey, Leanne V Burgin, and Richard M Aspden. Viscoelastic deformation of articular cartilage during impact loading. *Soft Matter*, 6(20):5206–5212, 2010.

[45] EL Elson and GM Genin. The role of mechanics in actin stress fiber kinetics. *Experimental cell research*, 319(16):2490–2500, 2013.

[46] Elliot L Elson and Guy M Genin. Tissue constructs: platforms for basic research and drug discovery. *Interface Focus*, 6(1):20150095, 2016.

[47] Igor Emri and Nicholas W Tschoegl. Generating line spectra from experimental responses. *Rheologica acta*, 36(3):303–306, 1997.

[48] Michael C Evans and Victor H Barocas. The modulus of fibroblast-populated collagen gels is not determined by final collagen and cell concentration: experiments and an inclusion-based model. *Journal of biomechanical engineering*, 131(10):101014, 2009.

[49] Fei Fang, Amrita S Sawhney, and Spencer P Lake. Different regions of bovine deep digital flexor tendon exhibit distinct elastic, but not viscous, mechanical properties under both compression and shear loading. *J. Biomech.*, 47(12):2869–2877, 2014.

[50] Z Feng, M Yamato, T Akutsu, T Nakamura, T Okano, and M Umezu. Investigation on the mechanical properties of contracted collagen gels as a scaffold for tissue engineering. *Artificial organs*, 27(1):84–91, 2003.

[51] John D Ferry. *Viscoelastic properties of polymers*. John Wiley & Sons, 1980.

[52] William N Findley and Francis A Davis. *Creep and relaxation of nonlinear viscoelastic materials*. Courier Corporation, 2013.

[53] Peter Fratzl. *Collagen: structure and mechanics, an introduction*. Springer, 2008.

[54] Harold J Frost and Michael F Ashby. *Deformation mechanism maps: the plasticity and creep of metals and ceramics*. Pergamon press, Oxford, UK, 1982.

[55] Yuan-Cheng Fung. *Biomechanics: mechanical properties of living tissues*. Springer Science & Business Media, 2013.

[56] Yuan-Cheng Fung, Nicholas Perrone, Max Anliker, et al. Biomechanics, its foundations and objectives. In *Symposium on Biomechanics, its Foundations and Objectives (1970: University of California, San Diego)*. NJ, Prentice-Hall, 1972.

[57] Maurizio Galderisi. Diastolic dysfunction and diabetic cardiomyopathy: evaluation by doppler echocardiography. *Journal of the American College of Cardiology*, 48(8):1548–1551, 2006.

[58] Guodong Gao, Sihua Yang, and Da Xing. Viscoelasticity imaging of biological tissues with phase-resolved photoacoustic measurement. *Optics letters*, 36(17):3341–3343, 2011.

[59] Alfonso Gautieri, Monica I Pate, Simone Vesentini, Alberto Redaelli, and Markus J Buehler. Hydration and distance dependence of intermolecular shearing between collagen molecules in a model microfibril. *Journal of biomechanics*, 45(12):2079–2083, 2012.

[60] Alfonso Gautieri, Simone Vesentini, Franco M Montevecchi, and Alberto Redaelli. Mechanical properties of physiological and pathological models of collagen peptides investigated via steered molecular dynamics simulations. *Journal of biomechanics*, 41(14):3073–3077, 2008.

[61] Alfonso Gautieri, Simone Vesentini, Alberto Redaelli, and Markus J Buehler. Hierarchical structure and nanomechanics of collagen microfibrils from the atomistic scale up. *Nano letters*, 11(2):757–766, 2011.

[62] Alfonso Gautieri, Simone Vesentini, Alberto Redaelli, and Markus J Buehler. Viscoelastic properties of model segments of collagen molecules. *Matrix Biology*, 31(2):141–149, 2012.

[63] Guy M Genin and Elliot L Elson. Mechanically guided cell migration: Less of a stretch than ever. *Biophysical journal*, 106(4):776, 2014.

[64] Guy M Genin and Elliot L Elson. Mechanics of cell-seeded ecm scaffolds. *Cell and Matrix Mechanics*, page 173, 2014.

[65] Guy M Genin, Alistair Kent, Victor Birman, Brigitte Wopenka, Jill D Pasteris, Pablo J Marquez, and Stavros Thomopoulos. Functional grading of mineral and collagen in the attachment of tendon to bone. *Biophysical journal*, 97(4):976–985, 2009.

[66] Jonathan A Gimbel, Joseph J Sarver, and Louis J Soslowsky. The effect of overshooting the target strain on estimating viscoelastic properties from stress relaxation experiments. *Journal of biomechanical engineering*, 126(6):844–848, 2004.

[67] Helen K Graham, Riaz Akhtar, Constantinos Kridiotis, Brian Derby, Tribikram Kundu, Andrew W Trafford, and Michael J Sherratt. Localised micro-mechanical stiffening in the ageing aorta. *Mech. Ageing Dev.*, 132(10):459–467, 2011.

[68] Farshid Guilak, John R Tedrow, and Rainer Burgkart. Viscoelastic properties of the cell nucleus. *Biochem. Biophys. Res. Commun.*, 269(3):781–786, 2000.

[69] Namrata Gundiah, Kimberly Kam, Peter B Matthews, Julius Guccione, Harry A Dwyer, David Saloner, Timothy AM Chuter, T Sloane Guy, Mark B Ratcliffe, and Elaine E Tseng. Asymmetric mechanical properties of porcine aortic sinuses. *The Annals of thoracic surgery*, 85(5):1631–1638, 2008.

[70] HS Gupta, J Seto, S Krauss, P Boesecke, and HRC Screen. In situ multi-level analysis of viscoelastic deformation mechanisms in tendon collagen. *Journal of structural biology*, 169(2):183–191, 2010.

[71] Lazarina Gyoneva, Carley B Hovell, Ryan J Pewowaruk, Kevin D Dorfman, Yoav Segal, and Victor H Barocas. Cell–matrix interaction during strain-dependent remodelling of simulated collagen networks. *Interface Focus*, 6(1):20150069, 2016.

[72] Hamed Hatami-Marbini and Abdolrasol Rahimi. Collagen cross-linking treatment effects on corneal dynamic biomechanical properties. *Experimental eye research*, 135:88–92, 2015.

[73] Roger C Haut. The influence of specimen length on the tensile failure properties of tendon collagen. *Journal of biomechanics*, 19(11):951–955, 1986.

[74] A Robert Hillman, Igor Efimov, and Karl S Ryder. Time-scale-and temperature-dependent mechanical properties of viscoelastic poly (3, 4-ethylenedioxythiophene) films. *J. Am. Chem. Soc.*, 127(47):16611–16620, 2005.

[75] Jeffrey W Holmes, Zachary Laksman, and Lior Gepstein. Making better scar: Emerging approaches for modifying mechanical and electrical properties following infarction and ablation. *Progress in Biophysics and Molecular Biology*, 2015.

[76] J. Honerkamp. Ill-posed problems in rheology. *Rheol. Acta*, 28(5):363–371, 1989.

[77] Paul A Hough, Emma Z Ross, and Glyn Howatson. Effects of dynamic and static stretching on vertical jump performance and electromyographic activity. *The Journal of Strength & Conditioning Research*, 23(2):507–512, 2009.

[78] Anna Huttenlocher and Alan Rick Horwitz. Integrins in cell migration. *Cold Spring Harbor perspectives in biology*, 3(9):a005074, 2011.

[79] James C Iatridis, Lori A Setton, Mark Weidenbaum, and Van C Mow. The viscoelastic behavior of the non-degenerate human lumbar nucleus pulposus in shear. *Journal of biomechanics*, 30(10):1005–1013, 1997.

[80] Bernadine D Idowu, Martin M Knight, Dan L Bader, and David A Lee. Confocal analysis of cytoskeletal organisation within isolated chondrocyte sub-populations cultured in agarose. *The Histochemical journal*, 32(3):165–174, 2000.

[81] Karin A Jansen, Rommel G Bacabac, Izabela K Piechocka, and Gijsje H Koenderink. Cells actively stiffen fibrin networks by generating contractile stress. *Biophysical journal*, 105(10):2240–2251, 2013.

[82] Martins Kalejs, Peteris Stradins, Romans Lacis, Iveta Ozolanta, Janis Pavars, and Vladimir Kasyanov. St jude epic heart valve bioprostheses versus native human and porcine aortic valves–comparison of mechanical properties. *Interactive cardiovascular and thoracic surgery*, 8(5):553–556, 2009.

[83] VM Kamath and MR Mackley. The determination of polymer relaxation moduli and memory functions using integral transforms. *Journal of non-newtonian fluid mechanics*, 32(2):119–144, 1989.

[84] D Karamichos, RA Brown, and V Mudera. Collagen stiffness regulates cellular contraction and matrix remodeling gene expression. *Journal of Biomedical Materials Research Part A*, 83(3):887–894, 2007.

[85] Joachim Kaschta and Florian J Stadler. Avoiding waviness of relaxation spectra. *Rheologica acta*, 48(6):709–713, 2009.

[86] R M Kenedi, T Gibson, and C H Daly. *Biomechanics and related bioengineering topics*, chapter Bio-engineering studies of the human skin II. Oxford: Pergamon Press, 1965.

[87] Virginia C. Klema and Alan J. Laub. The Singular Value Decomposition: Its Computation and Some Applications. *IEEE Trans. Autom. Control*, 1980.

[88] David M Knapp, Theodore T Tower, Robert T Tranquillo, and Victor H Barocas. Estimation of cell traction and migration in an isometric cell traction assay. *AIChE journal*, 45(12):2628–2640, 1999.

[89] MM Knight, DA Lee, and DL Bader. The influence of elaborated pericellular matrix on the deformation of isolated articular chondrocytes cultured in agarose. *Biochimica et Biophysica Acta (BBA)-Molecular Cell Research*, 1405(1):67–77, 1998.

[90] MM Knight, JM Ross, AF Sherwin, DA Lee, DL Bader, and CA Poole. Chondrocyte deformation within mechanically and enzymatically extracted chondrons compressed in agarose. *Biochimica et Biophysica Acta (BBA)-General Subjects*, 1526(2):141–146, 2001.

[91] M Kohandel, S Sivaloganathan, and G Tenti. Estimation of the quasi-linear viscoelastic parameters using a genetic algorithm. *Mathematical and Computer Modelling*, 47(3):266–270, 2008.

[92] Sanjay Kumar, Iva Z Maxwell, Alexander Heisterkamp, Thomas R Polte, Tanmay P Lele, Matthew Salanga, Eric Mazur, and Donald E Ingber. Viscoelastic retraction of single living stress fibers and its impact on cell shape, cytoskeletal organization, and extracellular matrix mechanics. *Biophysical journal*, 90(10):3762–3773, 2006.

[93] Michael K Kwan, Timothy HC Lin, and Savio LY Woo. On the viscoelastic properties of the anteromedial bundle of the anterior cruciate ligament. *Journal of biomechanics*, 26(4):447–452, 1993.

[94] Yeqi Lao, Da Xing, Sihua Yang, and Liangzhong Xiang. Noninvasive photoacoustic imaging of the developing vasculature during early tumor growth. *Physics in medicine and biology*, 53(15):4203, 2008.

[95] C. L. Lawson and R. J. Hanson. Solving least squares problems. In C. L. Lawson and R. J. Hanson, editors, *Prentice-Hall Series in Automatic Computation, Englewood Cliffs: Prentice-Hall, 1974*, pages 1–337. 3 edition, 1995.

[96] Sheng-Lin Lee, Ali Nekouzadeh, Boyd Butler, Kenneth M Pryse, William B McConnaughey, Adam C Nathan, Wesley R Legant, Pascal M Schaefer, Robert B Pless, Elliot L Elson, et al. Physically-induced cytoskeleton remodeling of cells in three-dimensional culture. *PloS one*, 7(12):e45512, 2012.

[97] Sheng-Lin Lee, Ali Nekouzadeh, Boyd Butler, Kenneth M Pryse, William B McConnaughey, Adam C Nathan, Wesley R Legant, Pascal M Schaefer, Robert B Pless, Elliot L Elson, et al. Physically-induced cytoskeleton remodeling of cells in three-dimensional culture. *PloS one*, 7(12):e45512, 2012.

[98] Sheng-Lin Lee, Ali Nekouzadeh, Boyd Butler, Kenneth M Pryse, William B McConnaughey, Adam C Nathan, Wesley R Legant, Pascal M Schaefer, Robert B Pless, Elliot L Elson, and GM Genin. Physically-induced cytoskeleton remodeling of cells in three-dimensional culture. *PloS one*, 7(12):e45512, 2012.

[99] Thay Q Lee and Savio LY Woo. A new method for determining cross-sectional shape and area of soft tissues. *Journal of biomechanical engineering*, 110(2):110–114, 1988.

[100] Wesley R Legant, Jordan S Miller, Brandon L Blakely, Daniel M Cohen, Guy M Genin, and Christopher S Chen. Measurement of mechanical tractions exerted by cells in three-dimensional matrices. *Nature methods*, 7(12):969–971, 2010.

[101] Catherine A Lemarié, Pierre-Louis Tharaux, and Stéphanie Lehoux. Extracellular matrix alterations in hypertensive vascular remodeling. *Journal of molecular and cellular cardiology*, 48(3):433–439, 2010.

[102] Jun Liao, Erinn M Joyce, and Michael S Sacks. Effects of decellularization on the mechanical and structural properties of the porcine aortic valve leaflet. *Biomaterials*, 29(8):1065–1074, 2008.

[103] Yanxin Liu, Andrea G Schwartz, Victor Birman, Stavros Thomopoulos, and Guy M Genin. Stress amplification during development of the tendon-to-bone attachment. *Biomechanics and modeling in mechanobiology*, 13(5):973–983, 2014.

[104] Yanxin Liu, Stavros Thomopoulos, Changqing Chen, Victor Birman, Markus J Buehler, and Guy M Genin. Modelling the mechanics of partially mineralized collagen fibrils, fibres and tissue. *Journal of The Royal Society Interface*, 11(92):20130835, 2014.

[105] Fl J Lockett. *Nonlinear viscoelastic solids*. Academic Press, 1972.

[106] Pengfei Lu, Ken Takai, Valerie M Weaver, and Zena Werb. Extracellular matrix degradation and remodeling in development and disease. *Cold Spring Harbor perspectives in biology*, 3(12):a005058, 2011.

[107] Trevor J Lujan, Clayton J Underwood, Nathan T Jacobs, and Jeffrey A Weiss. Contribution of glycosaminoglycans to viscoelastic tensile behavior of human ligament. *Journal of Applied Physiology*, 106(2):423–431, 2009.

[108] C Machiraju, A-V Phan, AW Pearsall, and S Madanagopal. Viscoelastic studies of human subscapularis tendon: Relaxation test and a wiechert model. *Comput. Methods Programs Biomed.*, 83(1):29–33, 2006.

[109] Akiko Mammoto, Tadanori Mammoto, Mathumai Kanapathipillai, Chong Wing Yung, Elisabeth Jiang, Amanda Jiang, Kristopher Lofgren, Elaine PS Gee, and Donald E Ingber. Control of lung vascular permeability and endotoxin-induced pulmonary oedema by changes in extracellular matrix mechanics. *Nature communications*, 4:1759, 2013.

[110] J Pablo Marquez, Elliot L Elson, and Guy M Genin. Whole cell mechanics of contractile fibroblasts: relations between effective cellular and extracellular matrix moduli. *Philosophical Transactions of the Royal Society of London A: Mathematical, Physical and Engineering Sciences*, 368(1912):635–654, 2010.

[111] J Pablo Marquez, Guy M Genin, and Elliot L Elson. On the application of strain factors for approximation of the contribution of anisotropic cells to the mechanics of a tissue construct. *Journal of biomechanics*, 39(11):2145–2151, 2006.

[112] J Pablo Marquez, Guy M Genin, Kenneth M Pryse, and Elliot L Elson. Cellular and matrix contributions to tissue construct stiffness increase with cellular concentration. *Annals of biomedical engineering*, 34(9):1475–1482, 2006.

[113] J Pablo Marquez, Guy M Genin, George I Zahalak, and Elliot L Elson. The relationship between cell and tissue strain in three-dimensional bio-artificial tissues. *Biophysical journal*, 88(2):778–789, 2005.

[114] J Pablo Marquez, Guy M Genin, George I Zahalak, and Elliot L Elson. Thin bio-artificial tissues in plane stress: the relationship between cell and tissue strain, and an improved constitutive model. *Biophysical journal*, 88(2):765–777, 2005.

[115] Dennis P McDaniel, Gordon A Shaw, John T Elliott, Kiran Bhadriraju, Curt Meuse, Koo-Hyun Chung, and Anne L Plant. The stiffness of collagen fibrils influences vascular smooth muscle cell phenotype. *Biophysical journal*, 92(5):1759–1769, 2007.

[116] John H McDonald. *Handbook of biological statistics*, volume 2. Sparky House Publishing Baltimore, MD, 2009.

[117] Inés G Mogilner, Graciela Ruderman, and J Raúl Grigera. Collagen stability, hydration and native state. *Journal of molecular Graphics and Modelling*, 21(3):209–213, 2002.

[118] Zachary D Molacek, Donovan S Conley, Tammy K Evetovich, and Kristi R Hinnerichs. Effects of low-and high-volume stretching on bench press performance in collegiate football players. *The Journal of Strength & Conditioning Research*, 24(3):711–716, 2010.

[119] Daniel K Moon, Savio LY Woo, Yoshiyuki Takakura, Mary T Gabriel, and Steven D Abramowitch. The effects of refreezing on the viscoelastic and tensile properties of ligaments. *Journal of biomechanics*, 39(6):1153–1157, 2006.

[120] Justin R Murphy, Mario C Di Santo, Thamir Alkanani, and David G Behm. Aerobic activity before and following short-duration static stretching improves range of motion and performance vs. a traditional warm-up. *Applied Physiology, Nutrition, and Metabolism*, 35(5):679–690, 2010.

[121] Volker Musahl, Steven D Abramowitch, Mary T Gabriel, Richard E Debski, Peter Hertel, Freddie H Fu, and Savio LY Woo. Tensile properties of an anterior cruciate ligament graft after bone–patellar tendon–bone press-fit fixation. *Knee Surgery, Sports Traumatology, Arthroscopy*, 11(2):68–74, 2003.

[122] Volker Musahl, Steven D Abramowitch, Thomas W Gilbert, Eiichi Tsuda, James H-C Wang, Stephen F Badylak, and Savio L-Y Woo. The use of porcine small intestinal submucosa to enhance the healing of the medial collateral ligamenta functional tissue engineering study in rabbits. *Journal of Orthopaedic Research*, 22(1):214–220, 2004.

[123] Abhilash Nair, Brendon M Baker, Britta Trappmann, Christopher S Chen, and Vivek B Shenoy. Remodeling of fibrous extracellular matrices by contractile cells: Predictions from discrete fiber network simulations. *arXiv preprint arXiv:1409.6216*, 2014.

[124] Ali Nekouzadeh, Guy M Genin, Philip V Bayly, and Elliot L Elson. Proc. r. soc. a. *Proceedings of the Royal Society of London A: Mathematical, Physical and Engineering Sciences*, 461(2058):1599–1626, 2005.

[125] Ali Nekouzadeh, Kenneth M Pryse, Elliot L Elson, and Guy M Genin. A simplified approach to quasi-linear viscoelastic modeling. *Journal of biomechanics*, 40(14):3070–3078, 2007.

[126] Ali Nekouzadeh, Kenneth M Pryse, Elliot L Elson, and Guy M Genin. A simplified approach to quasi-linear viscoelastic modeling. *J. Biomech.*, 40(14):3070–3078, 2007.

[127] Ali Nekouzadeh, Kenneth M Pryse, Elliot L Elson, and Guy M Genin. Stretch-activated force shedding, force recovery, and cytoskeletal remodeling in contractile fibroblasts. *Journal of biomechanics*, 41(14):2964–2971, 2008.

[128] CP Neu and GM Genin. *Handbook of imaging in biological mechanics*. Boca Raton, FL: CRC Press, 2014.

[129] HKP Neubert. A simple model representing internal damping in solid materials(frequency of stiffness variation determined by mathematical model representing basic characteristics of internal damping in solid materials). *Aeronautical Quarterly*, 14:187–210, 1963.

[130] TD Nguyen, RE Jones, and BL Boyce. A nonlinear anisotropic viscoelastic model for the tensile behavior of the corneal stroma. *Journal of biomechanical engineering*, 130(4):041020, 2008.

[131] Mark A Nicosia, Jeffrey S Kasalko, Richard P Cochran, Daniel R Einstein, and Karyn S Kunzelman. Biaxial mechanical properties of porcine ascending aortic wall tissue. *The Journal of heart valve disease*, 11(5):680–6, 2002.

[132] I Nigul and U Nigul. On algorithms of evaluation of fung's relaxation function parameters. *Journal of Biomechanics*, 20(4):343–352, 1987.

[133] Siobhan A O'Leary, Barry J Doyle, and Tim M McGloughlin. The impact of long term freezing on the mechanical properties of porcine aortic tissue. *Journal of the mechanical behavior of biomedical materials*, 37:165–173, 2014.

[134] K. Osaki. Viscoelastic properties of dilute polymer solutions. In *Fortschritte der Hochpolymeren-Forschung*, volume 12 of *Advances in Polymer Science*, pages 1–64. Springer Berlin Heidelberg, 1973.

[135] S Ottani, G Pezzin, and C Castellari. An investigation of the viscoelastic properties of molten polypropylene. *Rheologica acta*, 27(2):137–144, 1988.

[136] Alan J Pearce, Dawson J Kidgell, James Zois, and John S Carlson. Effects of secondary warm up following stretching. *European journal of applied physiology*, 105(2):175–183, 2009.

[137] S Pittaccio, F Migliavacca, V Hjordtal, M Smerup, ET Fründ, T Villa, E Morre-Pedersen, and MR De Leval. Aortic tissue properties in porcine models: a comparison of ex vivo mechanical test results after simulated aortic arch reconstructions. *Journal of Applied Biomaterials & Biomechanics*, 3(3):147–156, 2005.

[138] Rita T Prajapati, Mark Eastwood, and Robert A Brown. Duration and orientation of mechanical loads determine fibroblast cyto-mechanical activation: Monitored by protease release. *Wound repair and regeneration*, 8(3):238–246, 2000.

[139] Stephen W Provencher. A constrained regularization method for inverting data represented by linear algebraic or integral equations. *Comput. Phys. Commun.*, 27(3):213–227, 1982.

[140] Stephen W Provencher. Contin: a general purpose constrained regularization program for inverting noisy linear algebraic and integral equations. *Comput. Phys. Commun.*, 27(3):229–242, 1982.

[141] Kenneth M Pryse, Ali Nekouzadeh, Guy M Genin, Elliot L Elson, and George I Zahalak. Incremental mechanics of collagen gels: new experiments and a new viscoelastic model. *Ann. Biomed. Eng.*, 31(10):1287–1296, 2003.

[142] Kenneth M Pryse, Ali Nekouzadeh, Guy M Genin, Elliot L Elson, and George I Zahalak. Incremental mechanics of collagen gels: new experiments and a new viscoelastic model. *Annals of biomedical engineering*, 31(10):1287–1296, 2003.

[143] Kenneth M Pryse, Ali Nekouzadeh, Guy M Genin, Elliot L Elson, and George I Zahalak. Incremental mechanics of collagen gels: new experiments and a new viscoelastic model. *Annals of biomedical engineering*, 31(10):1287–1296, 2003.

[144] MA Puso and JA Weiss. Finite element implementation of anisotropic quasi-linear viscoelasticity using a discrete spectrum approximation. *Journal of Biomechanical Engineering*, 120(1):62–70, 1998.

[145] Zhao Qin, Alfonso Gautieri, Arun K Nair, Hadass Inbar, and Markus J Buehler. Thickness of hydroxyapatite nanocrystal controls mechanical properties of the collagen–hydroxyapatite interface. *Langmuir*, 28(4):1982–1992, 2012.

[146] Kim Ragaert, Filip De Somer, Pamela Somers, Ives De Baere, Ludwig Cardon, and Joris Degrieck. Flexural mechanical properties of porcine aortic heart valve leaflets. *journal of the mechanical behavior of biomedical materials*, 13:78–84, 2012.

[147] Andrew D Rouillard and Jeffrey W Holmes. Mechanical boundary conditions bias fibroblast invasion in a collagen-fibrin wound model. *Biophysical journal*, 106(4):932–943, 2014.

[148] Roger A Rowe, Kenneth M Pryse, Clara F Asnes, Elliot L Elson, and Guy M Genin. Collective matrix remodeling by isolated cells: Unionizing home improvement do-it-yourselfers. *Biophysical journal*, 108(11):2611–2612, 2015.

[149] Fatemeh Saadat, Victor Birman, Stavros Thomopoulos, and Guy M Genin. Effective elastic properties of a composite containing multiple types of anisotropic ellipsoidal inclusions, with the application to the attachment of tendon to bone. *Journal of the Mechanics and Physics of Solids*, 2015.

[150] S.E. Salcudean, Daniel French, S. Bachmann, R. Zahiri-Azar, X. Wen, and W.J. Morris. Viscoelasticity modeling of the prostate region using vibro-elastography. In Rasmus Larsen, Mads Nielsen, and Jon Sporring, editors, *Medical Image Computing and Computer-Assisted Intervention MICCAI 2006*, volume 4190 of *Lecture Notes in Computer Science*, pages 389–396. Springer Berlin Heidelberg, 2006.

[151] Joseph J Sarver, Paul S Robinson, and Dawn M Elliott. Methods for quasi-linear viscoelastic modeling of soft tissue: application to incremental stress-relaxation experiments. *Journal of biomechanical engineering*, 125(5):754–758, 2003.

[152] AAHJ Sauren and EPM Rousseau. A concise sensitivity analysis of the quasi-linear viscoelastic model proposed by fung. *J. Biomech. Eng*, 105(1):92–95, 1983.

[153] AAHJ Sauren and EPM Rousseau. A concise sensitivity analysis of the quasi-linear viscoelastic model proposed by fung. *J. Biomech. Eng*, 105(1):92–95, 1983.

[154] AAHJ Sauren, MC Van Hout, AA Van Steenhoven, FE Veldpaus, and JD Janssen. The mechanical properties of porcine aortic valve tissues. *Journal of biomechanics*, 16(5):327–337, 1983.

[155] Katharina Schregel, Eva Wuerfel née Tysiak, Philippe Garteiser, Ines Gemeinhardt, Timour Prozorovski, Orhan Aktas, Hartmut Merz, Dirk Petersen, Jens Wuerfel, and Ralph Sinkus. Demyelination reduces brain parenchymal stiffness quantified in vivo by magnetic resonance elastography. *Proc. Natl. Acad. Sci. U.S.A.*, 109(17):6650–6655, 2012.

[156] Katharina Schregel, Eva Wuerfel née Tysiak, Philippe Garteiser, Ines Gemeinhardt, Timour Prozorovski, Orhan Aktas, Hartmut Merz, Dirk Petersen, Jens Wuerfel, and Ralph Sinkus. Demyelination reduces brain parenchymal stiffness quantified in vivo by magnetic resonance elastography. *Proceedings of the National Academy of Sciences*, 109(17):6650–6655, 2012.

[157] HRC Screen, J Seto, S Krauss, P Boesecke, and HS Gupta. Extrafibrillar diffusion and intrafibrillar swelling at the nanoscale are associated with stress relaxation in the soft collagenous matrix tissue of tendons. *Soft Matter*, 7(23):11243–11251, 2011.

[158] Zhilei Liu Shen, Harold Kahn, Roberto Ballarini, and Steven J Eppell. Viscoelastic properties of isolated collagen fibrils. *Biophysical journal*, 100(12):3008–3015, 2011.

[159] Vivek S Shenoy. A free energy based approach to model durotaxis and extracellular stiffness-dependent contraction and polarization of cells. *Interface Focus*, 0(0):0–1, 2015.

[160] Frederick H Silver, David L Christiansen, Patrick B Snowhill, and Yi Chen. Transition from viscous to elastic-based dependency of mechanical properties of self-assembled type i collagen fibers. *Journal of applied polymer science*, 79(1):134–142, 2001.

[161] Jérôme Solon, Ilya Levental, Kheya Sengupta, Penelope C Georges, and Paul A Janmey. Fibroblast adaptation and stiffness matching to soft elastic substrates. *Biophysical journal*, 93(12):4453–4461, 2007.

[162] Florian J Stadler. Effect of incomplete datasets on the calculation of continuous relaxation spectra from dynamic-mechanical data. *Rheologica acta*, 49(10):1041–1057, 2010.

[163] Florian J Stadler and Christian Bailly. A new method for the calculation of continuous relaxation spectra from dynamic-mechanical data. *Rheologica Acta*, 48(1):33–49, 2009.

[164] Florian J Stadler, Joachim Kaschta, and Helmut Münstedt. Dynamic-mechanical behavior of polyethylenes and ethene-/α-olefin-copolymers. part i. α'-relaxation. *Polymer*, 46(23):10311–10320, 2005.

[165] Mark D Stevenson, Alisha L Sieminski, Claire M McLeod, Fitzroy J Byfield, Victor H Barocas, and Keith J Gooch. Pericellular conditions regulate extent of cell-mediated compaction of collagen gels. *Biophysical journal*, 99(1):19–28, 2010.

[166] T-J Stieltjes. Recherches sur les fractions continues. In *Annales de la Faculté des sciences de Toulouse: Mathématiques*, volume 8, pages 1–122, 1894.

[167] Triantafyllos Stylianopoulos and Victor H Barocas. Volume-averaging theory for the study of the mechanics of collagen networks. *Computer methods in applied mechanics and engineering*, 196(31):2981–2990, 2007.

[168] Hsing-Wen Sung, Yen Chang, Chi-Tung Chiu, Chiun-Nan Chen, and Huang-Chien Liang. Mechanical properties of a porcine aortic valve fixed with a naturally occurring crosslinking agent. *Biomaterials*, 20(19):1759–1772, 1999.

[169] Ariel Sverdlik and Y Lanir. Time-dependent mechanical behavior of sheep digital tendons, including the effects of preconditioning. *Journal of biomechanical engineering*, 124(1):78–84, 2002.

[170] Aaron M Swedberg, Shawn P Reese, Steve A Maas, Benjamin J Ellis, and Jeffrey A Weiss. Continuum description of the poisson s ratio of ligament and tendon under finite deformation. *Journal of biomechanics*, 47(12):3201–3209, 2014.

[171] Stavros Thomopoulos, Victor Birman, and Guy M Genin. *Structural interfaces and attachments in biology*. New York, NY: Springer Science & Business Media, 2012.

[172] Stavros Thomopoulos and Guy M Genin. Tendon and ligament biomechanics. *Orthopaedic Biomechanics*, page 49, 2012.

[173] Stavros Thomopoulos, Gerald R Williams, Jonathan A Gimbel, Michele Favata, and Louis J Soslowsky. Variation of biomechanical, structural, and compositional properties along the tendon to bone insertion site. *J. ORTHOP. RES.*, 21(3):413–419, 2003.

[174] James J Tomasek, Giulio Gabbiani, Boris Hinz, Christine Chaponnier, and Robert A Brown. Myofibroblasts and mechano-regulation of connective tissue remodelling. *Nature Reviews Molecular Cell Biology*, 3(5):349–363, 2002.

[175] Robert L Trelstad, Kimiko Hayashi, and Jerome Gross. Collagen fibrillogenesis: intermediate aggregates and suprafibrillar order. *Proceedings of the National Academy of Sciences*, 73(11):4027–4031, 1976.

[176] Xavier Trepat, Linhong Deng, Steven S An, Daniel Navajas, Daniel J Tschumperlin, William T Gerthoffer, James P Butler, and Jeffrey J Fredberg. Universal physical responses to stretch in the living cell. *Nature*, 447(7144):592–595, 2007.

[177] Kevin L Troyer, Donald J Estep, and Christian M Puttlitz. Viscoelastic effects during loading play an integral role in soft tissue mechanics. *Acta biomaterialia*, 8(1):234–243, 2012.

[178] Nicholas W Tschoegl. *The phenomenological theory of linear viscoelastic behavior: an introduction*. Springer Science & Business Media, 2012.

[179] Jessica Unick, H Scott Kieffer, Wendy Cheesman, and Anna Feeney. The acute effects of static and ballistic stretching on vertical jump performance in trained women. *The Journal of Strength & Conditioning Research*, 19(1):206–212, 2005.

[180] Ramji T Venkatasubramanian, Wim F Wolkers, Mithun M Shenoi, Victor H Barocas, Daniel Lafontaine, Charles L Soule, Paul A Iaizzo, and John C Bischof. Freeze–thaw induced biomechanical changes in arteries: role of collagen matrix and smooth muscle cells. *Annals of biomedical engineering*, 38(3):694–706, 2010.

[181] Ellen Wachtel and Alice Maroudas. The effects of ph and ionic strength on intrafibrillar hydration in articular cartilage. *Biochimica et Biophysica Acta (BBA)-General Subjects*, 1381(1):37–48, 1998.

[182] Jessica E Wagenseil, Tetsuro Wakatsuki, Ruth J Okamoto, George I Zahalak, and Elliot L Elson. One-dimensional viscoelastic behavior of fibroblast populated collagen matrices. *Journal of biomechanical engineering*, 125(5):719–725, 2003.

[183] Tetsuro Wakatsuki, Michael S Kolodney, George I Zahalak, and Elliot L Elson. Cell mechanics studied by a reconstituted model tissue. *Biophysical Journal*, 79(5):2353–2368, 2000.

[184] Tetsuro Wakatsuki, Bill Schwab, Nathan C Thompson, and Elliot L Elson. Effects of cytochalasin d and latrunculin b on mechanical properties of cells. *Journal of cell science*, 114(5):1025–1036, 2001.

[185] Hailong Wang, AS Abhilash, Christopher S Chen, Rebecca G Wells, and Vivek B Shenoy. Long-range force transmission in fibrous matrices enabled by tension-driven alignment of fibers. *Biophysical journal*, 107(11):2592–2603, 2014.

[186] Ning Wang and Donald E Ingber. Control of cytoskeletal mechanics by extracellular matrix, cell shape, and mechanical tension. *Biophysical journal*, 66(6):2181, 1994.

[187] Jeffrey A Weiss, Savio L-Y Woo, Karen J Ohland, Shuji Horibe, and Peter O Newton. Evaluation of a new injury model to study medial collateral ligament healing: primary repair versus nonoperative treatment. *Journal of Orthopaedic Research*, 9(4):516–528, 1991.

[188] DJ Wills, DCA Picton, and WIR Davies. An investigation of the viscoelastic properties of the periodontium in monkeys. *Journal of periodontal research*, 7(1):42–51, 1972.

[189] W Wilson, NJB Driessen, CC Van Donkelaar, and K Ito. Prediction of collagen orientation in articular cartilage by a collagen remodeling algorithm. *Osteoarthritis and Cartilage*, 14(11):1196–1202, 2006.

[190] A Wineman. Nonlinear viscoelastic solidsa review. *Mathematics and Mechanics of Solids*, 14(3):300–366, 2009.

[191] Pak Kin Wong, Winny Tan, and Chih-Ming Ho. Cell relaxation after electrodeformation: effect of latrunculin a on cytoskeletal actin. *Journal of biomechanics*, 38(3):529–535, 2005.

[192] T Wong, JA McGrath, and H Navsaria. The role of fibroblasts in tissue engineering and regeneration. *British Journal of Dermatology*, 156(6):1149–1155, 2007.

[193] Savio L-Y Woo, Michael I Danto, Karen J Ohland, Thay Q Lee, and Peter O Newton. The use of a laser micrometer system to determine the cross-sectional shape and area of ligaments: a comparative study with two existing methods. *Journal of biomechanical engineering*, 112(4):426–431, 1990.

[194] Bin Xu, Haiyue Li, and Yanhang Zhang. Understanding the viscoelastic behavior of collagen matrices through relaxation time distribution spectrum. *Biomatter*, 3(3):e24651, 2013.

[195] Bin Xu, Haiyue Li, and Yanhang Zhang. Understanding the viscoelastic behavior of collagen matrices through relaxation time distribution spectrum. *Biomatter*, 3(3):e24651, 2013.

[196] Yingjie Xu, Pan Zhang, and Weihong Zhang. Two-scale micromechanical modeling of the time dependent relaxation modulus of plain weave polymer matrix composites. *Compos. Struct.*, 123:35 – 44, 2015.

[197] Sihua Yang, Da Xing, Yeqi Lao, Diwu Yang, Lvming Zeng, Liangzhong Xiang, and Wei R Chen. Noninvasive monitoring of traumatic brain injury and post-traumatic rehabilitation with laser-induced photoacoustic imaging. *Applied physics letters*, 90(24):243902, 2007.

[198] Sihua Yang, Da Xing, Quan Zhou, Liangzhong Xiang, and Yeqi Lao. Functional imaging of cerebrovascular activities in small animals using high-resolution photoacoustic tomography. *Medical physics*, 34(8):3294–3301, 2007.

[199] W Yang, TC Fung, KS Chian, and CK Chong. Viscoelasticity of esophageal tissue and application of a qlv model. *Journal of biomechanical engineering*, 128(6):909–916, 2006.

[200] W Yang, TC Fung, KS Chian, and CK Chong. Viscoelasticity of esophageal tissue and application of a qlv model. *Journal of biomechanical engineering*, 128(6):909–916, 2006.

[201] Bangzheng Yin, Da Xing, Yi Wang, Yaguang Zeng, Yi Tan, and Qun Chen. Fast photoacoustic imaging system based on 320-element linear transducer array. *Physics in medicine and biology*, 49(7):1339, 2004.

[202] Lawrence Yoo, Hansang Kim, Vijay Gupta, and Joseph L Demer. Quasilinear viscoelastic behavior of bovine extraocular muscle tissue. *Investigative ophthalmology & visual science*, 50(8):3721, 2009.

[203] George I Zahalak, Jessica E Wagenseil, Tetsuro Wakatsuki, and Elliot L Elson. A cell-based constitutive relation for bio-artificial tissues. *Biophysical journal*, 79(5):2369–2381, 2000.

[204] Yaguang Zeng, Da Xing, Yi Wang, Bangzhen Yin, and Qun Chen. Photoacoustic and ultrasonic coimage with a linear transducer array. *Optics letters*, 29(15):1760–1762, 2004.

[205] Hao F Zhang, Konstantin Maslov, Meng-Lin Li, George Stoica, and Lihong V Wang. In vivo volumetric imaging of subcutaneous microvasculature by photoacoustic microscopy. *Optics Express*, 14(20):9317–9323, 2006.

[206] Wei Zhang, Henry Y Chen, and Ghassan S Kassab. A rate-insensitive linear viscoelastic model for soft tissues. *Biomaterials*, 28(24):3579–3586, 2007.

[207] Xinli Zhou, Lixin Ma, Javad Habibi, Adam Whaley-Connell, Melvin R Hayden, Roger D Tilmon, Ashley N Brown, Jeong-a Kim, Vincent G DeMarco, and James R Sowers. Nebivolol improves diastolic dysfunction and myocardial remodeling through reductions in oxidative stress in the zucker obese rat. *Hypertension*, 55(4):880–888, 2010.

Vita

Behzad Babaei

Degrees

B.S. Mechanical Engineering, September 2007
M.S. Mechanical Engineering, March 2010

Professional

Reviewed articles for:
ASME Journal of Biomechanical Engineering
Acta Mechanica Sinica
International Conference on Material Technology & Environmental Engineering
Proceedings of the National Academy of Sciences
Biomacromolecules
Journal of the Mechanical Behavior of Biomedical Materials
Journal of the Royal Society: Interface

Journal Publications

B. Babaei, A. Davarian, S. L. Lee. K., M. Pryse, W. B. McConnaughey, E. L. Elson, G. M. Genin, "Remodeling by fibroblasts alters the rate-dependent mechanical properties of collagen", Acta Biomaterialia., 2016.

R. M. Castile, N. W. Skelley, B. Babaei, R. H. Brophy, S. P. Lake, "Microstructural properties and mechanics vary between bundles of the human anterior cruciate ligament during stress-relaxation", J. Biomech., 2015.

B. Babaei, S. D. Abramowitch, E. L. Elson, S. Thomopoulos, G. M. Genin, "A discrete spectral analysis for determining quasi-linear viscoelastic properties of biological materials", J. R. Soc. Interface., 2015.

B. Babaei, A. Davarian, K. M. Pryse, E. L. Elson, G. M. Genin, "Efficient and optimized identification of generalized Maxwell viscoelastic relaxation spectra", J. Mech. Behav. Biomed. Mater., 2015.

R. Mohammadkhani, D. Nemati, B. Babaei, "Investigation of gear-cutter design modifications on decreasing gearbox noise", J. Basic Appl. Sci. Res., 2012.

R. Mohammadkhani, D. Nemati, B. Babaei, "Optimizing helical gear profile for decreasing gearbox noise", J . Basic. Appl. Sci. Res., 2012.

Babaei, Behzad, Mahmood M. Shokrieh, and Kamran Daneshjou. "The ballistic resistance of multi-layered targets impacted by rigid projectiles." Materials Science and Engineering: A, 2011.

Conferences

AJ Velasquez Mao, Behzad Babaei, Kenneth M. Pryse, William B. McConnaughey, Elliot L. Elson, Guy M. Genin. Remodeling by fibroblasts alters the rate-dependent mechanical properties of collagen submitted to the NEMB2016-6180. ASME International Congress on Nanoengineering for Medicine and Biology, Houston, TX, February 21-24, 2016.

AJ Velasquez Mao, Behzad Babaei, Kenneth M. Pryse, William B. McConnaughey, Elliot L. Elson, Guy M. Genin. Frequency dependent energy dissipation of cells and ECM. Paper NEMB2016-6181. 2016 ASME International Congress on Nanoengineering for Medicine and Biology, Houston, TX, February 21-24, 2016.

Behzad Babaei, Elliot Elson, Stavros Thomopoulos, Guy M. Genin, "Fast tools for viscoelastic spectral analysis of cells, collagen, and ECM remodeling In Intelligent design: multi-scale modeling of cells, tissues, and organs", Opening workshop at the 2015 TERMIS 4th International World Congress ("The Evolution of Regenerative Medicine"), Boston, MA, September 8, 2015.

Stavros Thomopoulos, Victor Birman, Markus J. Buehler, Ioannis Chasiotis, Mark Anastasio, Pedro Ponte-Castaeda, Asa Barber, B. Babaei, John C. Boyle, Baptiste Depalle, Alix C. Deymier-Black, Yizhong Hu, Kenna Middleton, Arun Nair, Fatemeh Sadaat, Guy M. Genin, "Multi-scale mechanics of the tendon-to-bone attachment", IMAG 2015 Multiscale Modeling Consortium Meeting, National Institutes of Health, Washington, DC, September 8-9, 2015.

Guy Genin, B. Babaei, John Boyle, Alix Deymier-Black, Yizhong Hu, Justin Lipner, Fatemeh Saadat, Victor Birman, Stavros Thomopoulos, "Multiscale modeling of partially mineralized tissues", Paper NEMB2015-8120. ASME 2015 4th Global Congress on NanoEngineering for Medicine and Biology, Minneapolis, MN, April 19-22, 2015.

B. Babaei, Ali Davarian, Kenneth M. Pryse, William B. Mc- Connaughey, Elliot L. Elson, Guy M. Genin. "Viscoelastic response spectra of living cells within a collagen extracellular matrix". Paper NEMB2015-8013. ASME 2015 4th Global Congress on Nano Engineering for Medicine and Biology, Minneapolis, MN, April 19-22, 2015.

B. Babaei, A. Davarian, S. L. Lee. K., M. Pryse, W. B. McConnaughey, E. L. Elson, G. M. Genin, "Remodeling of collagen by human fibroblasts", Washington University symposium, St.Louis, MO, April 19-22, 2015.

B. Babaei, S Abramowitch, EL Elson, S Thomopoulos, GM Genin. "Identifying Fung QLV Materials Through Spectral Analysis of Stress-relaxation Tests". SES 51st Annual Technical Meeting, Purdue University, West Lafayette, IN, February 21, 2015.

Guy M. Genin, Teresa M. Abney, Kenneth M. Pryse, T. Wakatsuki, B. Babaei, Nicholas Pittore, Dengfeng Gao, William McConaughey, Feng Xu, Elliot L. Elson, "Making a Hydrogel Very Sick: Fibrotic Cardiomyopathy Reconstituted in Engineered Tissue Constructs", The 7th World Congress of Biomechanics, Boston, MA, October 1-3, 2014.

Guy M. Genin, Teresa M. Abney, B. Babaei, Ali Davarian, Dengfeng Guo, William B. McConnaughey, Nicholas Pittore, Kenneth M. Pryse, Feng Xu, Tetsuro Wakatsuki, and Elliot L. Elson, "Fibrotic cardiomyopathy reconstituted in hydrogel scaffolds", IUTAM Symposium on Mechanics of Soft Active Materials", Haifa, Israel, May 12-15, 2014.

Guy M. Genin, Kenneth M. Pryse, Teresa M. Abney, Sheng-Lin Lee, B. Babaei, Ryan Blumenstein, Michael Knoedel, Ali Davarian, Ali

Nekouzadeh, William B. McConnaughey, Feng Xu, Tianjian Lu, Tetsuro Wakatsuki, Bryan Carlson, Elliot L. Elson. "Engineered heart tissue as a model of cardiac fibrosis". Tissue Engineering and Regenerative Medicine International Society (TERMIS) 2013 Annual Meeting, Shanghai, China, October 23-26, 2013.

B. Babaei, Alireza Sadeghian Motahar, Majid Sahravi, "Strength of reinforced composites with carbon nanotubes: an experimental study", The International Conference on Experimental Solid Mechanics and Dynamics (X-Mech-2012),Tehran, Iran, March 6-7, 2012.

Kamran Daneshjou, B. Babaei, Majid Sahravi, Alireza Sadeghian Motahar, "The Ballistic Resistance of Double-layered Metallic Plates", The 18th Annual International Conference on Mechanical Engineering, Tehran, Iran, May 19-21, 2010.

Kamran Daneshjou, Majid Shahravi, B. Babaei, "Ricochet of steel long-rod projectile from deformable steel plates", The 17th Annual International Conference on Mechanical Engineering, Tehran, Iran, May 19-21, 2009.

Kamran Daneshjou, B. Babaei, Majid Shahravi, "Resistant performance of perforation in multi-layered metallic targets", The 17th Annual International Conference on Mechanical Engineering, Tehran, Iran, May 19-21, 2009.

Mohammad Haghpanahi, Majid Shahravi, B. Babaei, "The Effect of Nose Shape in Rod Penetration", The 17th Annual International Conference on Mechanical Engineering, Tehran, Iran, May 19-21, 2009.

August 2016